Comprehensive Study of 1-bit Delta-Sigma Modulation in Digitized Radio over Fiber Fronthaul Systems

Yuxuan Xie

A Thesis

in the Department of

Electrical and Computer Engineering

Presented in Partial Fulfillment of the Requirements

For the Degree of

Master of Applied Science (Electrical and Computer Engineering)

at Concordia University

Montreal, Quebec, Canada

August 2021

CONCORDIA UNIVERSITY
SCHOOL OF GRADUATE STUDIES

This is to certify that the thesis prepared

By: Yuxuan Xie

Entitled: Comprehensive Study of 1-bit Delta-Sigma Modulation in Digitized Radio over Fiber Fronthaul Systems

and submitted in partial fulfillment of the requirements for the degree of

Master of Applied Science (Electrical and Computer Engineering)

Complies with the regulations of this university and meets the accepted standards with respect to originality and quality.

Signed by the final examining committee:

_____ Chair and Internal Examiner

Dr. Weiping Zhu

_____ External Examiner

Dr. Chadi Assi

_____ Supervisor

Dr. John Xiupu Zhang

Approved by: _____

Dr. Yousef R. Shayan
Chair of Department of Electrical and Computer Engineering

August 2021

_____

Dr. Mourad Debbabi
Dean of Gina Cody School of
Engineering and Computer Science

ABSTRACT

Comprehensive Study of 1-bit Delta-Sigma Modulation in Digitized Radio over Fiber Fronthaul Systems

Yuxuan Xie

Mobile access network includes backhaul and fronthaul transmission system. To support the requirements of high capacity, low cost and low power consumption in fronthaul transmission systems, radio over fiber (RoF) technology has become the most popular solution for fronthaul transmission. Current fronthaul transmission technology is based on digitized CPRI RoF transmission (CPRI- common protocol radio interface). However, the conventional CPRI RoF leads to fronthaul systems with high complexity, and high-power consumption. To simplify, 1-bit delta-sigma modulation based digital RoF fronthaul system was proposed, in which the complexity and power consumption of the antenna tower units by moving complicated signal processing to central baseband units are reduced. When 1-bit delta-sigma modulation is used, an electrical bandpass filter is only required at the antenna tower to convert a digital signal to an analog RF signal for a downlink fronthaul.

In this thesis, comprehensive studies and comparison of three 1-bit delta-sigma modulations (DSM) in fronthaul optical transmission are given, which are two bandpass and one envelope delta-sigma modulation. The first bandpass 1-bit DSM considered (type-I) is based on a mixed-signal and a bandpass ΔΣ modulator, and the second bandpass 1-bit DSM considered (type-II) is based on all-digital signal and two low-pass ΔΣ modulators.

First, the ΔΣ modulator, i.e. the core unit of the DSM, is designed for a long-term evolution (LTE) signal of 200 MHz. In the ΔΣ modulator, the loop filter plays a significant role, and thus it is first optimized. Based on theoretical analysis, simulations and experiments, the Chebyshev-based loop filter is selected because it has a narrower transition band and wider stopband. Moreover, it is found that the order of the loop filter should be matched with input signal bandwidth.

Among the three DSMs, it is found by simulations and experiments that bandpass DSM type I is the

simplest system, and it also leads to the best optical transmission. However, the bandpass DSM type I is the highest in the design difficulty because it uses a bandpass ΔΣ modulator. The bandpass DSM type II is the easiest system to be implemented by hardware for its all-digital structure. However, due to a wider signal spectrum, the type-II is more sensitive to fiber dispersion, and the wider signal spectrum is induced by digital carrier.

It is found that harmonic noise can be added to the signal band in the envelope DSM when the signal is not narrow, such as 200 MHz in this thesis. Further, it is shown that this noise becomes the dominating factor in transmission performance. Therefore, the envelope DSM leads to the worst transmission performance among the three DSMs.

DSM generated NRZ is also compared to conventional NRZ. It is found that the DSM generated NRZ leads to worse transmission performance than conventional NRZ, i.e., more sensitive to fiber dispersion, which is due to the fact that the DSM generated NRZ has a larger optical spectrum. To reduce the effect of fiber dispersion, it is demonstrated that the digital up-sampling after DSM can be used to reduce the optical bit rate, and thus transmission is much less sensitive to fiber dispersion.

ACKNOWLEDGEMENTS

First, I would like to express my thank to my parents, Li Feng and Yunfeng Xie, who offer me infinitive support and encouragement during my study in Canada.

Next, I would like to express my sincere gratitude to my supervisor Dr. John Xiupu Zhang, for his advice, help, and support for me to finish this thesis.

I also would like to express my appreciation to my colleague Xiaoran Xie, for his endless help and advice in the simulation of 1-bit DSM and experiment setups.

Finally, I would like to thank my groupmates included Fujuan Huang, Zijian Chen and Lara Juras, for their treasured support, which was really influential in shaping my experiment methods, critiquing my results as well as reviewing my writing.

Table of Contents

List of Figures

List of Tables

List of Acronyms

AP	access point
AMPS	advanced mobile phone system
AlGaAs	aluminum gallium arsenide
ASCII	American standard code for information interchange
AM	amplitude modulation
ADC	analog to digital converter
AWG	arbitrary waveform generator
APD	avalanche photodetectors
BTS	base transceiver station
BPSK	binary phase shift keying
BER	bit error rate
CSMA/CA	carrier-sense multiple access with collision avoidance
CPU	central processing unit
CDMA	code-division multiple access
CPRI	common public radio interface
CMOS	complementary metal-oxide-semiconductor
DSM	delta sigma modulation
ΔΣ modulator	delta sigma modulator
DSM	delta-sigma modulation
DPSK	differential phase-shift keying
DSP	digital signal processing
DSL	digital subscriber line
DAC	digital to analog converter
DC	direct current
DBR laser	distributed Bragg reflector
DFB laser	distributed-feedback laser
E/O	electric/optic
EAM	electrical-absorption modulator
EAM	electro-absorption modulator
EDSM	envelope delta-sigma modulation
EVM	error vector magnitude
FP laser	Fabry-Perot laser
FFT	fast Fourier transformation
FPGA	field-programmable gate array
5G	fifth generation
FIR	finite impulse response
1G	first generation
4G	fourth generation
FDM	frequency division multiplexing

FSK	frequency shift keying
FDMA	frequency-division multiple access
GVD	group-velocity dispersion
IIR	infinite impulse response
I/Q	in-phase and quadrature
IC	integrated circuit
IMDD	intensity modulation and direct-detection
ICI	inter-channel interference
IoT	Internet of things
IFFT	inverse fast Fourier transformation
LAN	local area network
LTE	long-term evolution
MZM	Mach-Zehnder modulator
MZM	Mach–Zehnder modulator
MAC	media access control
MOSFET	metal–oxide–semiconductor field-effect transistor
MIMO	multiple-input multiple-output
NTF	noise transfer function
NRZ	non-return to zero
O/E:	optic/electric
OTx	optical transmitter
OFDM	orthogonal frequency-division multiplexing
OSR	oversampling ratio
PSNR	peak signal to noise ratio
PM	phase modulation
PLL	phase-locked loop
PA	power amplifier
PSD	power spectral density
PCM	Pulse coding modulation
PDM	pulse density modulation
QAM	quadrature amplitude modulation
QPSK	quadrature phase-shift keying
QD	quantum dots
RF	radio frequency
RoF	radio over fiber
RIN	relative intensity noise
RIN	relative intensity noise
RRU	remote radio unit
RZ	return to zero
RMS	root mean square
2G	second generation

SNR	signal to noise ratio
STF	signal transfer function
SMF	single mode fiber
SISO	single-input single-output
SOPC	system on a programmable chip
3G	third generation
TDMA	time-division multiple access
WDM	wavelength division multiplexing
WAN	wide area networks

Chapter 1 Introduction

1.1 History of mobile communication networks

In the mid-1860s, the Scottish mathematician James Clerk Maxwell produced a pair of equations, which predicted that coupled electric and magnetic fields could travel through space as an "electromagnetic wave." Then in 1888, Heinrich Rudolf Hertz discovered electromagnetic radiation, which is predicted based on the Maxwell equations, by a series of experiments. These experiments were also the first wireless transmission in the world with four meters distance. About seven years later, Guglielmo Marconi achieved signal transmission and reception over a distance of about 2 km, which became the first patent of wireless signal transmission in the world [1]. After that, it took engineers about one century to move wired servers and technologies to wireless areas. Finally, in order to control the collision in telecommunication networks caused by the exponentially increasing number of users, cellular systems were launched. The most famous one was called advanced mobile phone system (AMPS), developed by Bell Labs, which was an analog network system based on frequency-division multiple access (FDMA). AMPS was also the first generation (1G) of telecommunication networks [2]. However, because of the limited semiconductor technologies, this system was a circuit-switched network, and it only supported voice service at that time.

With the development of integrated circuit technology, especially the metal–oxide–semiconductor field-effect transistor (MOSFET), the transformation from analog signals to digital signals became possible. As a result, in 1991, a set of protocols called global system for mobile communications (GSM) were published by the European, which was the first digital network, and GSM became the second generation (2G) telecommunication networks [2]. This system also introduced hybrid channelization techniques with time-division multiple access (TDMA) and FDMA. Several advanced digital modulation methods, such as differential phase-shift keying (DPSK), quadrature phase-shift keying (QPSK), and quadrature amplitude modulation (QAM), were also developed to replace the conventional analog modulation method like amplitude modulation (AM) because of their reliability. The applications of

information theory, such as source coding and channel coding, were also used in 2G networks to reduce the bit error rate (BER) and improve security. Unfortunately, although GSM optimized for full-duplex voice telephony, it was still an all circuit-switched network whose efficiency is not good enough to support the high data rate of the Internet. Therefore, packet-switched networks were invented for Internet service. In third generation (3G) networks [2], general packet radio service (GPRS) was designed for Internet service, and GSM was kept for voice service. With this hybrid switched network, as well code division multiple access (CDMA), 3G networks became the prototype of modern telecommunication networks. Besides, compared with 2G networks, 3G networks could support more users with the help of advanced media access control (MAC) methods such as carrier-sense multiple access with collision avoidance (CSMA/CA) [3]. Thus, 3G networks can support all kinds of portable devices like personal computers and tablets, while 2G is only for mobile phones.

Although 3G networks could provide both Internet and voice services, people never stop research from achieving as high speed as possible. So, the fourth generation (4G) standard was proposed in 2010, which was called long-term evolution (LTE) [4]. The most famous technology in 4G was orthogonal frequency-division multiplexing (OFDM), which significantly increased band utilization rate. In FDMA, there must be a gap between each channel to reduce inter-channel interference (ICI). When using OFDM, because the carrier of a channel is orthogonal with nearby channels, there could be an overlap between each channel in frequency domain [5]. Thus, the efficiency of frequency band utilization of OFDM could reach 100% in theory. Another essential improvement in 4G is multiple-input multiple-output (MIMO) technology. MIMO systems deploy multiple antennas at both the source (transmitter) and the destination (receiver). The capacity of the MIMO system is increased linearly with the increase of the number of transmitting and receiving antennas. The data throughput and link reliability of MIMO systems are essentially higher than that of conventional single-input single-output (SISO) systems [6]. Finally, the 4G systems could interoperate with 2G, 3G, and broadband digital broadcasting systems. In addition, 4G systems are also fully IP-based wireless Internet [7]. As Figure 1-1 shown, these features make 4G become a seamless connections network.

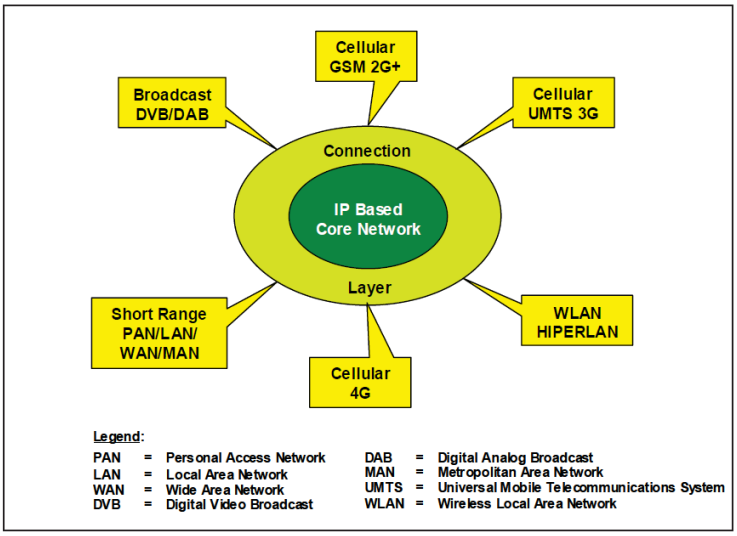

Figure 1-1 Seamless connections of 4G networks [7]

Nowadays, fifth generation (5G) standards have been defined, and some companies, such as Bell and Huawei, already work as pioneers to develop 5G in their products. Generally, continued increase in signal bandwidth, band utilization rate, and transmission speed are the main goals of 5G development. Additionally, 5G networks also focus on Internet of things (IoT), especially for automobiles. However, this technology is limited to the communications between vehicles and core networks, called "in coverage." Finally, direct communications between vehicles, called "out of coverage," is also a mission of 5G.

Table 1-1 shows a comparison from 1G to 5G. It is found that the transmission speed shows exponentially increasing trends. The channel bandwidth also becomes wider because 1G is designed for voice calls only, and next generation technologies want to support more and more services.

Table 1-1 Comparison of parameters from 1G to 5G [1]-[9]

Comparison	1G	2G	3G	4G	5G (phase 1)
Introduce in	1979	1991	2001	2010	Present
Technology	AMPN	GMS	W-CDMA	LTE MIMO	New radio
Access system	FDMA	FDMA&TMDA	CDMA	OFDM	OFDM
Switching type	Circuit switch	Circuit switch	Hybrid of Circuit switch and packet switch	Hybrid	Hybrid
Speed	2 kbps	64 kbps	2 Mbps	1 Gbps	Up to 100 Gbps
Bandwidth/channel	30 kHz	200 kHz	1.25 MHz	5-20 MHz	Up to 400 MHz
Applications	Voice calls	Voice calls and messages	Voice calls, messages and Internet	High-speed Internet	Extremely high-speed network, IoT

1.2 Radio over fiber system

With the advancement in fiber optical communication, the demand for broadband digital transmitter architecture with high data rates and capability is increased significantly. As a result, the radio over fiber (RoF) systems become the most popular solutions for the backbone of wide area networks (WAN). Furthermore, 5G speeds will be 13 times higher than the current average mobile connection in the next 5 years [10]. However, conventional transmission mediums, such as digital subscriber line (DSL) and coaxial cable, are difficult to support the capacity and speed requirement of 5G and next-generation networks. In that case, RoF system will also dominate the market of local area networks (LAN), like access points (AP), in future. Figure 1-2 shows the general structure of the RoF system. The central station is the data source of the whole system. The main cell is a base transceiver station (BTS) combined with radio frequency (RF) modulators and electric to optic (E/O) convertors. In addition, there are usually a set of parallel cells in a center station to support the large throughput of mobile telecommunication networks. The base station is usually an antenna array with optic to electric (E/O) convertors, whose responsibility is handling traffic and signaling between mobile devices by wireless channel. Optical fiber usually works as link to connect central station and base station, and their distance is always less than 20 km because of fiber attenuation.

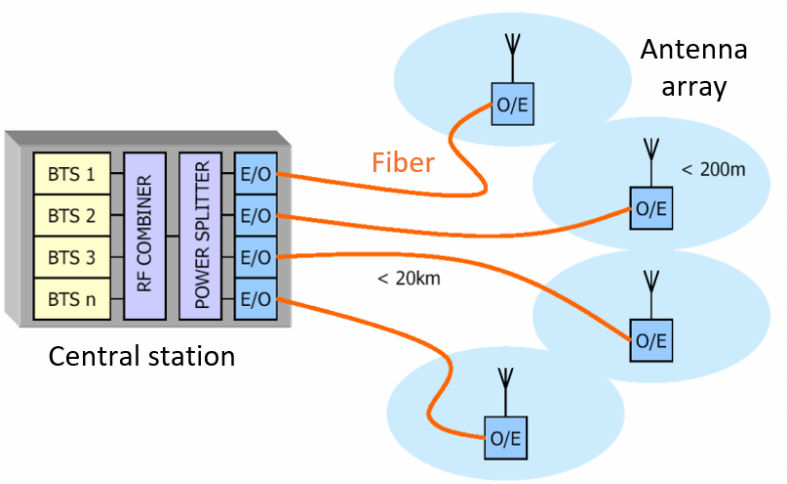

Figure 1-2 General structure of RoF system [11].

Generally, there are two types of RoF transmission methods: analog RoF and digital RoF. To realize

a cost-effective fronthaul network, analog RoF transmission systems for transmitted mobile data to antennas are applied as the common solution for access networks. Additionally, it is also able to simplify the remote radio unit (RRU) antennas sites and is also transparent and flexible to remote carrier frequencies and protocols [12]. However, because the optical carriers are modulated by analog radio signal directly, the transmission performance of analog RoF is strongly influenced by the nonlinearity of power amplifiers, memory effect, and arising from in-line transmission nonlinearity. In other words, the distortion requirement of analog RoF standards is stricter as compared to wireless standards [14]. Thus, digital RoF is expected to overcome the issue because of its strong resistance to nonlinearity.

Figure 1-3 illustrates the details of an analog RoF link. First, most signal processing operations happen in the central station. After the original signal is modulated and up-converted to a proper RF frequency, the RF signal is transmitted to an optical transmitter (OTx). Usually, intensity modulation and direct-detection (IMDD) systems are primary choices for short reach links [15]. For intensity modulation, the direct modulators are the most popular solution because of its low cost and simple structure. However, if the system requires a higher bit rate (≥10 Gbps), external modulators, such as Mach–Zehnder modulator (MZM) and electrical-absorption modulator (EAM), usually show better performances than direct modulators. Moreover, an independent laser is required for external modulators. So, the system can use some faultless laser products, such as quantum dots (QD) lasers, to achieve narrow lightweight and low relative intensity noise (RIN). At the receiver side, the optical receiver (ORx) transfers the received optical signal into an electrical RF signal. After that, the RF signal will be amplified and transmitted into the antenna directly. Generally, there should be no additional digital signal processing (DSP) device in RRH to keep the antenna tower as simple as possible. However, in order to reduce the fiber dispersion effect, IMDD systems have to use high laser power, which will intensify the fiber nonlinear effect, such as Kerr effect. On the other hand, compared with IDMM systems, coherent optical transmissions provide strong mitigation to dispersion, greater capacity, and flexibility. Nevertheless, it relies on DSP technology to compensate for fiber dispersion, which will significantly increase the complexity of the whole system.

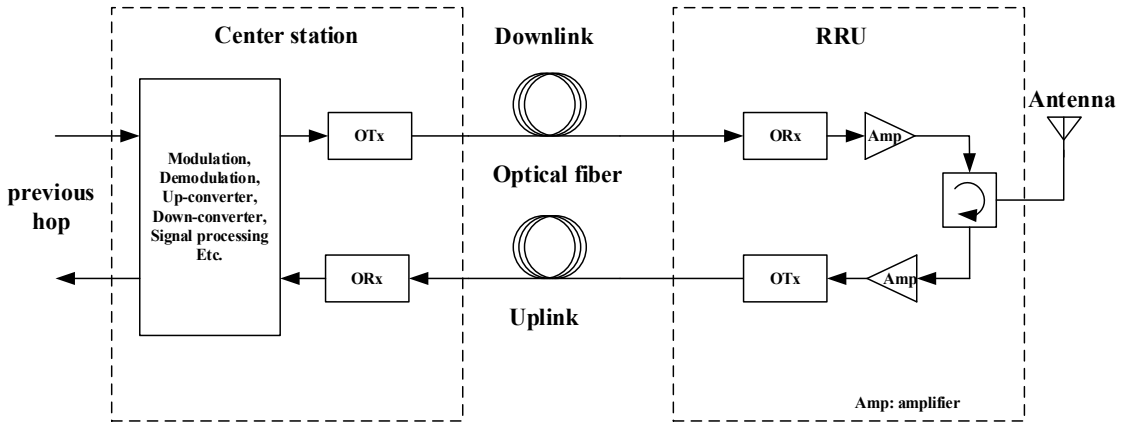

Figure 1-3 Schematic of an analog RoF link

Conventionally, the structure of digital RoF downlink systems can be illustrated in Figure 1-4. By using high-speed sampling and multi-bit quantization with analog to digital converters (ADC) and digital to analog converters (DAC), the digitized RF signal has been digitized and gets great resistance to nonlinearity because there are only two voltages levels in a digital signal. Moreover, a new technology called photonic ADC can combine ADC and electrical to optical converter together. It can save a lot of space and energy cost in integrated circuit design. Additionally, the time jitter of photonic ADC can reach about 100 times less than normal ACD [16]. As a result, digital RoF systems become popular solutions in access point and common public radio interface (CPRI) design. However, according to the development trend of 5G and next-generation technology, the bit rate of transmission systems will continue increasing, which may reach 100 Gb/s or higher. Moreover, conventional ADC also requires a multi-bit quantizer to decrease quantizing noise. Under current conditions of very large-scale integration (VLSI) technology, implementing both high sampling speed and multi-quantizing bits together is always too expensive to afford. Fortunately, it is possible to only focus on achieving high sampling frequency, and 1-bit delta-sigma modulation (DSM) is introduced [17].

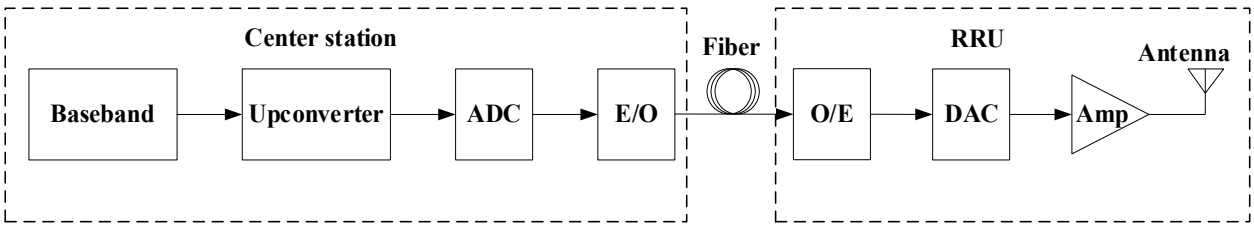

Figure 1-4 Block diagram of conventional digitized RoF transmission system (downlink)

A digitized RoF transmission system with 1-bit DSM is shown in Figure 1-5. A baseband signal is injected into a 1-bit delta-sigma modulation subsystem, and a digitized NRZ signal is created at its output, which drives an electric-optic converter. After optical to electrical conversion, an RF wireless signal can be created by letting the digital electric signal going through an RF bandpass filter with a required central frequency and bandwidth. Finally, the RF wireless signal is radiated by an antenna. Comparing to conventional RoF system, the DSM-based digitized RoF systems use a bandpass filter instead of a DAC. This operation can significantly reduce the complexity of RHH because DAC is a DSP device, and the bandpass filter could be analog circuits. As a result, in DSM based RoF system, most calculations and signal processing operations happen at center stations. So, this system requires high-speed central processing units (CPU), such as digital signal processor, field-programmable gate array (FPGA) and system on a programmable chip (SOPC), for signal generation and transmission control.

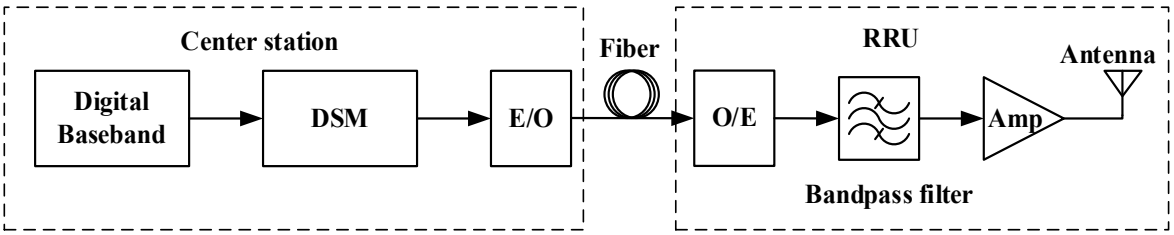

Figure 1-5 Block diagram of 1-bit digitized RoF transmission system based on DSM (downlink).

1.3 Thesis outline

The rest of the thesis is organized as follows:

Chapter 2 is the literature review about the details of RoF systems and delta-sigma modulations.

Chapter 3 gives the theoretical principles of delta sigma modulations, including delta sigma modulator and three types of delta sigma modulations, as well as how they have been incorporated into RoF systems.

Chapter 4 presents the simulation results with comparisons.

Chapter 5 present the experiment setup and procedures.

Chapter 6 make the conclusion of this thesis and give suggestions for future work to achieve better improvement in DSM.

Chapter 2 Background and literature review

Chapter 2 first introduces several important techniques used in RoF links. These include lasers, optical modulators, optical receivers, and power amplifiers. Next, general principles and applications of ADC are discussed in section 2.2. Finally, section 2.3 introduces N-bit and 1-bit DSM, as well as their implementations.

2.1 Radio over fiber system

2.1.1 Digital modulations and OFDM

Digital modulation is the process of encoding a digital information signal into the amplitude, phase, or frequency of the transmitted signal. The original signal before modulation is called baseband signal, and the waveform (usually sinusoidal) that is modulated is defined as the carrier signal. In digital baseband, there are two types of line codes for binary bitstream called return to zero (RZ) and non-return to zero (NRZ). In addition, there are also two common power level patterns: unipolar and bipolar. Thus overall, there are four waveform patterns which are the permutations of line code patterns and power level patterns. They are unipolar RZ, unipolar NRZ, bipolar RZ, and bipolar NRZ waveform. Figure 2-1 shown the sequential waveform of them with same input bit pattern "10101100".

The first discussion is about power levels. Assumed that the distance between two power level is 2A, the power level of unipolar signal is 0 and 2A. For bipolar signal, the power level should be -A and +A. Now, support that the system suffers additional Gaussian white noise with power spectrum density $S_n(f) = \frac{N_0}{2}$, where N_0 is constant. And the bitrate of the system is $R_b = \frac{1}{T_b}$. Hence, the variance of white noise is $\sigma^2 = \frac{N_0}{2T_b}$ [18]. Thus, the bit error rates of both unipolar and bipolar signals are

$$BER = Q\left(\sqrt{\frac{2A^2T_b}{N_0}}\right) \tag{2.1}$$

where Q is the q function.

It looks like those unipolar and bipolar signals have same the performances while suffering white

noise. However, the average power of a unipolar signal is

$$P_{\mathrm{u}} = 0.5 \times 0^2 + 0.5 \times (2A)^2 = 2A^2 \tag{2.2}$$

And the average power of a bipolar signal is

$$P_{\mathrm{b}} = 0.5 \times A^2 + 0.5 \times (-A)^2 = A^2 \tag{2.3}$$

In conclusion, in order to get same performance, the unipolar signal costs double energy more than the bipolar signal. Furthermore, there is a direct current (DC) component in unipolar waveforms, which leads to voltage droop problems, especially in passing an amplifier. This characteristic means that unipolar waveform always requires a special designed RF amplifier in applications. Therefore, the bipolar waveform is an energy-efficient solution in transmissions.

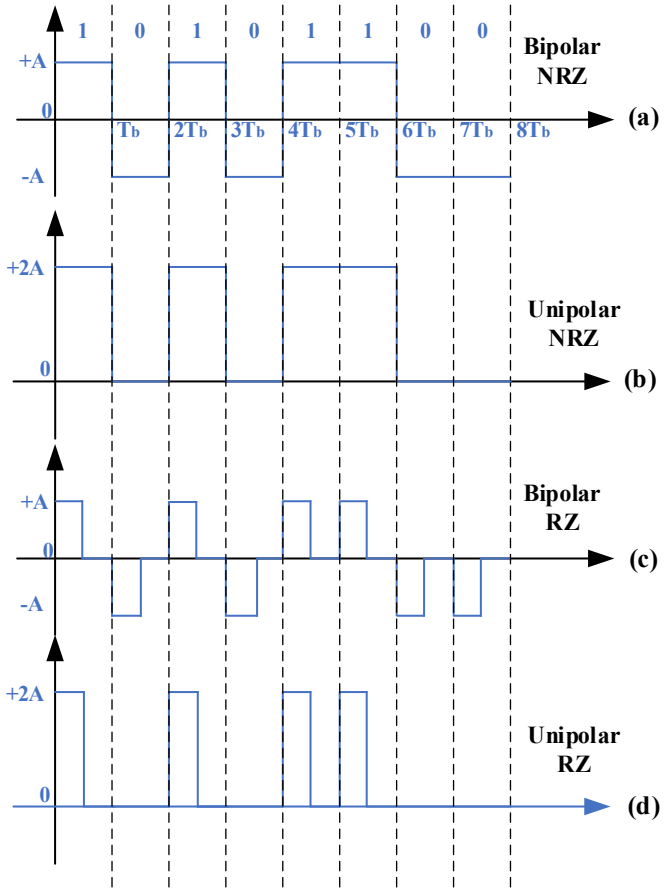

Figure 2-1 Sequential waveforms of bipolar NRZ, unipolar NRZ, bipolar RZ and unipolar RZ.

The next discussion is about RZ and NRZ. As Figure 2-1 shown, the amplitude of an RZ pulse will always return to zero at half of a bit period. As a result, the RZ signal does not require an additional clock signal for synchronizations. This is called self-synchronization [18]. On the other hand, the RZ signal has wider bandwidth. The RZ and NRZ signal can be treated as random processes and using NRZ as example here. Suppose that there is a bipolar NRZ signal $X(t)$, as Figure 2-1 shown

$$X(t) = \sum_{n=-\infty}^{+\infty} A_n p(t - nT_b) \tag{2.4}$$

where $A_n = [-A, A]$ is amplitude of signal, *p* is the probability of each power level, $T_b = \frac{1}{R_b}$ is the bit period, and R_b is the bitrate [19].

The mean of $X(t)$ is

$$m_X(t) = E\left[\sum_{n=-\infty}^{+\infty} A_n p(t - nT_b)\right] = \sum_{n=-\infty}^{+\infty} E[A_n] p(t - nT_b) \tag{2.5}$$

As NRZ signal, $E[A_n] = 0$. So $m_X(t) = 0$, and the autocorrelation function of *X(t)* is

$$\begin{aligned} R(t_1, t_2) &= E[X(t_1) \cdot X(t_2)] \\ &= \begin{cases} E[X(t_1)^2] = A^2 & if\ nT \le t_1, t_2 < (n+1)T_b \\ E[X(t_1)] \cdot E[X(t_2)] = 0 & otherwise \end{cases} \end{aligned} \tag{2.6}$$

Since this process is wide-sense stationary, the autocorrelation function can be written as

$$R(\tau) = R(t_1 - t_2) = \begin{cases} A^2\left(1 - \frac{|\tau|}{T_b}\right) & if\ |\tau| < T_b \\ 0 & otherwise \end{cases} \tag{2.7}$$

According to the Einstein-Wiener-Khinchin theorem, the power spectral density (PSD) of a wide-sense stationary random process is given by the Fourier transform of the autocorrelation function. Thus, the PSD of a NRZ signal $S_{NRZ}(f)$ is

$$S_{NRZ}(f) = \mathcal{F}[R(\tau)] = A^2 T_b sinc^2(fT_b) \tag{2.8}$$

Same as above, the PSD of an RZ signal is $S_{RZ}(f)$

$$S_{RZ}(f) = \frac{A^2 T_b}{4} sinc^2\left(\frac{fT_b}{2}\right) \tag{2.9}$$

Figure 2-2 plots the PSD of RZ and NRZ signal. For $sinc^2$ function,

$$\int_{-1}^{1} sinc^2(x)dx = 0.9028 \ and \ \int_{-\infty}^{\infty} sinc^2(x)dx = 1 \tag{2.10}$$

This formula shows that the main lobe of a $sinc^2$ function obtains 90.28% energy of the whole signal. Therefore, the value first zero is defined as the bandwidth in digital signal processing. Based on this conclusion, the bandwidth of the NRZ signal is R_b, and the bandwidth of the RZ signal is $2R_b$. In conclusion, the bipolar NRZ signal is the most energy and bandwidth efficiency signal

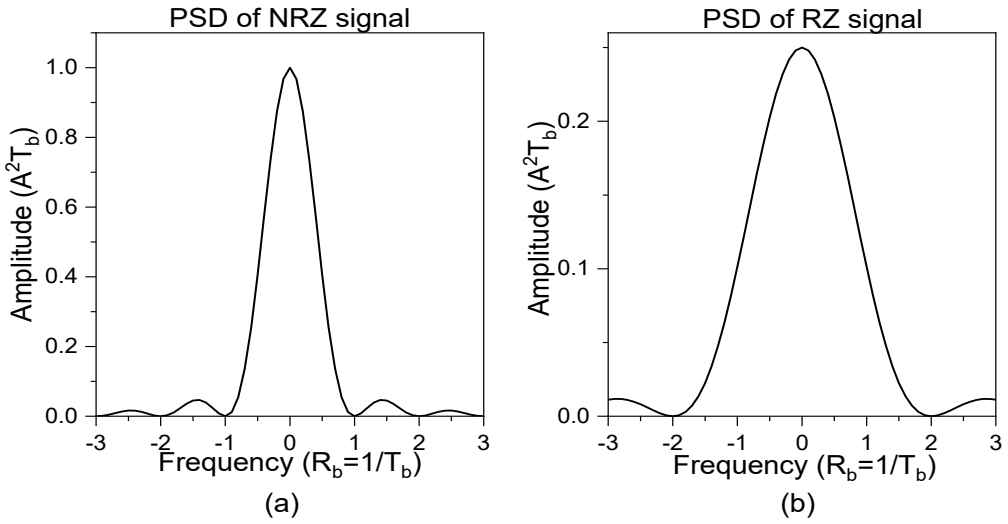

Figure 2-2 power spectral density of NRZ signal (a) and RZ (b) signal

In this thesis, the digital modulation methods are classified into orthogonal modulation and non-orthogonal modulation. The orthogonal modulation is defined as modulation whose carriers are orthogonal. For example, A modulation using *sin(x)* and *cos(x)* as carriers is orthogonal modulation, such as QPSK and QAM. On the contrary, modulation methods with a single carrier, like amplitude shift keying (ASK), or non-orthogonal carriers, such as frequency shift keying (FSK), are defined as non-orthogonal modulations. The devices to implement modulation is called modulators or up-convertors. Additionally, in orthogonal modulation, the modulated signal can be decomposed into two amplitude-modulated sinusoids, whose phases are offset by one-quarter cycle (90 degrees, π/2 radians or 1/4 period), known as the in-phase and quadrature (I/Q) components. Figure 2-3 provides a block diagram of an I/Q up-convertor [20].

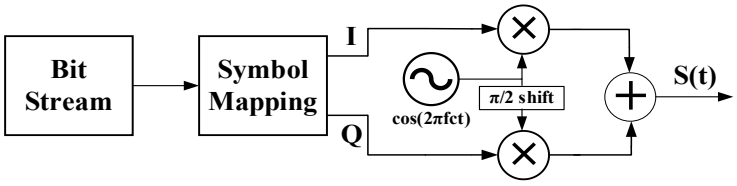

Figure 2-3 Standard I/Q up-convertor

Based on the figure above, the modulated signal *S(t)*

$$\begin{aligned} S(t) &= I \cdot \cos(2\pi f_c t) + Q \cdot \sin(2\pi f_c t) \\ &= A \cdot \cos(2\pi f_c t + \varphi) \end{aligned} \tag{2.11}$$

where $A = \sqrt{I^2 + Q^2}$ *and* $\varphi = arctan\frac{Q}{I}$.

By comparing the form of *S(t)* with Euler's formula, it is found that there is just an imaginary unit "*j*" between them. After adding a "*j*" in quadrature component, *S(t)* becomes a complex exponential signal:

$$\begin{aligned} S_c(t) &= I \cdot \cos(2\pi f_c t) + j \cdot Q \cdot \sin(2\pi f_c t) = A \cdot e^{j(2\pi f_c t + \varphi)} \\ &= \left(A \cdot e^{j\varphi}\right) \cdot e^{j2\pi f_c t} = (I + jQ) \cdot e^{j2\pi f_c t} \end{aligned} \tag{2.12}$$

Thus, after removing the carrier part $e^{j2\pi f_c t}$, we can describe any modulated signal using a lowpass complex function. This is called the lowpass equivalent of bandpass signals [20]. The *I* and *Q* are defined as the in-phase and quadrature components. It can also be expressed in terms of the envelope (A) and the phase (φ). Since the spectrum of equivalent signal $(I + jQ) = \left(A \cdot e^{j\varphi}\right)$ is also a lowpass signal, just like the digital baseband signal. It can also be defined as equivalent baseband, and the equivalent baseband signal could be described as a discrete set $\{S_e(k) = I_k + jQ_k, k = 1,2, \dots N\}$, where N is the total number of samples. In equivalent baseband, the constellation diagram is a representation of a signal modulated by a digital modulation scheme such as QAM. It displays the signal, i.e., $S_e(k)$, as a two-dimensional XY-plane scatter diagram in the complex plane. And the error vector magnitude (EVM) is a measure used to quantify the performance of a digital transmission based on the constellation diagram. The EVM used in this thesis is based on IEEE 802.11 [21], whose unit is dB instead of percentage. Figure 2-4 uses the simplest orthogonal modulation, QPSK, as example to show the constellation diagram and the principle of EVM. The EVM is calculated by the formula below. Since this formula calculates the root mean square (RMS) value of EVM vectors, some references also name it as EVM_{rms}.

$$EVM\ (dB) = 20log_{10}\left(\sqrt{\frac{1}{NP_{avg}}\sum_{k=1}^{N}[(I_k - I_k{}^*)^2 + (Q_k - Q_k{}^*)^2]}\right) \tag{2.13}$$

where N is the number of symbols, P_{avg} is the power of constellation diagram, (I_k, Q_k) is the complex coordinates of the measured symbol k, and $(I_k{}^*,\ Q_k{}^*)$ is the complex coordinates of the reference symbol k.

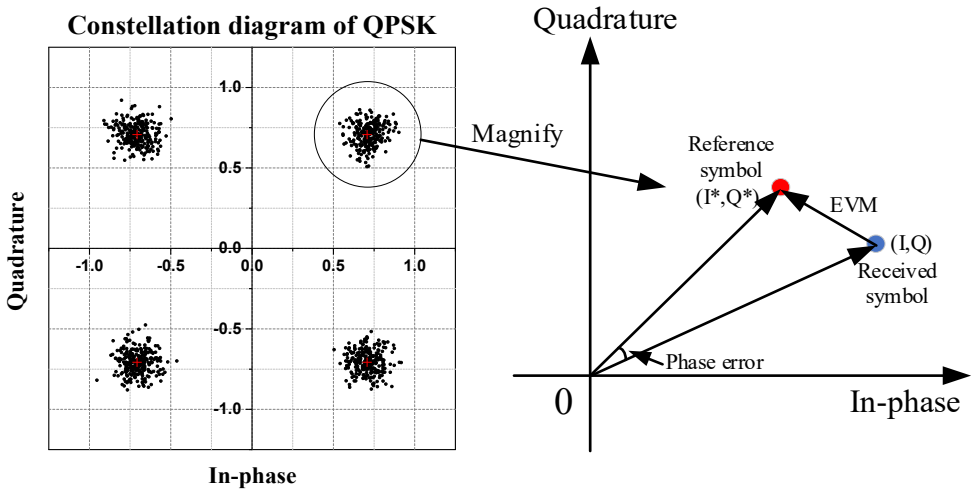

(a) (b)

Figure 2-4. (a) Example and (b) principle of EVM

Finally, while suffering amplitude noise, such as additional Gaussian white noise, the EVM can be directly converted to signal to noise ratio (SNR) by the below formula in [22]:

$$EVM\ (1) \approx \left(\frac{1}{SNR(1)}\right)^{\frac{1}{2}} \tag{2.14}$$

where $EVM\ (1)$ and $SNR\ (1)$ mean the units of them are dimensionless. And the transformation between unit one to unit dB is known as:

$$EVM\ (dB) = 20log_{10}\big(EVM\ (1)\big) \text{ and } SNR(dB) = 10log_{10}(SNR(1))$$

Thus, after transferring unit of EVM and SNR into dB, it becomes:

$$EVM\ (1) = 10^{\frac{EVM(dB)}{20}} \approx \left(\frac{1}{SNR(1)}\right)^{\frac{1}{2}} = \left(\frac{1}{10^{\frac{SNR(dB)}{10}}}\right)^{\frac{1}{2}} \tag{2.15}$$

$$EVM(dB) \approx -1 \times SNR(dB)$$

In digital communications, orthogonal frequency-division multiplexing (OFDM) is also a typical

method whose equivalent baseband signal is a complex function. First, in OFDM, the orthogonality of two functions is defined as the inner product of them is zero. Because the carriers used in OFDM are sinusoid, the orthogonality of two carriers $f(t)$ and $g(t)$ is defined as:

$$\int_T f(t) \cdot g(t) = 0 \tag{2.16}$$

Let $f(t) = \cos(2\pi f_m t)$, $g(t) = \sin(2\pi f_n t)$ and $T = LCM(\frac{1}{f_m}, \frac{1}{f_n})$, where $m \neq 0, n \neq 0$ and LCM means least common multiple. Then, we have:

$$\begin{gathered} \int_T \cos(2\pi f_m t) \cdot \sin(2\pi f_n t) = 0, \qquad for\ all\ m \neq 0, n \neq 0 \\ \int_T \cos(2\pi f_m t) \cdot \cos(2\pi f_n t) = 0, \qquad for\ m \neq 0, n \neq 0\ and\ m \neq n \\ \int_T \sin(2\pi f_m t) \cdot \sin(2\pi f_n t) = 0, \qquad for\ m \neq 0, n \neq 0\ and\ m \neq n \end{gathered} \tag{2.17}$$

These results show the carriers (henceforth called subcarriers) in set

$$\{(\cos(2\pi f_m t), \sin(2\pi f_n t)),\ \ m \neq 0, n \neq 0\} \tag{2.18}$$

are mutually orthogonal.

Based on these three formulas above, the principles of OFDM can be described as a specialized frequency division multiplexing using a set of distinct orthogonal subcarriers. Specifically, let subcarriers be at the frequencies $f_k = \frac{kW}{N}$, where k is a positive integer, W is the total available bandwidth, and N is the total number of subcarriers. In equivalent baseband, the subcarriers set can be written as a complex exponential function $e^{j2\pi f_k t} = e^{j\frac{2\pi}{N}kWt}$. As explained above, the equivalent baseband signal is $S_e(k) = I_k + jQ_k$. Thus, the OFDM signal in equivalent baseband can be written as:

$$S_{OFDM}(t) = \sum_{k=1}^{N} S_e(k) \cdot e^{j\frac{2\pi}{N}kWt} \tag{2.19}$$

It is clear that the implementation of OFDM is similar with inverse discrete Fourier transformation (IDFT):

$$x[n] = \frac{1}{N}\sum_{k=1}^{N} X[k] e^{j\frac{2\pi}{N}kn} \tag{2.20}$$

where $x[n]$ is a discrete-time signal and $X[k]$ is $x[n]$ in frequency domain.

Hence, the best implementation method of OFDM is the inverse fast Fourier transformation (IFFT) algorithm. This approach is much easier to implement with integrated circuits because hardware implementation requires *N* local oscillators, each of which oscillates at a frequency at $f_k = \frac{kW}{N}$. On the contrary, the software approach can be directly implemented by a programable IC such as FPGA. Figure 2-5 illustrates the algorithm structure of the OFDM software approach [22]. There are converters between serial to parallel (S/P and P/S) required because the input and output of IFFT and fast Fourier transformation FFT algorithm must be parallel, and the data structure of signal sources, sinks, and channels must be serial. Finally, the signal after OFDM in equivalent baseband is still a complex exponential function. Therefore, it can be modulated by an I/Q up-convertor. In other words, OFDM can be treated as orthogonal modulation.

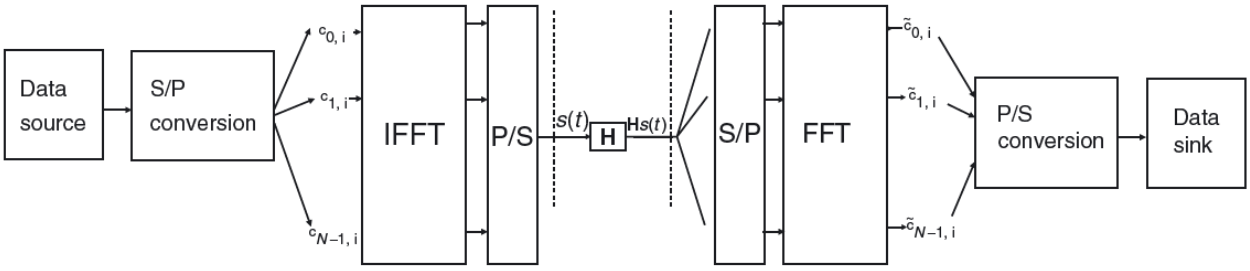

Figure 2-5 Block diagram of OFDM using IFFT in [22]

2.1.2 Optical transmitters and receivers

Generally, there are two typical transmission methods in fiber communications: intensity modulation and direct-detection (IMDD) and coherent transmission. No matter what type of modulation method, the optical signal is initially generated by lasers. The classic laser structure is called Fabry-Perot laser, shown in Figure 2-6 (a). The active region between the N-type layer and the P-type layer is a PN junction with large bandgap material, such as aluminum gallium arsenide (AlGaAs), and the energy pump of lasers is usually electrical current. The cleaved facet in the Fabry-Perot laser act as mirrors, which can be replaced by Bragg gratings, as shown in Figure 2-6 (b). This type of laser is known as distributed Bragg reflector (DBR) laser. Since the Bragg gratings are formed as periodically changing the reflective index, it can filter out the longitudinal modes, which makes the DBR laser as a single-longitudinal mode laser. However, the corrugated

region in the DBR laser is part of the cavity, and it is somewhat lossy, which lowers the efficiency of the devices. By fabricating the Bragg gratings above the active region, the distributed-feedback laser (DFB) laser is introduced as a solution, as shown in Figure 2-6 (c). Therefore, the DFB laser is selected as the main laser source in this thesis.

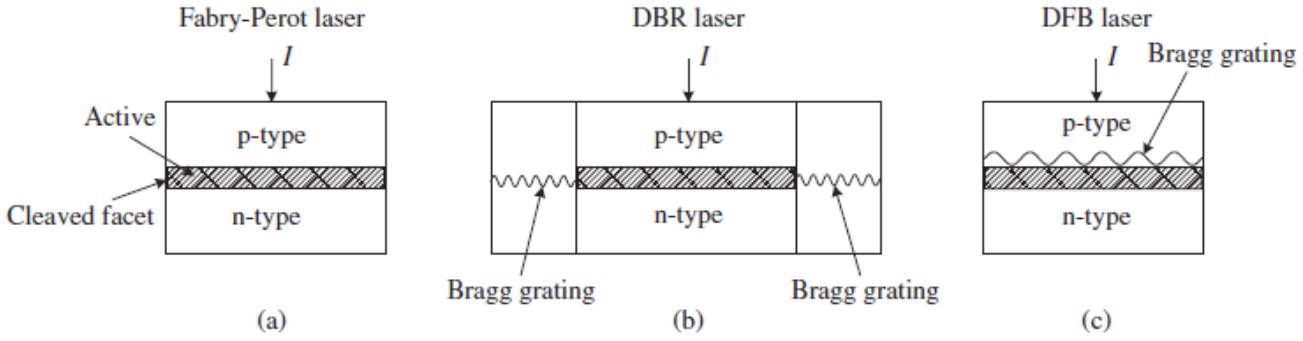

Figure 2-6 Different laser configurations: (a) FP laser, (b) DBR laser, (c) DFB laser [24].

Optical direct modulation is the simplest modulation method in RoF links, whose principles are shown in Figure 2-7. Since the laser power is too small to carrier information if the input electrical current is less than the threshold current, there must be a DC bias at the input side to make the input current always higher than the threshold current. However, the direct modulator is limited by nonlinearity distortion. Moreover, it is sensitive to laser chirp, which makes direct modulators not suitable for high bit rate (higher than 10 Gbps) transmission [24]. Finally, this modulation method can only modulate amplitude information, so the direct modulator can only be applied in IMDD RoF links.

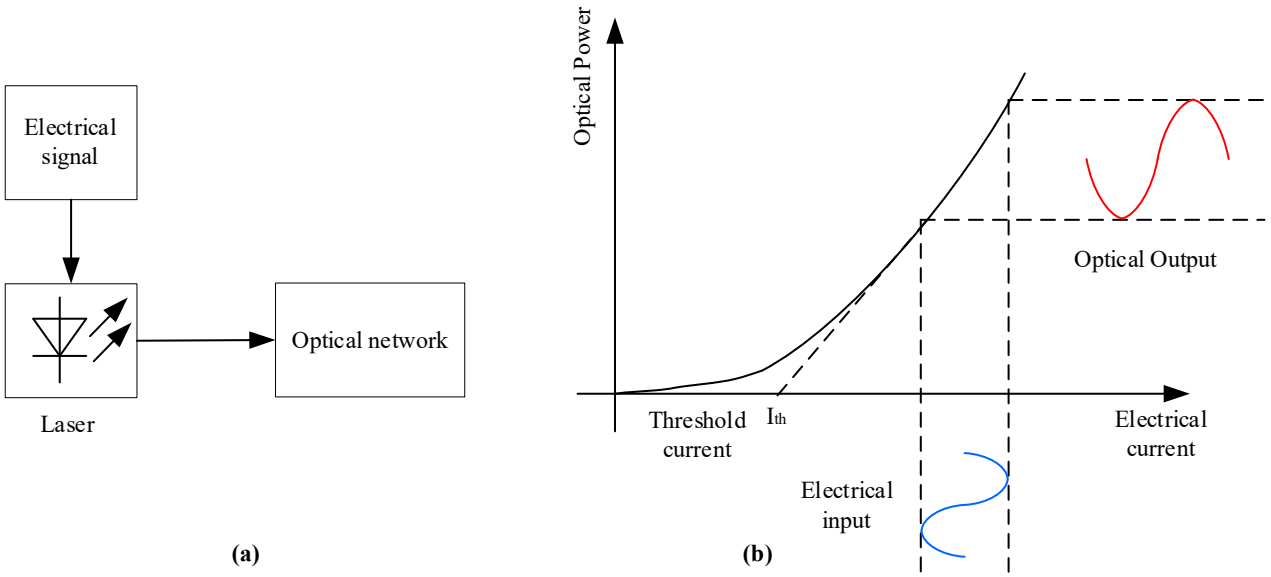

Figure 2-7 Principles of optical direct modulation including (a) general structure and (b) characteristic.

In order to overcome the disadvantages of direct modulators, the external modulator is introduced. Figure 2-8 provides the structure of external modulation. Generally, there are three widely used external modulators: the phase modulator, the Mach-Zehnder modulator (MZM), and the electro-absorption modulator (EAM). The main applications of phase modulators are coherent transmissions which will introduce later. The principle of EAM is the dependence of the absorption coefficient of a semiconductor on the applied electric field, and the band of this semiconductor material decreases as the applied field increases [24]. Figure 2-9 provides an example of NRZ signal modulation. For bit "zero", V(t)=0, there is no absorption for the input laser signal since the photon energy is less than the semiconductor bandgap. When transmitting bit "one", the photon energy is higher than the bandgap, and the optical carrier is absorbed. This makes the intensity of the electric field of output optical signal of bit "one" less than bit "zero". Thus, the information in the electrical domain is translated into the optical domain.

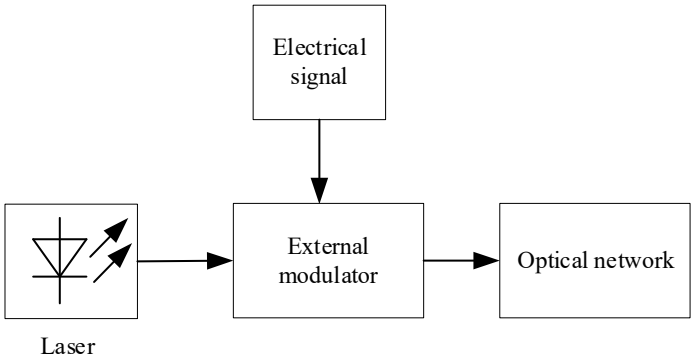

Figure 2-8 General structure of optical external modulator

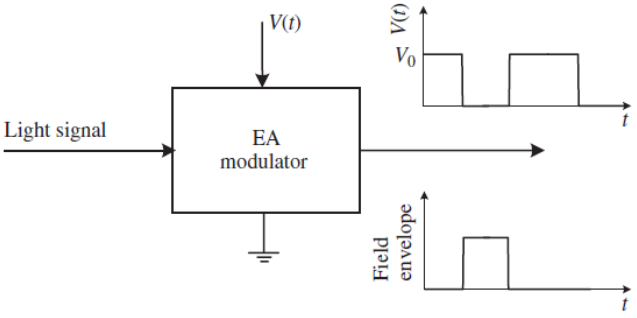

Figure 2-9 Modulation of NRZ signal using an EAM [24]

MZM is another widely used external modulator, and it is a multi-function modulator which means it can modulate both amplitude and phase information. An MZM usually consists of two arms, as shown in Figure 2-10. For modulation of NRZ signal, the relationship of input and output optical signal is given by [24]:

$$P_{out} = |A_{out}|^2 = {A_0}^2 cos^2\left\{\frac{[V_1(t) - V_2(t)]\pi}{2V_\pi}\right\} \tag{2.21}$$

where V_π is known as half-wave voltage. And instantaneous frequency shift (or frequency chirp) of output is zero if

$$V_1(t) + V_2(t) = V_{bias} \tag{2.22}$$

where V_{bias} is the bias voltage. Let $V_1(t)$ be the message signal $m(t) = \begin{cases} +V_\pi/4, & for\ bit\ "1" \\ -V_\pi/4, & for\ bit\ "0" \end{cases}$ and $V_{bias} = V_\pi/2$. The output of MZM is

$$P_{out} = \begin{cases} P_0 = {A_0}^2 & for\ bit\ "1" \\ 0 & for\ bit\ "0" \end{cases} \tag{2.23}$$

In that case, the MZM acts as an amplitude modulator.

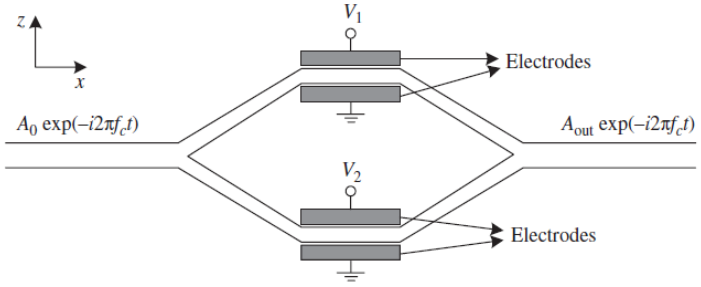

Figure 2-10 Cross-section of a dual-drive MZM [24].

Both optical direct modulation and external modulation can be defined as intensity modulation or amplitude modulation. In order to expand the capacity of fiber networks, coherent optical transmission is proposed. Similar to coherent electrical modulation, the optical coherent modulation can modulate both amplitude and phase information. The main structure of optical coherent modulation is a phase modulator whose structure is given in Figure 2-11 [24]. For some special materials such as $LiNbO_3$, the refractive index change is directly proportional to the applied electric field intensity, which is known as the Pockels effect or linear electro-optic effect. For the $LiNbO_3$ crystal in Figure 2-11, the relationship between the refractive index and the driving voltage is

$$n = n_0 - \frac{1}{2} {n_0}^3 r_{33} E_z \; and \; E_z = \frac{V}{d} \tag{2.24}$$

where n_0 is the refractive index without applying electric field, and r_{33} is a constant coefficient to describe the electro-optic effect. Thus, the phase of output optical signal is

$$\Phi = \frac{2\pi}{\lambda_0} nL = \frac{2\pi L}{\lambda_0} (n_0 - \frac{1}{2} {n_0}^3 r_{33} \frac{V}{d}) \tag{2.25}$$

where λ_0 is the wavelength of the input signal. And we define half-wave voltage V_π as

$$V_\pi = \frac{\pi \lambda_0 d}{{n_0}^3 r_{33} L} \tag{2.26}$$

We obtain the phase of the output signal

$$\Phi = \frac{2\pi L}{\lambda_0} (n_0 - \frac{\pi V}{V_\pi}) \tag{2.27}$$

By setting the driving voltage V as electrical message signal V(t), the phase of the output optical signal changes following the message signal. For example. By setting V(t)=0 for bit "zero" and V(t)= V_π for bit "one", there is no phase shift for "0" and π phase shift for "1". That is optical binary phase shift

keying (BPSK). Finally, it is seen that the structure of MZM is a combination of two-phase modulators. So, the MZM can also work as a phase modulator.

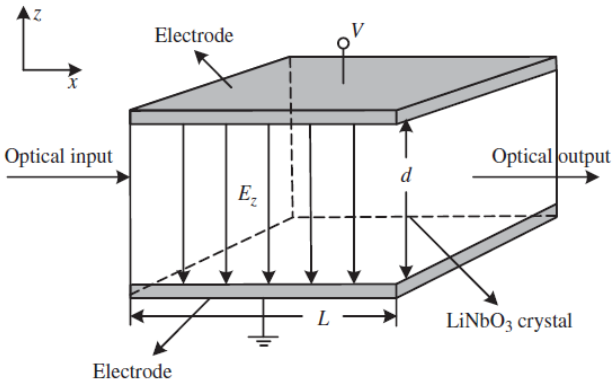

Figure 2-11 Phase modulation of an optical signal in a $LiNbO_3$ crystal [24].

Basically, there are two main noise sources in optical modulations of NRZ signals, relative intensity noise (RIN) and laser chirp. The laser chirp means the sudden change in laser center frequency during time caused by laser instability. This phenomenon will lead to a strong overshoot at the rising and falling edge of NRZ pulses. In direct-modulated lasers, the presence of the data signal produces large changes in the effective refractive index. This results in large phase shifts during the transitions of the data (transient chirp) as well as a long-term shift in the laser frequency (adiabatic chirp). Direct modulated lasers generally produce more chirp for higher extinction ratios. Another noise is intensity noise which is always generated from spontaneous emission and electron-hole recombination (known as shot noise). Since the power of noise is normalized to the average power level of the whole signal, it is named as relative intensity noise. Finally, the RIN can then be statistically described with a power spectral density (PSD), and it is always given in the unit of dB/Hz.

On the receiver side, an optical receiver is used to convert the optical signals into electronic signals. The core of the receiver is a photodiode. PN photodiode is the simplest category. As its name shows, there is a PN junction diode operation under reverse bias. However, the PN photodiode is limited by the compromise between quantum efficiency and bandwidth. i.e., a PN photodiode wants a wider absorption region to achieve higher quantum efficiency, but this operation will also increase the whole size of the device and resulting in a decreasing bandwidth of systems. Next, the PIN photodiode adds an intrinsic

region between N-type layer and P-type layer. Since most of photon absorption occurs at the intrinsic region, which could be tailored, the PIN photodiode can obtain optimum quantum efficiency and achieve bandwidth to a few tens of gigahertz. Finally, in order to get the gain to detect extremely low-intensity optical signals, avalanche photodetectors (APD) are invented by adding a gain layer between the N-type region and absorption region.

As its name shows, optical direct detection means a receiver that detects the power of the received signal only, which is the demodulation of optical intensity modulation. Usually, it is composed of a photodiode, a pre-amplifier, and a signal processing unit, as shown in Figure 2-12 [24]. For direct receivers, one of the main noise sources is thermal noise, which results from thermally induced random fluctuations in the charge carrier in load resistance. Because it is hard to keep the temperature of photodiodes as constant in experiments, thermal noise is always the dominated noise in direct receiver. Another common noise source is dark current caused by the current leakage path in the photon detector and thermal excitation of carriers across the PN junction. However, the dark current always works as the noise base of a photodiode, and it is negligible for large power detection. The last common noise source is shot noise which is associated with the quantum nature of the light. Since each incident photon produces an electron's worth of current, the power spectral density of shot noise is similar to white noise, which is proportional to the photocurrent.

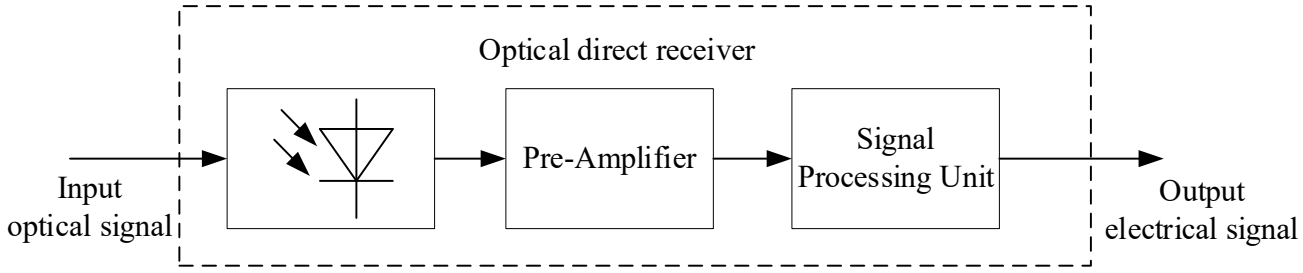

Figure 2-12 Structure of optical direct detection.

The optical direct receiver can only demodulate optical amplitude modulation. For optical coherent modulation, a coherent receiver is required. The difference between coherent and direct receivers is that there is a local oscillator in optical coherent receivers. Figure provides a block diagram of a single-branch coherent receiver [24]. Support that the received signal $q_r(t)$ and local oscillator output $q_{LO}(t)$ are

$$q_r(t) = A_r s(t) e^{-j(\omega_c t+\varphi)}$$
$$q_{LO}(t) = A_{LO} e^{-j(\omega_{LO} t+\varphi_{LO})} \tag{2.28}$$

where A_r and A_{LO} is the amplitude of received and local optical carrier, ω_c and ω_{LO} are frequency of them, φ and φ_{LO} are phase and $s(t)$ is the complex field envelope. The photocurrent is proportional to the absolute square of the incident optical field with slope R which is defined as responsivity of photodiodes. Therefore, the photocurrent is

$$I(t) = R\left|\frac{q_r(t)+q_{LO}(t)}{\sqrt{2}}\right|^2$$
$$= \frac{R}{2}\left\{|A_r s(t)|^2 + |A_{LO}|^2 + 2A_r A_{LO} Re\left[s(t)e^{-j[(\omega_c-\omega_{LO})t+(\varphi-\varphi_{LO})]}\right]\right\} \tag{2.29}$$

By setting the local laser power to be much higher received power, i.e., $|A_{LO}|^2 \gg |A_r|^2$, the first term $|A_r s(t)|^2$ can be neglected. Then, let $\omega_c - \omega_{LO}$ equal to the carrier frequency of RF signal ω_{RF} and $\varphi_{LO} = 0$. Since $|A_{LO}|^2$ is a constant, it will become a DC component and can be removed by a capacitance. Thus, the signal that goes to the front end is

$$I(t) = RA_r A_{LO} Re\left[s(t)e^{-j(\omega_{RF} t+\varphi)}\right] \tag{2.30}$$

That is the principle of coherent optical receivers. Compared with direct receiver, first, the sensitivity of coherent optical receivers is higher than direct receivers because there is a high-power local oscillator. On the contrary, the bit error rate of coherent optical receivers is always worse than direct receivers. It also requires more signal processing to keep good performance, because it is hard to keep $\varphi_{LO} = 0$ in applications which means that there is phase error in coherent optical receivers.

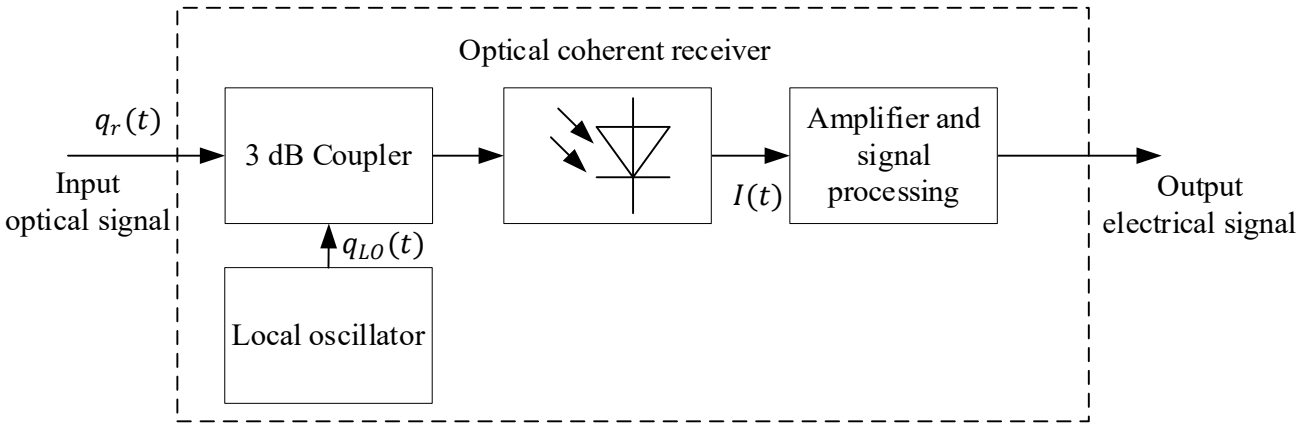

Figure 2-13 Structure of optical coherent detection.

2.1.3 Optical fiber

Optical fiber is the channel of RoF fronthaul systems. Compared with wireless networks, optical fiber network has high reliability, capacity, and security, which makes it become the solution for the backbone of modern telecommunication networks. Figure 2-14 [24] illustrates a cross-section of a step-index fiber where step-index means the refractive index of the core is constant. First, guided mode (usually abbreviated to mode) is an important parameter that is decided by the radius of fiber core as well as materials of core and cladding, and it can be written as

$$V = \frac{2\pi a}{\lambda}\sqrt{{n_1}^2 - {n_2}^2} \tag{2.31}$$

where a is the radius of the fiber core, λ is the wavelength of light, n_1 is the reflective index of the fiber core, and n_2 is the reflective index of the cladding. If V is less than or equal to 2.405, this fiber is a single mode fiber (SMF) at wavelength λ. And the wavelength that $V = 2.405$ is defined as the cutoff wavelength of this SMF. In this thesis, all fibers used in simulations and lab experiments are SMF at C-band (from 1530 nm to 1565 nm). Attenuation is also a basic parameter of optical fiber which is also called fiber loss. As its name implies, it is the energy loss of light after transmitting a distance in the optical fiber, which is always described in unit dB/km, and it is determined by the materials of fiber. This parameter is also the limitation of earlier optical fiber development. For example, the loss of fiber in 1966 is close to 20 dB/km, and it is just around 0.2 dB/km nowadays. The next typical parameter is dispersion. Dispersion happens because the group speed of light changes with the frequency of the optical wave. For the IM-DD link, the main dispersion type is chromatic dispersion, and it is also called group-velocity dispersion (GVD). It is defined as the differentiation of group velocity from the wavelength. Since it is a function of wavelength, a value at a typical wavelength will always be provided in fiber datasheets. For example, the GVD of standard SMF, e.g., SMF-28 [25], at 1550 nm is around $15\sim18\ ps/(km\cdot nm)$. For some special fibers, such as dispersion compensating fiber (DCF), the GVD is a negative value. Finally, Kerr nonlinearity will also suffer distortion in the IM-DD link since the reflective index varies with the power of optical field. The nonlinearity index (also called Kerr constant) is also decided by material. For silica core, the Kerr constant is approximately $2.6\times10^{-20}\ m^2/W$.

Since there are just two power levels for NRZ waveforms, the Kerr nonlinear effect will only happen at the rising and falling edges of NRZ waveforms. On the contrary, it will affect analog RoF and coherent transmission.

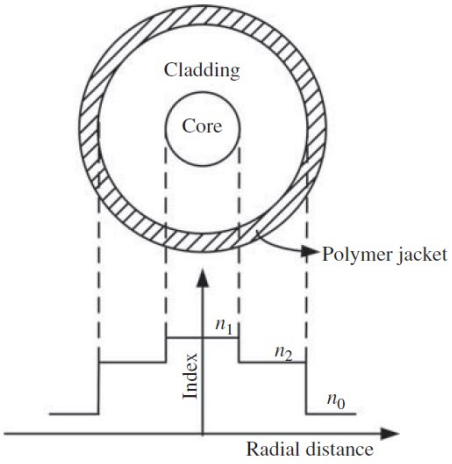

Figure 2-14 Cross-section of optical fiber and its reflective index profile

2.1.4 RF Power amplifier

A power amplifier (PA) is required in RoF links, and it is always located after photodiode because the output current of the photodiode is usually too weak for antenna tower systems. One of the significant characteristics of the power amplifier is nonlinear effect. Since the fundamental devices used in PAs, such as transistors and capacitors, are nonlinear devices whose output voltage is a function of high order terms of input voltage [26], it results in the nonlinear input-output characteristics of PA. Figure 2-15 provides the input-output characteristic of PA used in this thesis [27]. It is seen that the input power and output power are not proportional by analyzing the green line, and the gain of this amplifier (red line) is not constant can also prove this pattern. This nonlinear effect will suffer a distortion on the output signal, especially for high peak to average ratio signals, such as OFDM signal. On the other hand, for NRZ signals, there are just two power levels, and the nonlinear distortion only happens at the rising and falling edges. Thus, compared with OFDM signals, the nonlinear effect on NRZ signals is usually negligible.

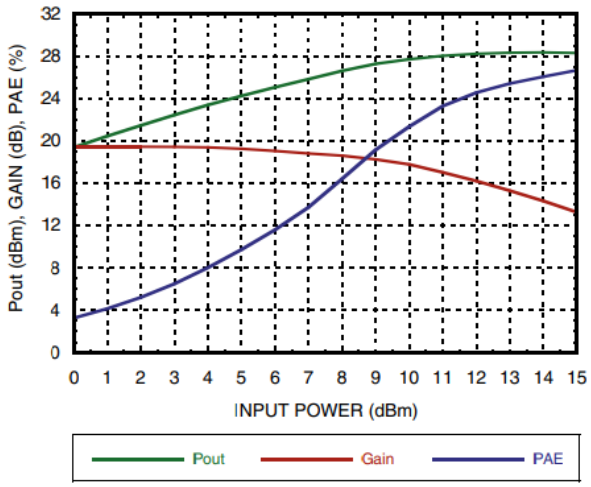

Figure 2-15 Profiles of power amplifier used in this thesis.

The mode of PA can be classified based on its conduction angle. In general, if the conduction angle is greater than zero, i.e., from 0 to 2π, these amplifiers are classified as conventional power amplifiers. In detail, they are class A, class B, class AB and class C [26], and the PA used in this thesis is a class C. On the contrary, if the conduction angle of PA is zero, which means that transistors work at on-off mode. These PAs are classified as switching mode power amplifiers, including class D-T. The switching mode power amplifiers are usually special designed for NRZ form signals, such as pulse coding modulation. For conventional RF power amplifiers, the working frequency range usually does not involve the DC component. For example, the frequency range of PA used in this thesis is from 800 MHz to 21 GHz, and the transmitted NRZ signal is sampled at 10 GHz. Thus, the PA is a high-pass system, instead of an all-pass system, for transmitted signals. As the step response of this PA, as shown in Figure 2-16, the time constant τ is 2.23 ns which is the time when the amplitude attenuates 3dB with a unit step signal input at $t=0$. This parameter shows that this PA can only hold a power level for about 22 bit period with input NRZ signal at 10 Gbps. In other words, if there is continuous bit "1" (or bit "0") bitstreams as input to this PA at 10 Gbps, this PA can only hold a power level for 22 bits period, and the rest of the bits will suffer from distortion.

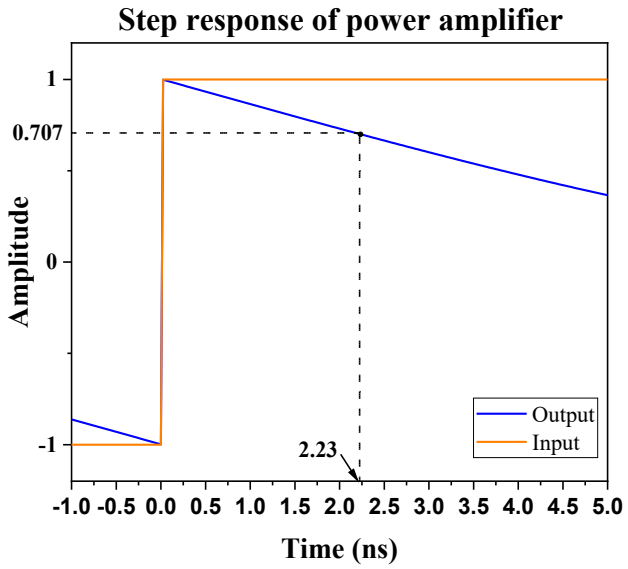

Figure 2-16 Step response of power amplifier used in thesis.

2.2 Analog to digital converters

This section introduces the basic theories and structures of analog to digital converters (ADC) including sampling, quantizing, and coding. Next, there is a thorough discussion about changing sampling frequency methods such as over-sampling, up-sampling, and down-sampling. Firstly, the original signal is a continuous-time signal whose time and amplitude are continuous. After sampling, the time of the signal becomes discrete, but the amplitude is still continuous. So, this signal is defined as the discrete-time signal. Finally, the output of the whole process becomes a digital signal after quantizing and coding.

2.2.1 Sampling

Basically, sampling is an operation that reduce a continuous-time signal to a discrete-time signal, which is also the margin between analog and digital systems. The principle of sampling is multiplexing the original signal with a period impulse train, as Figure 2-17 shown. Additionally, The Nyquist sampling theorem states that a bandlimited continuous-time signal can be sampled and perfectly reconstructed from its samples if the waveform is sampled over twice as fast as its highest frequency component [28], and the twice of the maximum frequency of the original signal is defined as Nyquist frequency, also

called Nyquist rate. Sometimes, the sampling at Nyquist frequency is not enough to get a good resolution. In that case, oversampling is proposed. In signal processing, oversampling is the process of sampling a signal at a sampling frequency significantly higher than the Nyquist frequency. Oversampling can improve resolution and signal-to-noise ratio, and it can be helpful in avoiding aliasing and phase distortion by relaxing anti-aliasing filter performance requirements. Finally, the oversampling ratio (OSR) is defined as the quotient of real sampling frequency over Nyquist frequency.

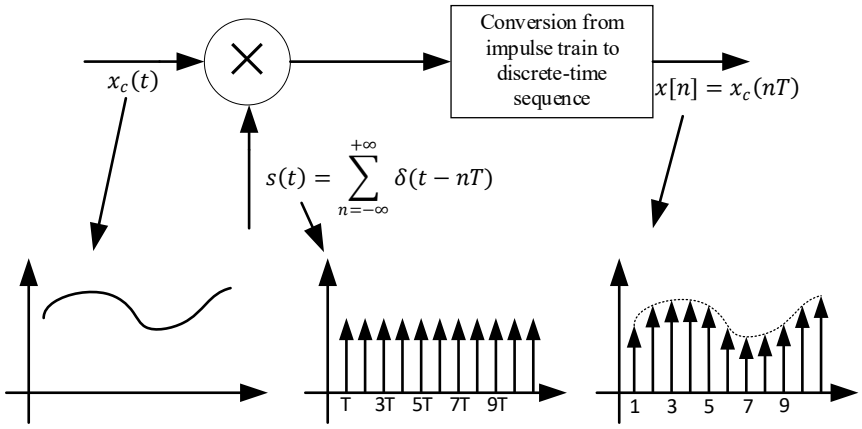

Figure 2-17 Principle of impulse sampling with sampling period T

In digital signal processing, up-sampling and down-sampling are operations changing sampling frequency after sampling. As their names suggest, the increasing sampling frequency is defined as up-sampling, and the decreasing sampling frequency is down-sampling. By comparing up-sampling and over-sampling, both of them are increasing sampling frequency. But the object of over-sampling is $x_c(t)$, and up-sampling is applied on $x(n)$ in Figure 2-17. For down-sampling, there is only one implementation method by keeping just one sample in every M samples and eliminating the rest samples, where M is the down-sampling ratio. Thus, the signal after down-sampling can be written as $x_d[n] = x[Mn] = x_c(nMT)$. On the other hand, the implementation of up-sampling is more complex than down-sampling since the original signal $x_c(t)$ is usually not available after sampling. One of the methods is padding $N - 1$ zeros between each sample then applying a low-pass filter with gain N and cutoff frequency π/N, where N is the up-sampling ratio. For NRZ signal, interpolation is the common method, i.e., by repeating each bit by N-1 times. One of the typical applications of up-sampling is jitter

simulation. Since the bit rate of NRZ in this thesis is only 10 Gbps, and the RMR of jitter is around a few picoseconds to tens of picoseconds, the time resolution of the original signal is not enough for simulation. Hence, there is an up-sampling operation before adding jitter.

2.2.2 Quantizing and coding

After sampling, the time of the signal is discrete, but the amplitude is still continuous. Quantization is a process of mapping the continuous amplitude set into a countable discrete set. And the device for quantization is a quantizer which is a nonlinear device. One-bit quantizing is the simplest one whose principle is a sign function, i.e., if the input value is greater than zero, the system will quantize it as bit "1". Otherwise, the system will map it as bit "0". This quantizer is usually designed for delta-sigma modulation, which will discuss later in detail. Another quantizing algorithm is uniform quantization. Figure 2-18 [29] (a) plots the principle of uniform quantization where Δ is quantizing step. It is uniform because the steps between each quantizing level are equal. After quantizing, the system needs a coding operation to transfer the quantized powers into bitstreams. Pulse coding modulation (PCM) is the common method for coding. One of the coding methods is uniform coding by direct transfer the power level into binary code. For example, the binary code in Figure 2-18 (a) is a uniform PCM based on American standard code for information interchange (ASCII). On the contrary, non-uniform PCM applies a technique called companding (compressing-expanding) [29]. This technique can get a high resolution for non-uniform distributed signal, i.e., a signal which exists a high probability for smaller amplitudes and a low probability for larger amplitudes, like the OFDM signal. There are two non-uniform PCM standards in the world including North American standard μ-law and A-law, which is European and Asian standard. Figure 2-18 (b) illustrates the characteristic of A-law at the first quadrant. It is shown that it involves more detail when the input amplitude is close to zero. Another coding method is pulse density modulation (PDM) which always works with delta-signa modulations.

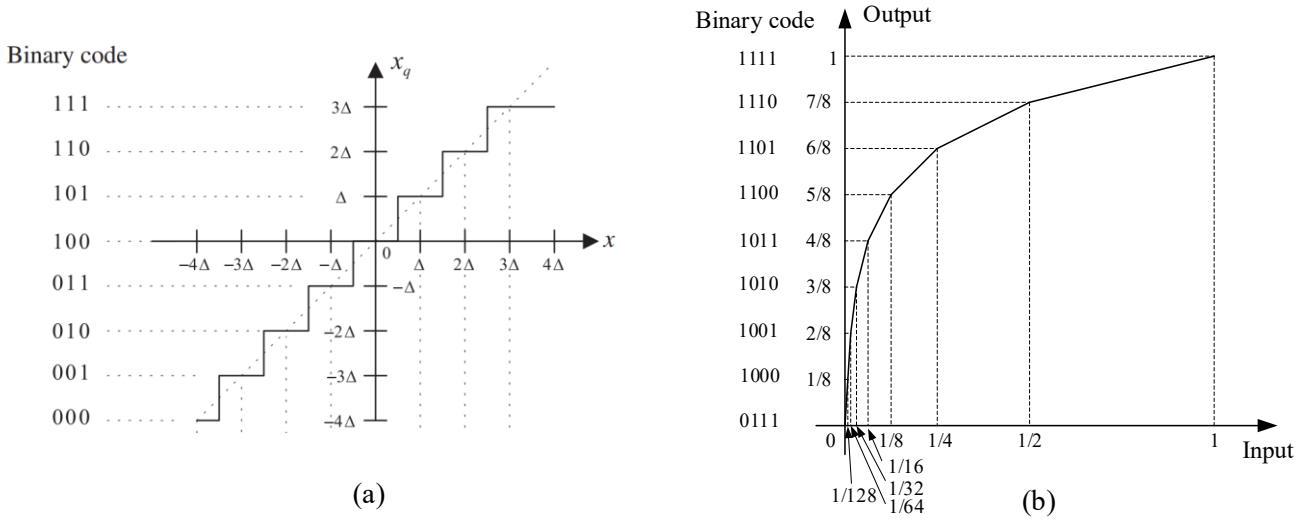

Figure 2-18 (a) uniform 3-bit quantization and (b) A-law non-uniform quantization and PCM.

2.3 Delta-sigma modulation

This section just gives a general introduction and current research topics of delta-sigma modulation. The block diagram and mathematical principles of delta-sigma modulation will discuss in chapter 3.

2.3.1 N-bits delta-sigma modulation

The delta-sigma modulation (DSM) is first presented in Japan by professor Y. Yasuda in 1960s [30]. It is a 3.5 bits DSM, i.e., there are $2^3 + 1 = 9$ power levels from -4 V to 4V, where 0.5 is a specially designed bit pattern for zero. At that time, the maximum sampling frequency of DSM is just 3 kHz because of the limitation of transistors. Thus, this technology is not applied in industrials, and most of research topics are theoretical. Nowadays, the main application of multi-bits DSM is delta-sigma ADC, and the purpose of DSM is shaping the quantizing noise to improve SNR. Support that there is a signal with bandwidth f_b sampled at Nyquist frequency and quantized by an N-bit quantizer, the PSD of quantizing noise is [31]

$$P(f) = \frac{1}{2^{N-1}\sqrt{12 f_b}} \tag{2.32}$$

One solution to control the quantizing noise is to increase the quantizing bit N, which is what conventional ADC does. For the delta-sigma ADC, it applies a negative feed-back loop with a loop filter

to shape the quantizing noise. Since the bandwidth of the loop filter is limited, the sampling frequency of delta-sigma ADC is always higher than Nyquist frequency, i.e., oversampling. Thus, the PSD of quantizing noise of delta-sigma ADC is

$$P(f) = \frac{1}{2^{N-1}\sqrt{12OSRf_b}} \cdot NTF(f) \tag{2.33}$$

where OSR is oversampling ratio, and NTF is noise transfer function. The principles of noise shaping will discuss in chapter 3, and NTF could be treated as a high-pass filer here.

2.3.1 One-bit delta-sigma modulation

One-bit DSM is first introduced in the late 1990s. The principles of one-bit DSM are similar with delta-sigma ADC by setting the quantizer bit equal to one, i.e., there is just one threshold. This makes sense in theory, but it requires a much higher sampling frequency than delta-sigma ADC. Until around 2010, the working frequency of DSM, which is implemented by complementary metal-oxide-semiconductor (CMOS), reaches 4 GHz [14] and [34]-[33], which can meet the requirement of LTE standards. This outcome makes the implementation of DSM become a popular topic. One implementation method is using CMOS very-large-scale integration (VLSI) technology [34]-[33]. Another method is using programmable IC, such as FPGA [35]-[38]. The advantage of FPGA based DSM is programmable, which means that it can use additional signal processing algorithms, such as digital pre-distortion (DPD), to enhance transmission performance and reliability. However, additional high-frequency clock sources, such as phase-locked loops (PLL), are required for FPGA to generate an RF signal. The last popular topic is amplifier design [39]-[41]. As discussed in section 2.1.4, conventional PAs cannot hold a power level for a long time, and the output of DSM is an NRZ signal. As a result, the output signal of DSM will suffer distortion if using conventional PAs. In RoF link, the fact is that the output power of the photodiode is too small for antenna systems. Thus, there should be a switching-mode power amplifier for the DSM signal.

2.4 Motivation and contributions

In all the previous works about DSM over RoF system, each work only focused on one structure of DSM, and there were no comprehensive comparisons between the three DSMs. In addition, harmonic noise in narrowband signals is negligible, and was not considered in envelope DSM. However, when a wideband signal is considered, harmonic noise becomes a main limiting factor in performance, which means that the impact of the harmonic noise must be studied. Moreover, high-order DSM systems are also ignored in most previous works. For example, some researchers use a very high sampling frequency (up to 100 GHz) to achieve high OSR. As a result, they avoid the problems of high-order loop filter design and system stability. But the cost of the whole system becomes unaffordable for industrial applications. Finally, an area hardly addressed in the literature is the detail of transmission performances in RoF links. Many papers only consider transmission performances with and without RoF links, but they do not discuss the effect of different parameters in RoF links, such as fiber dispersion, optical power, Kerr effect, and RF power amplifier. Therefore, it is necessary to conduct a comprehensive study of all typical DSMs in RoF transmissions.

In this thesis, three types of DSMs by MATLAB are studied, which are two bandpass DSMs and one envelope DSM. The studies include simulation and experimental verification. One of the main contributions of this work is to design high-order loop filters for DSMs under the condition of a limited sampling frequency. The different structures of loop filters, as well as their characteristics, are discussed based on theories and simulations. It is found that the Chebyshev-based loop filter is the best structure for wideband signals. Furthermore, another contribution of this work is to investigate optical transmission limitation for three DSMs, such as GVD, Kerr effect, and quantizing noise. It is found that the most straightforward DSM structure shows the best performance, and the simplest structure EDSM, which is also the best structure of narrowband signals, gets the worst results for wideband signals because of harmonic noise. The results of an all-digital structure are fair, but it can use up-sampling to enhance its performances. Based on the results, some new characteristics of DSMs are analyzed and demonstrated. This comprehensive study clearly classifies the structures and features of different types of DSMs, which can help our research team understand and directly use them in future research work.

Chapter 3 Theoretical analysis of delta-sigma modulation

This chapter discusses the principles of DSM in theory, including the noise shaping, delta-sigma modulators, and different type of delta-sigma modulations.

3.1 Noise shaping and delta-sigma modulator

Delta-sigma modulator (ΔΣ modulator) is the core unit of delta-sigma modulation (DSM), which has a negative feedback loop with a loop filter and a 1-bit quantizer in addition to an oversampling unit, as shown in Figure 3-1. The input signal of ΔΣ modulator could be any band-limited signal. For example, it could be a digital equivalent baseband signal, i.e., a non-modulated signal or a modulated RF signal. The output of the ΔΣ modulator is an NRZ form signal. NRZ form means the power level of signal is identical with NRZ signal, i.e., there are only two power levels, and the power levels do not return to zero at half bit period. However, the probability distribution of bit "0" and "1" is different with a perfect NRZ signal, i.e., the spectrum of this signal is different from the PSD of NRZ signals.

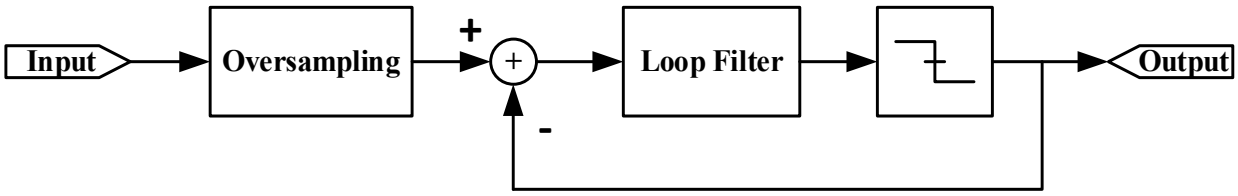

Figure 3-1 Block diagram of 1-bit delta-sigma modulator

Oversampling is the first step of ΔΣ modulator by setting the sampling frequency much higher than Nyquist frequency. The over-sampling ratio (OSR) of a lowpass input signal, e.g., non-modulated signal, is defined as

$$OSR_{LP} = \frac{f_s}{2f_{max}} = \frac{f_s}{BW} \tag{3.1}$$

where f_s is the sampling frequency, f_{max} is the maximum frequency of the input, and BW is the total bandwidth of the input signal. Since the spectrum of a non-modulated signal distributes around the Y-axis, see Figure 3-2 (a), the maximum frequency is just half of the signal bandwidth. For bandpass input signal, such as modulated signal shown in Figure 3-2 (b), the ORS is defined as [17]

$$OSR_{BP} = \frac{f_s}{2BW} \tag{3.2}$$

It is found that the center frequency f_c does not appear in the above formula. The reason is that the noise shaping system is only interested in the frequency component carried with information, and f_s/f_c could be any ratio if f_s is greater than Nyquist frequency. However, the f_s is always set as $4f_c$ to make the peak of the input signal located at the center of the whole spectrum in applications.

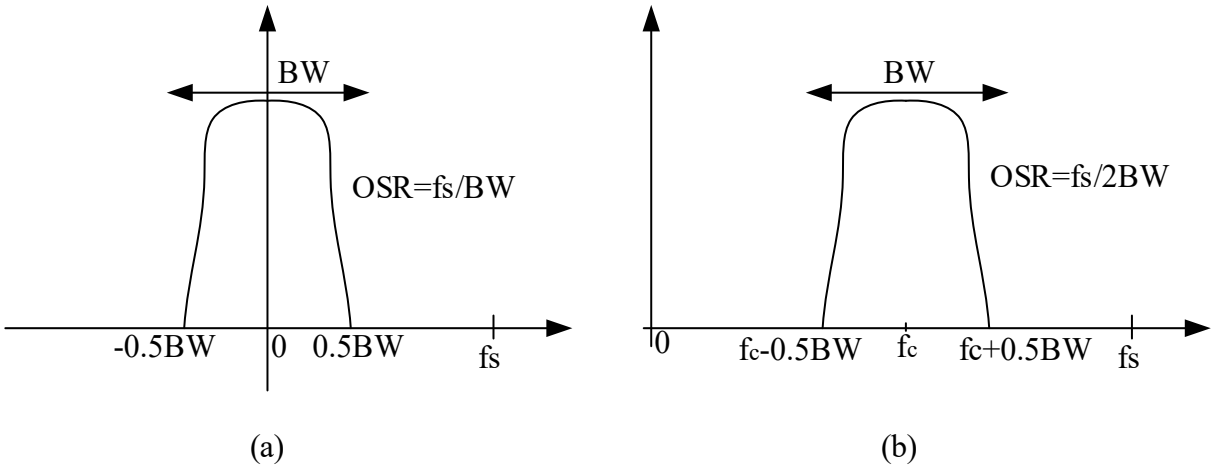

Figure 3-2 Spectrum of a (a) lowpass signal and (b) bandpass signal

3.1.1 Lowpass delta-sigma modulator

The feedback loop is the significant component of a ΔΣ modulator. Because the one-bit quantizer is a nonlinear device, i.e., a sign function in mathematics which does not meet the conditions of Fourier transformation, it is impossible to write the system function of the feedback loops directly. As discussed in section 2.3, the PSD of quantizing is same as white noise. Thus, the quantizer could be simplified as a mixer that adding the quantizing noise to the original signal, and the signal flow chat is plotted in Figure 3-3.

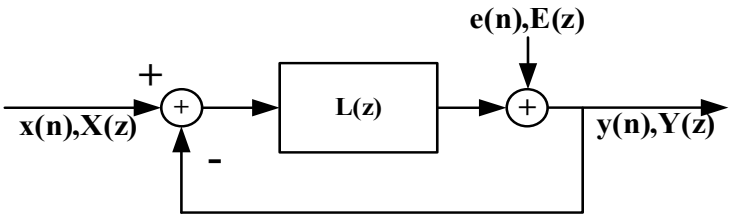

Figure 3-3 Signal flow chart of ΔΣ modulator

where $x(n)$ is sampled input signal, $e(n)$ is quantizing noise, and $y(n)$ is the output signal. $L(z)$ is the transfer function of the loop filter. $X(z), E(z)$, and $Y(z)$ are z-transforms of the above quantities. The relationship between them can be described by

$$\begin{aligned} Y(z) &= E(z) + L(z) \cdot [X(z) - Y(z)] \\ Y(z) &= \frac{L(z)}{1 + L(z)} \cdot X(z) + \frac{1}{1 + L(z)} \cdot E(z) \end{aligned} \tag{3.3}$$

Thus, the signal transfer function (STF) and noise transfer function (NTF) are given respectively by

$$\begin{aligned} STF(z) &= \frac{L(z)}{1 + L(z)} \\ NTF(z) &= \frac{1}{1 + L(z)} \end{aligned} \tag{3.4}$$

First, consider that the input signal is a non-modulated signal, i.e., a lowpass signal in frequency domain. By setting NTF as a highpass filter, the quantizing noise in the low-frequency range will be filtered out. At the same time, since $STF(z) + NTF(z) = 1$, the STF is a lowpass filter, and most of frequency components of input signal will be kept. Moreover, the PSD of quantizing is known as white noise. Hence, the system function of NTF is the PSD of shaped noise. Therefore, while designing the ΔΣ modulator, we always design NTF first instead of the loop filter. Finally, about the naming rule, the first adjunct is the order of feedback loops, which is equal to the order of the loop filter. The second adjunct is characteristic of frequency selection for input signal, i.e., lowpass or bandpass.

For example, one of ΔΣ modulators used in this thesis is shown in the following flow chart:

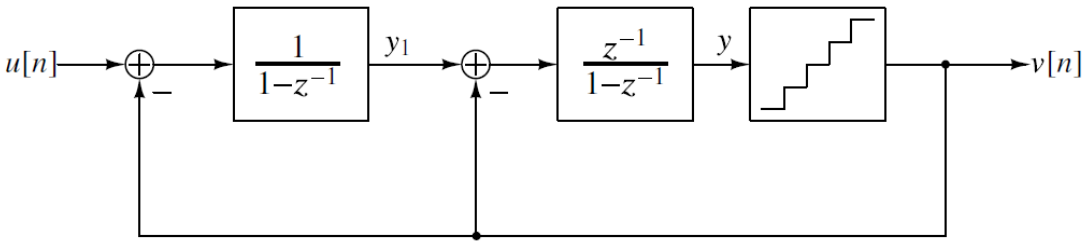

Figure 3-4 2nd order lowpass ΔΣ modulator

The NTF of this ΔΣ modulator is

$$NTF(z) = 1 - 2z^{-1} + z^{-2} \tag{3.5}$$

As Figure 3-5 (a) shown, the NTF is a highpass filter, which means that the quantizing noise at the low-

frequency range will be shaped. Moreover, most of the frequency components of the input signal are located at the low-frequency range. Thus, on the output side, there is only little quantizing noise mixed with the input signal. That is the principle of noise shaping in feedback loops. Furthermore, based on the naming rules, this feedback loop is named as 2nd order lowpass ΔΣ modulator. Finally, in Figure 3-5 (b), all of poles are located inside the unit circle, which proves that this NTF is stable. And all zeros are placed at point (1,0), which shows that this NTF is a Butterworth-based function.

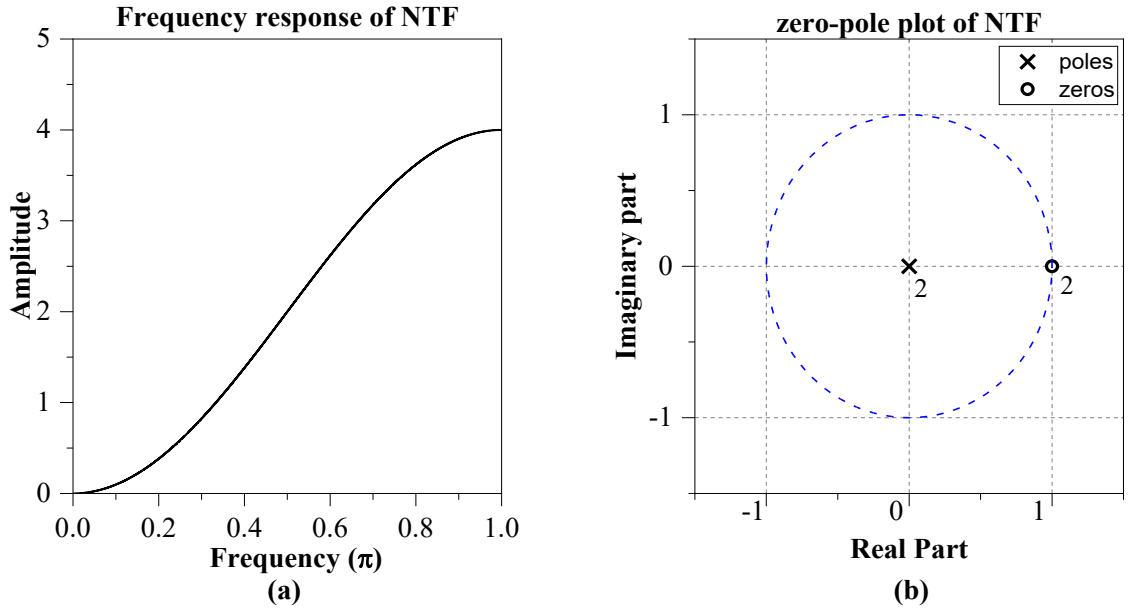

Figure 3-5 (a) Frequency response and (b) zero-pole plot of noise transfer function

3.1.2 Bandpass delta-sigma modulator

As discussed in section 3.1.1, the input signal of ΔΣ modulator in that section must be a lowpass signal because the stopband of NTF is located at the low-frequency range. This structure may still work for baseband transmission of voice channels since the Nyquist frequency of voice signal is just 48 kHz, and we have enough space for oversampling. However, for LTE signals, the center frequency is always around a few gigahertz. As a result, if lowpass ΔΣ modulators are used, there is a very high sampling frequency required to let the peak of LTE signal locate at low-frequency range in the spectrum, which is hard to implement. In order to solve this problem, the bandpass ΔΣ modulator is introduced.

Generally, there are two methods for bandpass NTF design. One is directly design based on a

bandpass filter which is always used in high order ΔΣ modulator and will be discussed in section 3.1.3. Another method is applying N-path transformation, i.e., let $z = -z^N$, [17] to a lowpass ΔΣ modulator. The principle of N-path transformation is that there are N solutions of Nth root of a complex number. i.e.,

$$\sqrt[n]{Ae^{j\varphi}} = \left(Ae^{j\varphi}\right)^{\frac{1}{n}} = A^{\frac{1}{n}} \cdot e^{j\frac{\varphi+2k\pi}{n}} \tag{3.6}$$

where $Ae^{j\varphi}$ is a complex number with amplitude A and phase φ, n is a positive integer, and $k = \{0,1,\cdots,n-1\}$. Thus, after using N-path transformation, there are interleaving N copies of the original system with alternating polarity on each of the path inputs and outputs, which realizes a transfer function $H'(z) = H(-z^N)$. Especially when $N = 2$, the copies of zeros and poles will locate near $z = j$ and $z = -j$ in the complex plane if the original zeros and poles are placed near $z = 1$. As shown in Figure 3-6 [17].

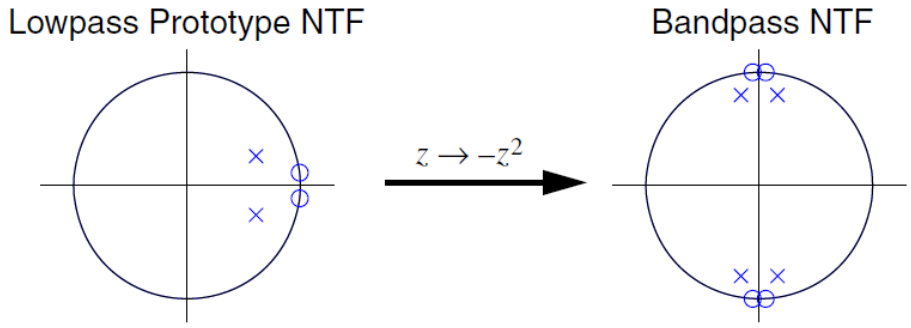

Figure 3-6 Applying a two-path transformation ($z \rightarrow -z^2$) to a lowpass NTF

For example, applying a two-path transformation to the ΔΣ modulator in Figure 3-4, it will become a bandpass ΔΣ modulator, which is used for a 20MHz signal in later simulations. It is shown that the frequency response of NTF becomes a bandstop filter in Figure 3-7 (a) because all of zeros is copied and placed at $z = j$ and $z = -j$, as shown in Figure 3-7 (b).

One of the problems for N-path transformation is that the passband for the input signal is always located at the center of the spectrum, i.e., $\omega = 0.5\pi$. Therefore, the sampling frequency f_s of oversampling operation must equal four times of center frequency of modulated signal f_c, i.e., $f_s = 4f_c$. Another disadvantage is that it will increase the order of loop filter by N times. This characteristic will affect the stability of feedback loops. Thus, N-path transformation does not work for high order ΔΣ

modulator design.

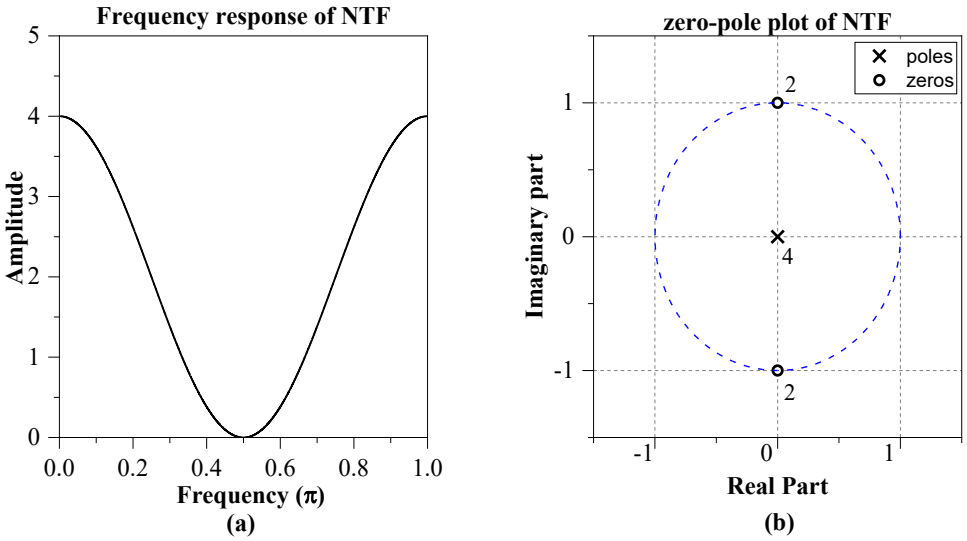

Figure 3-7 (a) Frequency response and (b) zero-pole plot of bandpass NTF using two-path transformation

3.1.3 High order delta-sigma modulator

All ΔΣ modulators introduced in the previous section are low order system, whose structure is just a series connection of first order ΔΣ modulators. One of their disadvantages is that the bandwidth is not wide enough for 5G signals, i.e., bandwidth up to 200MHz. For example, the bandwidth support of ΔΣ modulators in Figure 3-5 and Figure 3-7 is just 20MHz. Another problem for the series connection is stability. As Figure 3-5 and Figure 3-7 shown, the maximum value of NTF frequency response is 4, which means that the out of band noise will be amplified by four times. However, it is impossible to make this out of band gain less than one because of conservation of energy, i.e., noise shaping just moves the noise out of the signal band but does not remove noise. At the same time, it is better to keep the maximum value of NTF of ΔΣ modulator as less as possible for stability. As a result, a specially designed high order loop filter is required for a wider bandwidth input signal.

The process of high-order NTF design is similar to digital filter design. Here, we use the 6th ΔΣ modulator for a 200 MHz signal as example. First, we need a continuous-time filter as model, such as Butterworth filter and Chebyshev filter. The transfer function of high pass Butterworth filter is

$$H(j\omega) = 1 - \frac{1}{\sqrt{1 + \left(\frac{\omega}{\omega_c}\right)^{2n}}} \tag{3.7}$$

where ω_c is the cut-off frequency and n is the order of filter. And the transfer function of high pass Chebyshev filter is

$$H(j\omega) = 1 - \frac{1}{\sqrt{1 + \varepsilon^2 T_n^2\left(\frac{\omega}{\omega_c}\right)}} \tag{3.8}$$

where ε is the ripple factor and $T_n(x)$ is Chebyshev polynomials. Please notice that all Chebyshev filters used in this thesis are Chebyshev type I. Chebyshev type II filters are not selected because it does not roll off as fast as Type I.

By comparing the frequency response of Butterworth filter (a) to Chebyshev filter (b) in Figure 3-8 with the same cut-off frequency 0.5π, it is found that Chebyshev filter does not as good as Butterworth filter in one and two orders. That is why all NTFs in Figure 3-5 and Figure 3-7 are Butterworth-based. Additionally, the transition band of Chebyshev filters is narrow than Butterworth filters in four and six orders. This characteristic makes high order Chebyshev-based NTF works better than Butterworth because high order Chebyshev-based NTF can achieve wider bandwidth than Butterworth-based NTF. On the contrary, the stopband of Chebyshev filters is not flatness which causes additional noise mixed with the transmitted signal. Overall, a Butterworth based NTFs are much suitable for low order ΔΣ modulator (i.e., 1 and 2 order), and Chebyshev based NTF always works for high order ΔΣ modulator (higher than 6 order). Four order is a middle-order because the overall performance of Butterworth and Chebyshev NTFs are similar.

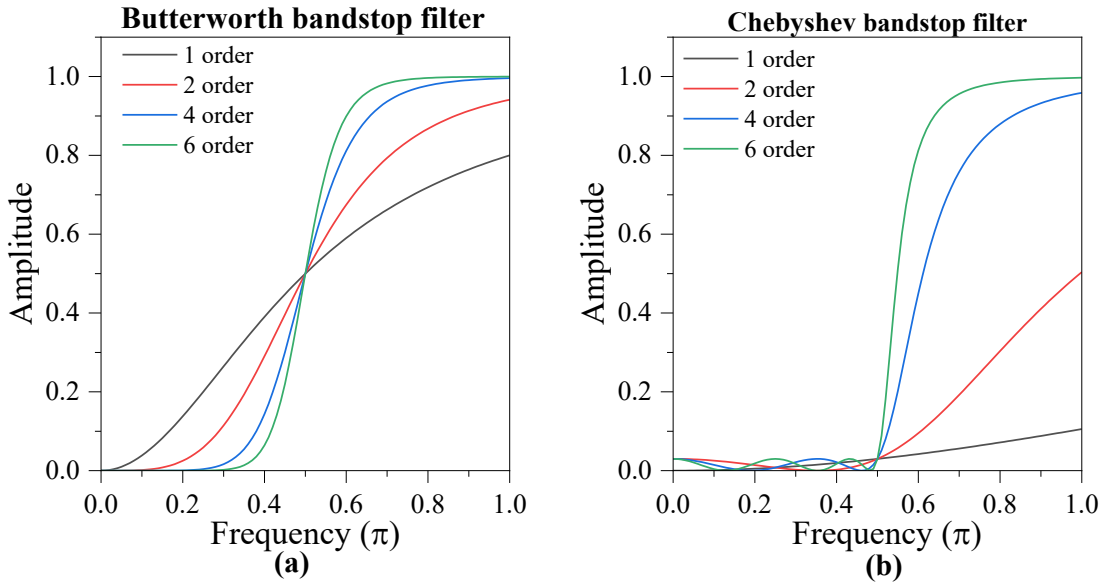

Figure 3-8 frequency response of (a) Butterworth filter and (b) Chebyshev filter with different order

After choosing the model of NTF, i.e., Butterworth-based or Chebyshev-based, the next step is transferring the continuous-time transfer function to a discrete system function. Generally, there are two types of digital filter structure, finite impulse response (FIR) filter and infinite impulse response (IIR). FIR filter is always used to achieve linear phase, and the application in this thesis is the received filter. The technique for IIR filter design in this thesis is bilinear transformation since another common method, impulse invariance only works for lowpass and bandpass filter. The principle of bilinear transformation is the mapping between s-plane and z-plane. With $H_c(s)$ denoting the continuous-time system function and $H(z)$ for discrete-time system function, the bilinear transformation corresponds to replace *s* by [28]

$$s = \frac{2}{T}\left(\frac{1-z^{-1}}{1+z^{-1}}\right) \tag{3.9}$$

where *T* is the sampling period. While using frequency, known that $s = j\Omega$ and $z = e^{j\omega}$, where Ω is the continuous frequency and ω is the discrete frequency, the mapping of frequency response between continuous-time to discrete-time is given by

$$\omega = 2arctan\left(\frac{\Omega T}{2}\right) \tag{3.10}$$

With these two steps, we get a high-order NTF based on a classical filter model. For example, NTF

of the 6 order lowpass ΔΣ modulator used in this thesis is

$$NTF(z) = \frac{\sum_{i=0}^{6} b_i z^{-i}}{\sum_{i=0}^{6} a_i z^{-i}} \tag{3.11}$$
$$b[n] = [1, -5.963, 14.852, -19.779, 14.852, -5.963, 1]$$
$$a[n] = [1, -5.441, 12.390, -15.109, 10.407, -3.837, 0.592]$$

where $a[n]$ and $b[n]$ are defined as the coefficient matrix of polynomials of the transfer function. In the rest of part, we will only use coefficient matrix to describe a polynomial. The frequency response of NTF is shown in Figure 3-9 (a). The sampling frequency of this ΔΣ modulator is set as 5 GHz in simulation. Thus, the bandwidth of this NTF, i.e., the stopband of bandstop filter in Figure 3-9 (a), is about $0.05 \times 5\ GHz = 250MHz$, which is wider enough for a 200MHz input signal. In Figure 3-9 (b), all zeros distribute around point (1,0), which causes the non-flatness stopband of NTF. That is a typical characteristic of Chebyshev-based NTF. This property provides a narrow transition band to NTF to achieve wider bandwidth. However, it also leads up to the non-flatness stopband.

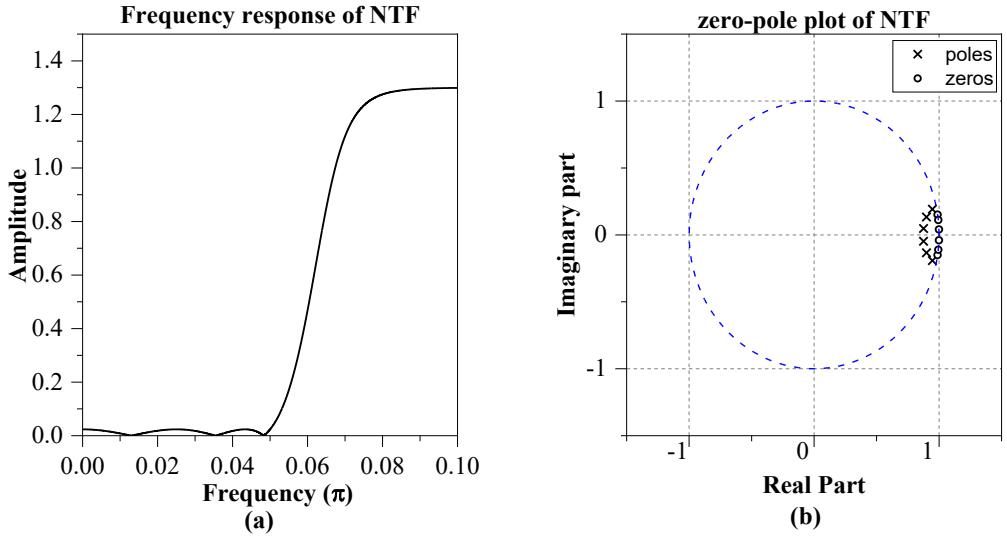

Figure 3-9 (a) frequency response and (b) zero-pole plot of a Chebyshev based NTF for 6 order lowpass ΔΣ modulator

Figure 3-10 provides the frequency response and zero-pole plot of NTF of bandpass ΔΣ modulator. The coefficient matrixes are

$$b[n] = [1, -1.332 \times 10^{-15}, 2.995, -2.803 \times 10^{-15}, 2.995, 1.464 \times 10^{-15}, 1] \tag{3.12}$$
$$a[n] = [1, -1.776 \times 10^{-15}, 2.805, -3.109 \times 10^{-15}, 2.633, 1.369 \times 10^{-15}, 0.826]$$

First, it is shown that the center of the stopband for quantizing noise is located at 0.5π. Therefore, the peak of the input signal in frequency domain must be located at 0.5π by setting the sampling frequency equal to four times of carrier frequency, i.e., 10 GHz in simulation. Moreover, the bandwidth of NTF is $0.023 \times 10\ \text{GHz} = 230\ \text{MHz}$, which is enough for a 200 MHz signal. Finally, the zeros and poles are distributed around $z = j$ and $z = -j$, and they are symmetric about both real axis and imaginary axis. The symmetry about the real axis is mandatory because there is a copy in the spectrum at range $[\pi, 2\pi]$ (or $[-\pi, 0]$, $(-\infty, 0]$ for continuous-time signal spectrum). The symmetry about the imaginary axis is optional, but it can improve the stability of feedback loops for high-order ΔΣ modulators.

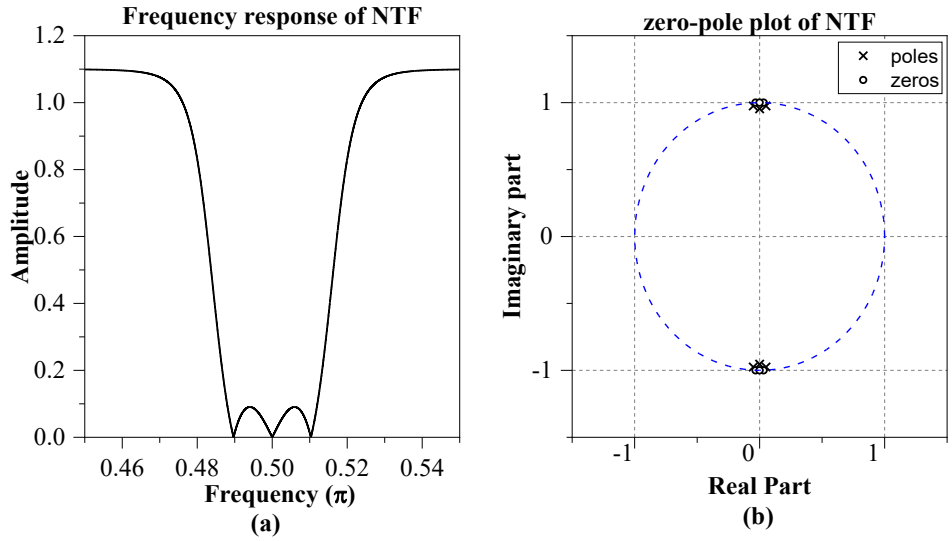

Figure 3-10 (a) frequency response and (b) zero-pole plot of a Chebyshev based NTF for 6 order bandpass ΔΣ modulator

3.1.4 Stability of delta-sigma modulator

This section discusses the stability of feedback loops of ΔΣ modulators, including independent stability and signal-dependent stability. Unfortunately, there is no necessary and sufficient condition of stability for ΔΣ modulator, and all conditions discussed in this section are approximate criteria. The stability of a system is defined by [28]:

"A system is stable in the bounded-input, bounded-output sense if and only if every bounded input sequence produces a bounded output sequence."

However, since the ΔΣ modulator is a nonlinear system (quantizer is a nonlinear device), it is hard

to provide a condition related to system function and stability. The widely used approximate criterion is the modified Lee's rule [17][42][43] that a 1-bit ΔΣ modulator is likely to be stable if

$$\max(\left\|\mathrm{NTF}\left(e^{j\omega}\right)\right\|) < 1.5 \tag{3.13}$$

where $\|\cdot\|$ represents the Euclidean norm of a complex variable function. The original limitation of Lee's rule is 2 [42], but [17] modifies it as 1.5 for high order ΔΣ modulator, and the experiment in [43] can also prove it. Nevertheless, Lee's rule is still not a perfect condition, and it can only work as a reference for high order NTF design. For example, the maximum value of NTF for 2nd order ΔΣ modulator in Figure 3-5 and Figure 3-7 do not meet Lee's rule, but both of them can work stable in simulation. As a result, simulation is the best method to evaluate the stability of systems.

The stability of the ΔΣ modulator also depends on the input signal, called signal-dependent stability [17]. The input signal will also affect the system stability because it may cause the overdriven of the 1-bit quantizer, i.e., there are many continuous bits one (or bits zero) output from the quantizer. This phenomenon always happens at the peak of input signal in time domain, especially for the OFDM signal because it has a very high peak to average ratio. Figure 3-11 provides an example of instability because of the input signal. The input signal is the real part of a 200 MHz non-modulated OFDM signal whose amplitude is normalized, i.e., the maximum amplitude is limited at [-1, 1], and the loop filter is shown in Figure 3-9. The input signal and signal before the quantizer are measured by a real-time oscilloscope in MATLAB. It is clearly found that when the input signal reaches the peak in time domain, the output of the loop filter suffers an oscillation whose amplitude reaches 10^5. To avoid signal-dependent instability, one of possible solutions is adding an attenuator before feedback loops.

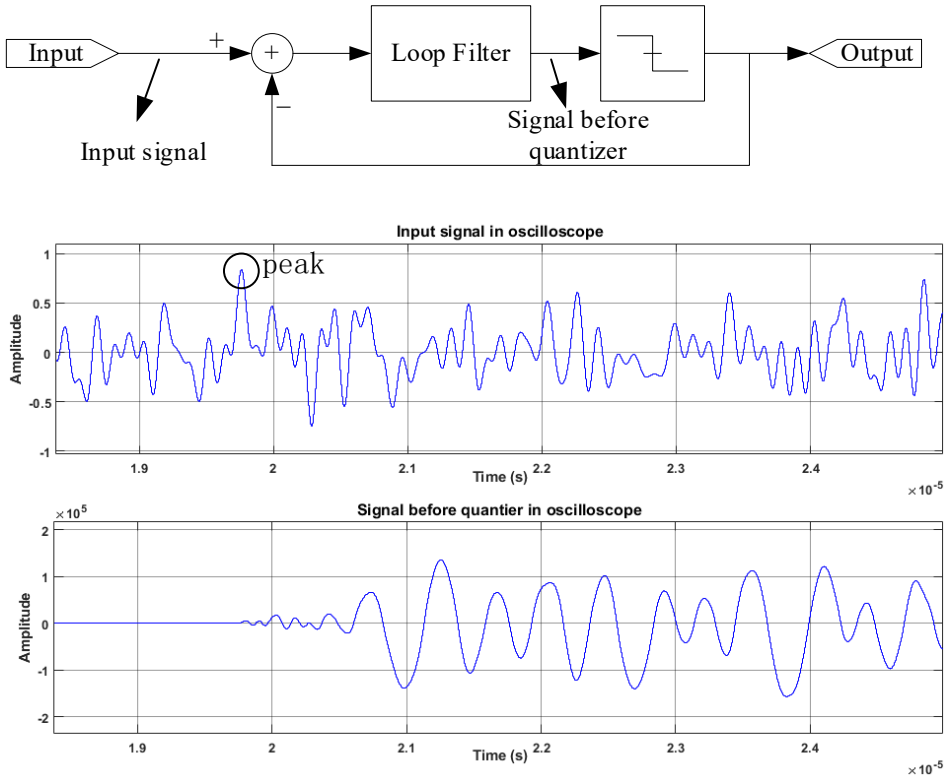

Figure 3-11 An example of signal-dependent instability.

3.2 Pulse density modulation and demodulation

3.2.1 Pulse density modulation

Similar to PCM, pulse density modulation (PDM) is also a form of modulation used to represent an analog signal with a binary signal. For the PDM signal, the amplitude value of original signal is relative to the density of binary pulses. A PCM signal is always generated by a conventional ADC, i.e., a PCM encoder directly transfers the quantized value into a binary bitstream. Figure 3-12 (a) provides an example of PCM signal. It is generated by a sinusoid sampled at 4 times of Nyquist frequency and quantized by an 8-bits ADC. Generally, it is hard to find the pattern without a decoder, and there must be a DAC to recover it to a sinusoid. On the other hand, as shown in Figure 3-12 (b), a PDM signal is generated by a ΔΣ modulator with OSR=32 to make it have the same resolution as the PCM signal in Figure 3-12 (a). It is clear that the density of pulses is high when the amplitude of the input signal is around zero. At the same time, the density of pulses becomes sparse when the amplitude is close to the

peak.

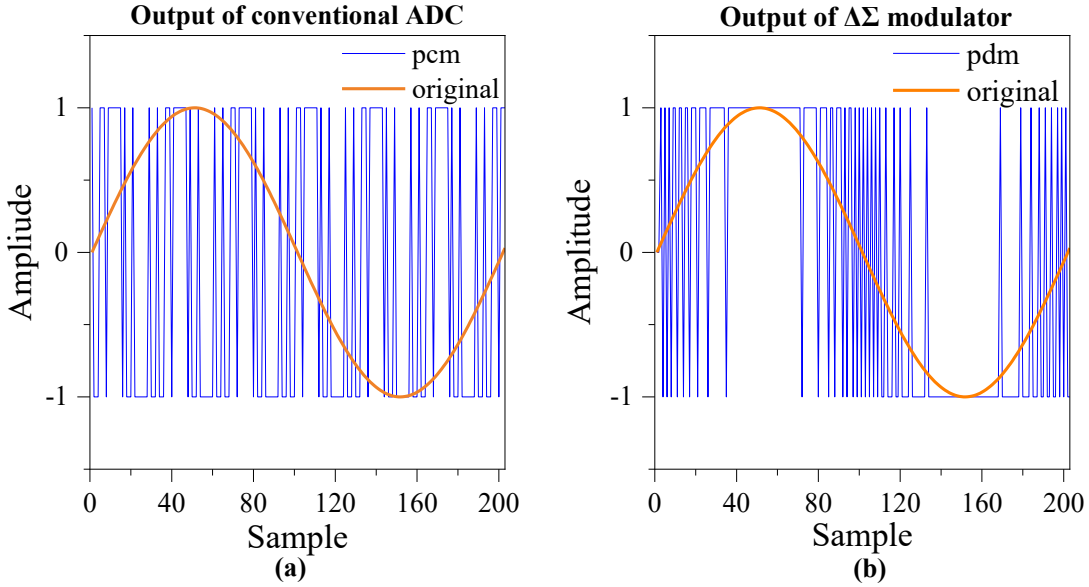

Figure 3-12 Comparison of (a) PCM signal and (b) PDM signal in NRZ form with same original signals.

3.2.2 Demodulation of delta-sigma modulator

In Figure 3-12 (b), it is hard to find the bit pattern of the PDM signal in time domain. In fact, the demodulation of PDM happens in frequency domain instead of time domain. Based on the system function of ΔΣ modulator discussed in section 3.1.1, the output signal of ΔΣ modulator could be written as

$$Y(z) = STF(z) \cdot X(z) + NTF(z) \cdot E(z) \tag{3.14}$$

where $Y(z)$, $X(z)$, and $E(z)$ are output signal, input signal, and quantizing noise in frequency domain. Support that we have a filter function $F(z)$ which is matched with input signal $X(z)$, i.e., $F(z)$ is a lowpass filter if $X(z)$ is a lowpass signal, $F(z)$ is a bandpass filter if $X(z)$ is a bandpass signal, and their bandwidth is also matched. Thus, after applying this filter to $Y(z)$, we have recovered signal

$$R(z) = Y(z)F(z) = STF(z)F(z)X(z) + NTF(z)F(z)E(z) \tag{3.15}$$

Since $NTF(z)$ is a bandstop filter and $F(z)$ is a bandpass filter, and they have same bandwidth, $NTF(z)F(z) \approx 0$. So, the quantizing noise is filtered out by the received filter. Thus,

$$R(z) = STF(z)F(z)X(z) \tag{3.16}$$

Because $STF(z)$ and $F(z)$ are matched with input signal $X(z)$, only a few of noise will be introduced

by the filter. In AD/DA technology, this noise is defined as the internal noise of systems. Therefore, the recovered signal could be given by

$$R(z) = X(z) + \text{Internal noise} \tag{3.17}$$

And $F(z)$ is defined as the recover filter of ΔΣ modulator.

Figure 3-13 illustrates the PSD of the signal shown in Figure 3-12 (b). It is found that the peak of the input signal overlapped with the PDM signal, and the quantizing noise is shaped out of the peak. The normalized frequency is given by logarithm based 10 to provide more details in the peak range. Therefore, after applying a lowpass filter, the original sinusoid could be recovered from the PDM signal.

Finally, about the recover filter, it is impossible to design an ideal filter in applications. The solution in this thesis is to design a high-order FIR filter whose bandwidth is wider than the signal bandwidth. This could make the passband of the filter close to an ideal filter. Next, we design a phase equalizer to get a constant phase shift. Since the FIR filter can achieve a linear phase, it is not difficult for phase equalizer design.

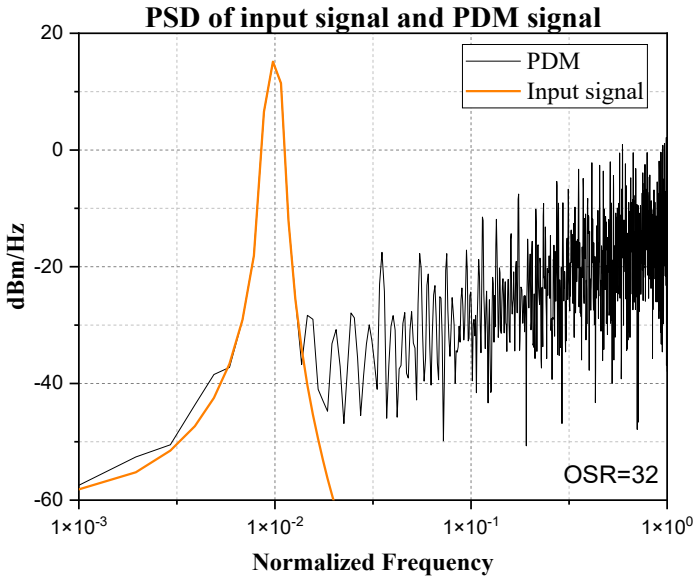

Figure 3-13 Power spectral density of signals in Figure 3-12 (b).

3.3 Type I bandpass delta-sigma modulation

Section 3.1 and 3.2 propose the structures and principles of ΔΣ modulator, which is the core of

delta-sigma modulation (DSM). The delta-sigma modulation is defined as the process that transfers the signal from digital equivalent baseband to RF. It usually includes one or more ΔΣ modulator(s), upconvert(s) and additional signal processing units. Finally, the oversampling in ΔΣ modulators will be simplified by directly giving the sampling frequency in the block diagram of DSMs.

3.3.1 Structure and analysis

There are three types of DSMs. Figure 3-14 shows a conventional bandpass 1-bit DSM, i.e., Type-I called in this thesis [17]. Note that all digital basebands in the block diagrams mean digital equivalent baseband, which has been discussed in section 2.1.1. First, the digital baseband signal is upconverted to in-phase and quadrature (I/Q) band-limited RF signal with an analog sinusoid as the RF carriers. Thus, the signal after upconverter and before ΔΣ modulator, i.e., positions (a) in Figure 3-14, is an analog RF signal given by

$$\begin{aligned} s_a(t) &= I \cdot \cos(2\pi f_c t) + Q \cdot \sin(2\pi f_c t) \\ &= A \cdot cos(2\pi f_c t + \varphi) \end{aligned} \tag{3.18}$$

where I and Q are the in-phase and quadrature parts of the equivalent baseband signal, A is amplitude, and φ is the phase of baseband signal, and f_c is the center frequency of the carrier, which is set as 2.5 GHz in this thesis. Obviously, the spectrum properties of $s_a(t)$ is a peak located at f_c whose bandwidth is equal to baseband bandwidth. Therefore, the analog RF signal is sampled and converted to an NRZ form signal by a 1-bit bandpass ΔΣ modulator, as discussed in section 3.1.2, in which the oversampling frequency f_s of $4f_c$ is used. It is known that the system function of a ΔΣ modulator is

$$Y(z) = STF(z) \cdot X(z) + NTF(z) \cdot E(z) \tag{3.19}$$

Because the STF does not affect the input signal in the determined bandwidth range, we can simplify it as

$$output = input + noise \tag{3.20}$$

where *noise* means out of band quantizing noise. Hence, the digitized RF signal in NRZ form could be described by $A\cos(2\pi f_c t + \theta) + noise$.

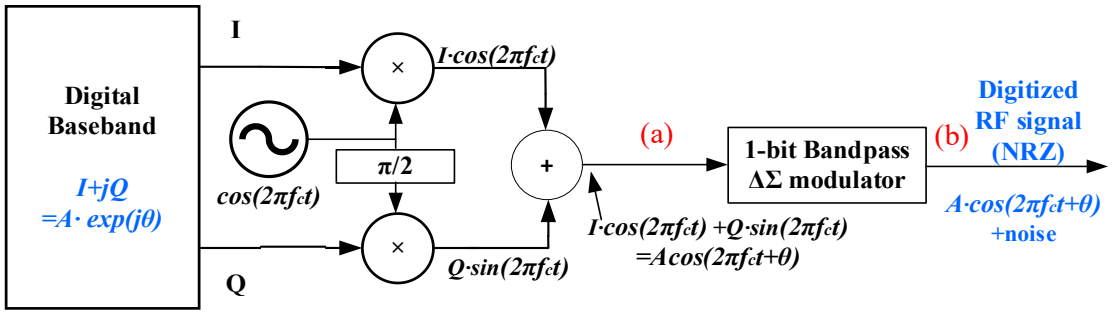

Figure 3-14 Block diagram of a bandpass 1-bit DSM (Type I). f_c is carrier frequency. Noise means quantizing noise. The signal at the positions of a and b will be illustrated in simulation chapter.

3.3.2 Typical applications

Overall, bandpass type I DSM is a mixed-signal system. First, the I/Q upconverter is absolutely an analog device because it uses analog sinusoids as carriers. At the same time, the bandpass ΔΣ modulator is a digital system since there is a sampling operation. This structure is also named as "discrete-time system processes continuous-time signal" in [28]. In this thesis, we treat the I/Q upconverter and ΔΣ modulator together as one system. In fact, they can be broken down and regroup to adapt to different modulation methods. For example, by changing the I/Q upconverter to a frequency modulator, this structure can still work by redesigning the loop filter because the spectrum of an FM signal is still a bandpass signal. Therefore, bandpass type I DSM is potential to adapt some point-to-point transmission systems.

Another typical application for bandpass type I DSM is multi-band modulation [44][45]. It is known that the ΔΣ modulator is a nonlinear system because it does not meet the law of additivity, i.e., the summation of digitized RF signals is not an NRZ form anymore. In other words, we cannot apply FDM after DSM in electric domain. One of the solutions is moving FDM to digital baseband, which is also the solution used in this work. Another solution is setting the FDM between upconverter and bandpass ΔΣ modulator. For example, the author team in [44] design a dual-band NTF shown in Figure 3-15. With this ΔΣ modulator, two signal bands are modulated at 1.923 GHz and 2.076 GHz with 5 MHz bandwidth for each band. However, this system, i.e., dual-band bandpass type I DSM, is limited by the signal bandwidth and separation between each signal band. Thus, this structure can only be applied for narrow bandwidth signals.

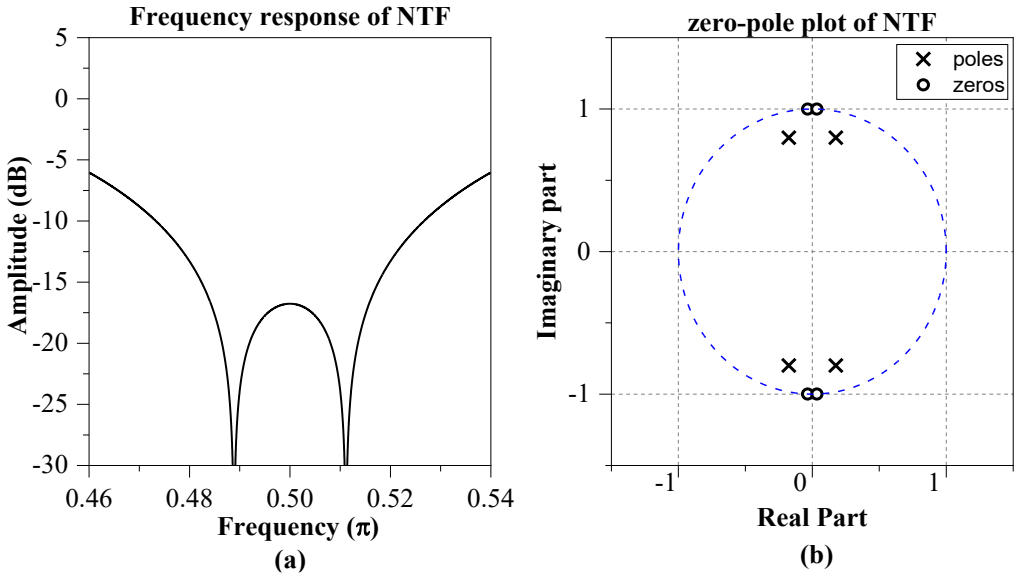

Figure 3-15 Configuration of a dual-band NTF with (a) frequency and (b) zero-pole plot in [44]

3.4 Type II bandpass delta-sigma modulation

3.4.1 Structure and analysis

Figure 3-16 shows the other bandpass DSM [13], and we name it as bandpass DSM Type-II, which can be used only for orthogonal modulated signals. The baseband signal is first divided into in-phase and quadrature parts. Then they are oversampled with an oversampling frequency of $f_s = 2f_c$, where f_c is the carrier frequency, and f_c of 2.5 GHz is used. Next, each of the I and Q signal is digitized by each 1-bit lowpass ΔΣ modulator. Because bandpass DSM Type-II uses lowpass ΔΣ modulators, the sampling frequency of ΔΣ modulators just need half of sampling frequency Type-I to achieve same OSR (see the definition of OSR in section 3.1). However, since the I and Q signals have been already digitized, and we want the final output of the system also to be digitized, an analog sinusoid can not be applied as the carrier in bandpass DSM Type-II. Therefore, a digital carrier at a central frequency f_c, the pulses of which are corresponding to four points of a sinusoidal period $T=1/f_c$, is used to upconvert the baseband I/Q signal to an RF signal. The principle of digital carrier is shown in Figure 3-17. It is a sampled sinusoid with $f_s = 4f_c$, i.e., there are 4 samples in each period, and the samples are located at $t = 0, t = T/4, t = T/2,$ and $t = 3T/4$.

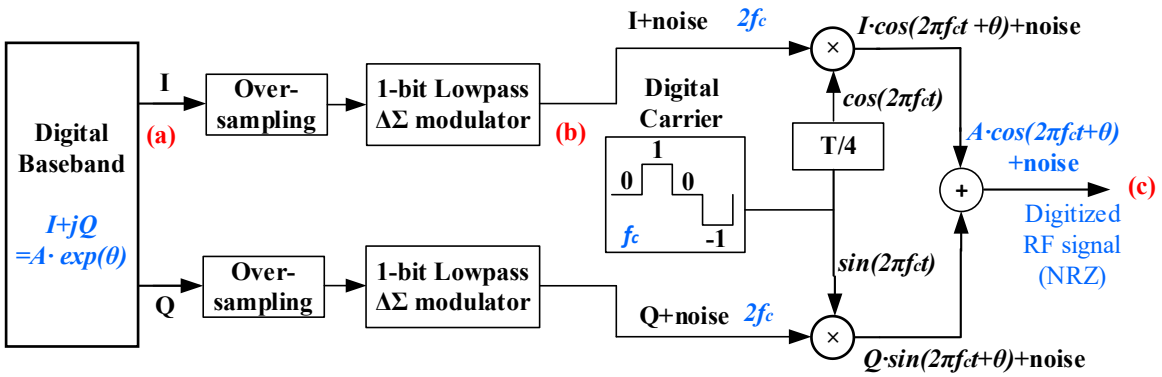

Figure 3-16 Block diagram of a bandpass DSM (Type II). f_c is carrier frequency, and $T=1/f_c$ is the period of digital carrier. Noise means quantizing noise.

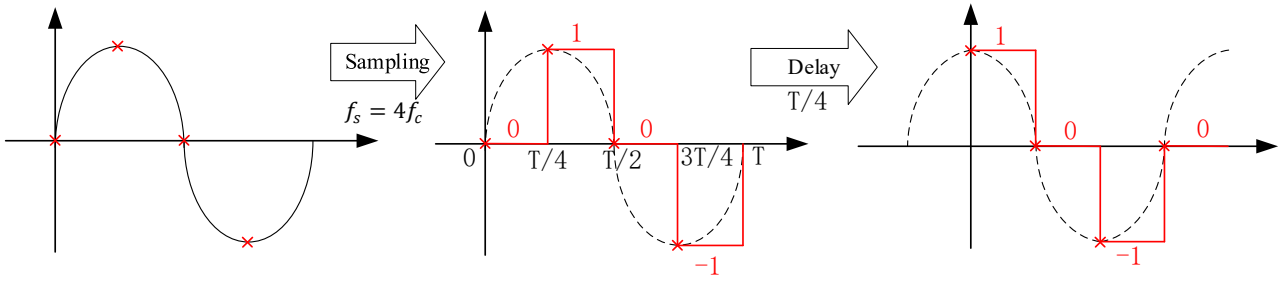

Figure 3-17 Principle of digital carrier. f_c is carrier frequency and f_s is sampling frequency.

Compared to the DSM Type-I, the lowpass ΔΣ modulator in the DSM Type-II only needs $2f_c$ to achieve the same OSR as the bandpass ΔΣ modulator. Since the sampling frequency of the digital carrier must be $4f_c$, the digitized RF signal is sampled with $4f_c$, which is the same as the DSM Type-I. In fact, the sampling frequency of ΔΣ modulator in the DSM Type-II could be set as $1/N$ times of final sampling frequency, i.e., $4f_c$, where N is a positive integer [44]. $2f_c$ is selected as sampling frequency in this thesis because we want the same OSR of DSM Type-I and Type-II for a fair comparison.

3.4.2 Bandwidth expansion effect

One of the problems for DSM Type-II is that the spectrum of digital carriers is not an ideal impulse function. Since the digital carrier is a periodic rectangular waveform instead of a sinusoid, the bandwidth of the digital carrier is not zero or negligible. In Figure 3-18, overall, the digital carrier is an impulse in frequency, but its bandwidth is about 1 MHz. In the LTE standard, the frequency offset of conventional

sinusoid carriers must be less than $\pm 25\ ppm\ (25 \times 10^{-6})$ times of center frequency [21]. If this carrier multiplies with a non-modulated signal, i.e., the signal after ΔΣ modulator in Figure 3-17, the bandwidth of the result will be wider than the input signal. For example, if the bandwidth set up in the digital baseband is 200 MHz, the bandwidth of the final digitized RF signal will be about 250 MHz.

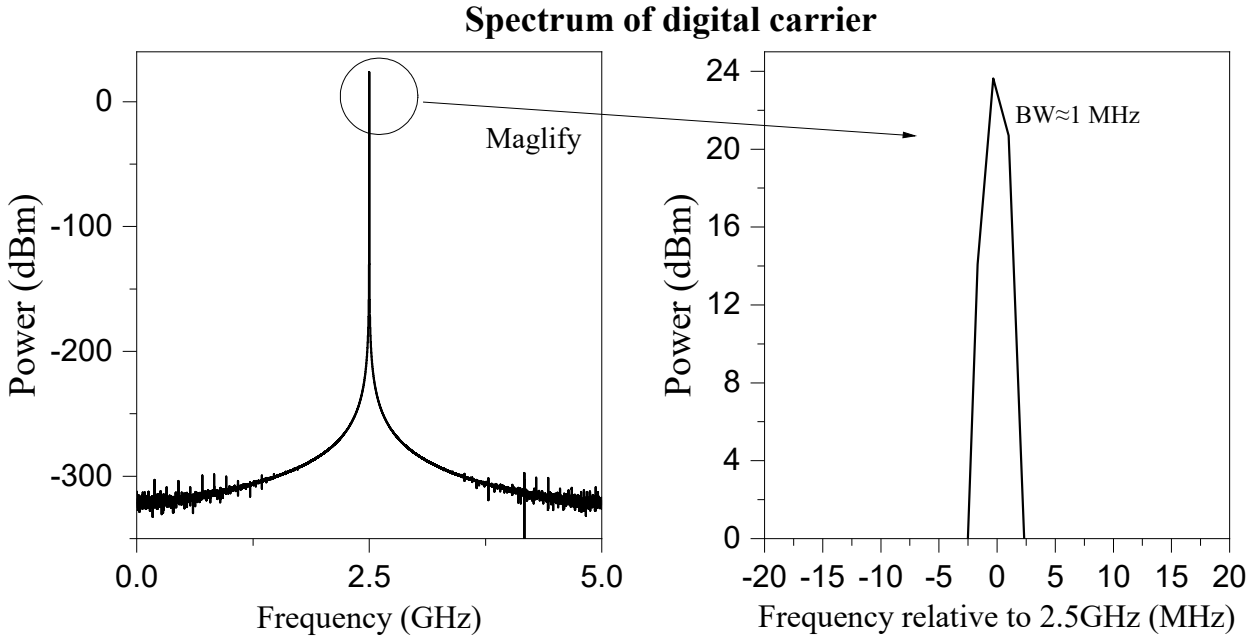

Figure 3-18 The spectrum of digital carriers.

3.4.3 Typical applications

Based on Figure 3-16, all devices used in bandpass DSM Type-II are digital (or discrete-time). Thus, DSM Type-II is an all-digital system, and the whole system can be implemented by FPGA directly. Of course, it can also be implemented by CMOS integrated circuit (IC). However, in that case, there is additional clock sources required to make synchronization between I and Q branches.

Moreover, the DSM Type II is an all-digital system, so that up-sampling (interpolation) can be easily used to equalize a lower bit rate of the digitized RF signal after the DSM [28]. Thus, the transmission induced penalty due to the high bit rate can be reduced. For 1-bit signal, up-sampling is to repeat and pad each bit by N-1 times, where N is the up-sampling ratio, e.g., “0101” becomes “00110011” by an up-sampling ratio of 2. Note that the transmitted bit sequence length is increased by N times, and therefore

system transmission efficiency is reduced by N times. In that case, we need to treat the output of DSM as a bit frame. Since the size of the bit sequence increase by N time but the bit rate setup in fiber transmission does not change, the pulse width of NRZ signal transmitted in fiber expands N times, as shown in Figure 3-19. It just like reduce the bit rate by N times. Since the dispersion in fiber is relative to pulse width, it could reduce the waveform distortion caused by the GVD impact. Note that the bit rate reduction is just an equivalent. The real bit rate does not change and what is reduced is the efficiency.

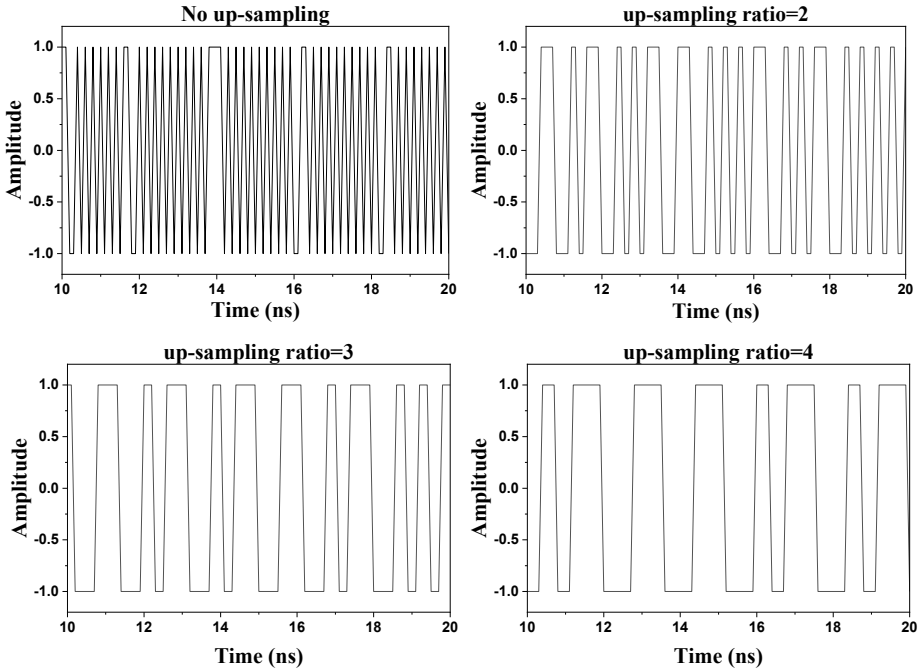

Figure 3-19 Waveform transmitted in fiber with different up-sampling ratios.

3.5 Envelope delta-sigma modulation

3.5.1 Structure and analysis

Figure 3-20 shows the structure of envelope delta-sigma modulation (EDSM) [17]. As discussed in section 2.1.1, an orthogonal modulated signal in the baseband can be divided into the envelope and phase parts. For the phase branch, the phase signal is first modulated by a standard I/Q modulator using analog sinusoids as carriers with frequency f_c. Thus, the signal before *sign(x)* in Figure 3-20 is a standard phase modulation (PM) signal with constant envelope. And it can be digitized by a 1-bit quantizer, i.e., *sign(x)*

in Figure 3-20, directly without generating in-band quantizing noise [17]. However, the quantizing noise will become harmonics, as shown in Figure 3-21. It is found that the main lobe of PM signal, the signal before *sign(x)* in Figure 3-20, is absolutely overlapped with the fundamental frequency component in 1-bit PM signal, i.e., the signal after *sign(x)*, and there are odd-order harmonics in the spectrum of 1-bit PM signal. In the envelope branch, since the spectrum of an envelope signal is lowpass, it could be oversampled and digitalized by a lowpass ΔΣ modulator. After both envelope and phase signals are digitalized, the system multiplies them together, and a digitized RF signal in NRZ format is created. Additionally, because the envelope and phase signal are NRZ format before multiplication, this operation can be implemented by an "AND" gate instead of an RF mixer. In that case, the EDSM requires unipolar NRZ, i.e., 0 and 1 instead of -1 and 1, because most of the common logic gates do not accept negative power.

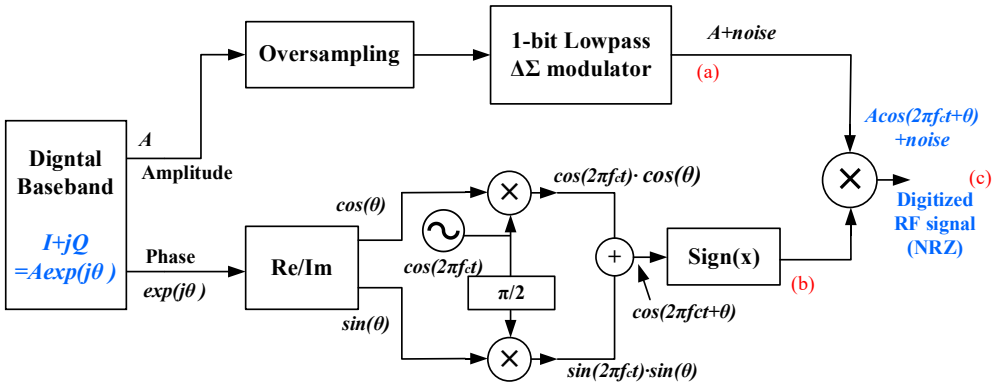

Figure 3-20 Block diagram of envelope DSM. f_c is carrier frequency. Noise means quantizing noise.

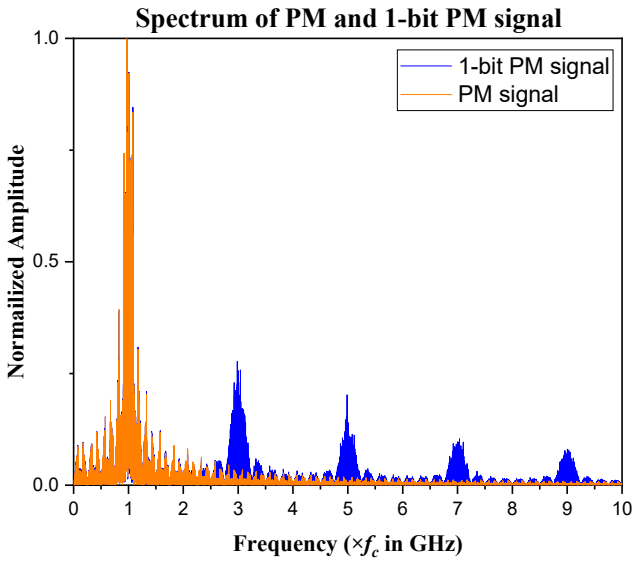

Figure 3-21 Spectrum of PM and 1-bit PM signal. f_c is carrier frequency and f_c=2.5 GHz

3.5.2 Harmonic effect

In the phase branch, the PM signal is a perfect sinusoid at one symbol period. To simplify the mathematics analysis, we set the phase θ as zero. Assumed the original PM signal is $Acos(2\pi f_c t)$, and the signal after sign quantizer is a bipolar NRZ rectangular pulse called *x(t)* with amplitude=A, Period = T = $1/f_c$ and duty cycle = 50%.

$$x(t) = \begin{cases} A, & 0 < t \leq \dfrac{T}{2} \\ -A, & -\dfrac{T}{2} < t \leq 0 \end{cases}, \qquad -\frac{T}{2} < t < \frac{T}{2} \tag{3.21}$$

Then apply the Fourier series:

$$x_T(t) = a_0 + \sum_{n=1}^{\infty} (a_n \cos n\omega_0 t + b_n \sin n\omega_0 t) \tag{3.22}$$

where $\omega_0 = 2\pi f_c = \frac{2\pi}{T}$, and

$$a_0 = \int_T x(t)\, dt = 0$$

$$a_n = \frac{2}{T}\int_T x(t) \cos(n\omega_0 t)\, dt, \quad n \neq 0$$

$$b_n = \frac{2}{T}\int_T x(t) \sin(n\omega_0 t)\, dt, \quad n \neq 0$$

$$a_n = \frac{2}{T}\int_{-\frac{T}{2}}^{0} -A\cos(n\omega_0 t)\,dt + \frac{2}{T}\int_{0}^{\frac{T}{2}} A\cos(n\omega_0 t)\,dt$$

$$= \frac{4}{T}\frac{A}{n\omega_0}\sin(n\omega_0 T) = \frac{4}{T}\frac{A}{n\omega_0}\sin(n\pi) = 0\,, for\ all\ n$$

$$b_n = \frac{2}{T}\int_{-\frac{T}{2}}^{0} -A\sin(n\omega_0 t)\,dt + \frac{2}{T}\int_{0}^{\frac{T}{2}} A\sin(n\omega_0 t)\,dt$$

$$= \frac{4}{T}\frac{A}{n\omega_0}[\cos(0) - \cos(n\pi)] = \begin{cases} \frac{4A}{n\pi}\left(-1^{\frac{n-1}{2}}\right), & n\ odd \\ 0, & n\ even, n \neq 0 \end{cases} \quad (3.23)$$

So, there are always odd-order harmonics in the phase branch. In frequency domain, the spectrum of 1-bit PM signal is $X(j\omega)$:

$$X(j\omega) = \mathcal{F}[x(t)] = \mathcal{F}[x_T(t)]$$

$$= \sum_{n=1}^{\infty}\left(\frac{8A}{jn}\left(-1^{\frac{n-1}{2}}\right)\delta(\omega - n\omega_0)\right) \quad (3.24)$$

Note: it is a single-sided spectrum. The spectrum is shown in Figure 3-21.

In the envelope branch, the signal after DSM is $\mathcal{F}[y(t)] = Y(j\omega) = E + noise$ in frequency domain. Where *E* is a band-limited signal from 0 to $0.5 \cdot BW$, and *noise* is the shaped quantizing noise from $0.5 \cdot BW$ to infinity (or the sampling frequency). It can be shown by the figure below:

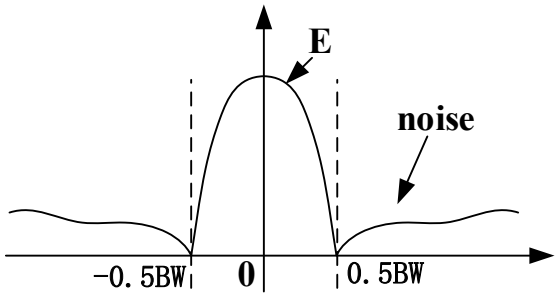

Figure 3-22 Spectrum of signal after DSM in frequency domain, i.e., $Y(j\omega)$

So, the final one-bit RF signal is $z(t) = x(t) \cdot y(t)$. And in frequency domain, multiplication will transfer into convolution:

$$Z(j\omega) = X(j\omega) \circledast Y(j\omega)$$

$$= \left[\sum_{n=1}^{\infty}\left(\frac{8A}{jn}\left(-1^{\frac{n-1}{2}}\right)\delta(\omega - n\omega_0)\right)\right] \circledast [E + noise]$$

$$= \left[\frac{8A}{j}\delta(\omega - \omega_0)\right] \circledast E + \left[\frac{8A}{j}\delta(\omega - \omega_0)\right] \circledast noise$$

$$+ \left[\sum_{n=3}^{\infty}\left(\frac{8A}{jn}\left(-1^{\frac{n-1}{2}}\right)\delta(\omega - n\omega_0)\right)\right] \circledast E$$

$$+ \left[\sum_{n=3}^{\infty}\left(\frac{8A}{jn}\left(-1^{\frac{n-1}{2}}\right)\delta(\omega - n\omega_0)\right)\right] \circledast noise \tag{3.25}$$

$$Z(j\omega) \propto S(j\omega_c) + noise(j\omega_c) + S(j3\omega_c) + noise(j3\omega_c) + \cdots$$

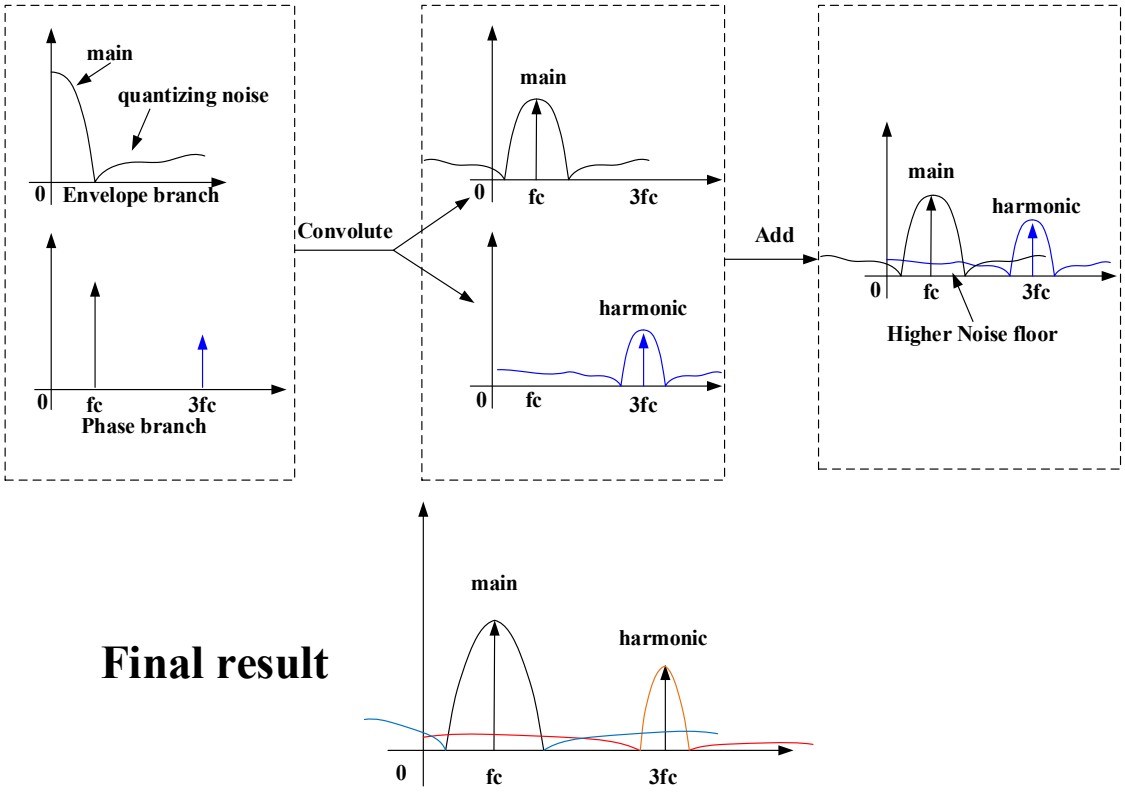

Figure 3-23 Principle of harmonic effect in EDSM

$Z(j\omega)$ is the output of EDSM, in which the first term is the desired signal at ω_c, i.e., main lobe, which is illustrated in black in Figure 3-23. The second term is the quantizing noise at ω_c, which is very

small since the DSM shapes the quantizing noise away from the main lobe, which is illustrated in blue in Figure 3-23. The third term is the third-order harmonic of the signal, which is illustrated in orange in Figure 3-23. And the fourth term is the quantizing noise convoluting with the third-order harmonic, i.e., 3rd order harmonic quantizing noise, which may be overlapped with the main lobe, which is illustrated in red in Figure 3-23. When the quantizing noise out of the signal band (main lobe) usually is not very low, the third-order harmonic quantizing noise may be large enough to degrade the signal significantly.

It is concluded that the envelope DSM introduces 3rd and higher-order harmonic quantizing noise, which may be overlapped with the signal. This noise can be reduced by using a high sampling frequency, i.e., high OSR, to spread the quantizing noise over a large bandwidth.

Chapter 4 Simulation results and discussions

4.1 Simulation system setup

The general process of simulation is outlined in the flowchart below:

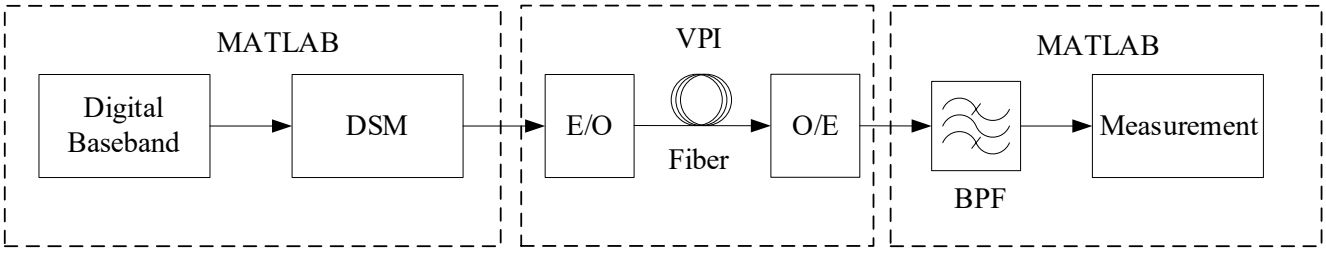

Figure 4-1 Simulation setup flowchart

All simulations about the electric domain, including digital baseband, DSMs, demodulation, etc., are implemented by MATLAB. For fiber links, including lasers, photodiodes, and fibers, are simulated in VPI Photonics Transmission Systems (VPI). The DSM signal is first generated by MATLAB. then it is grouped into bit frames, because VPI software does not accept MATLAB data directly. Then in VPI, the system reconstructs the NRZ form signal based on the input bit frame and bitrate setup. After the optical transmission is finished, VPI samples the output signal of photodiodes and transfers it back to MATLAB. Finally, the demodulation, signal processing and measurement will be processed by MATLAB.

The digital baseband signal is created based on the LTE standard [46][47]. However, when this project starts, the 5G standard [47] does not update the details about baseband signal parameters for bandwidth higher than 20 MHz. So, we use the 4G standard [46] to create a 20 MHz baseband signal first. Then, the 200 MHz is generated by applying FDM to ten 20 MHz signals. Since there is already a reserved gap in the 4G standard, there is no additional gap between each band while doing FDM. The parameters about 20 MHz LTE signal are available in Table 4-1.

Conventionally, absolute EVM is measured from the constellation diagram directly. However, this paper concentrates on the penalty of EVM after transmission. So, relative EVM is used, which focuses on the increased ratio of received EVM to a referenced EVM. Assumed $EVM_{\%}$ is the absolute EVM of

the received signal, and $Ref_{\%}$ is the referenced EVM. The relative EVM is defined as

$$\Delta EVM = EVM_{dB} - Ref_{dB} = 20 \cdot log_{10}(\frac{EVM_{\%}}{Ref_{\%}}) \quad (4.1)$$

Table 4-1 Summarization of LTE Standards for 20 MHz bandwidth

Baseband parameters		RF parameters	
Bandwidth (BW)	20/200 MHz	Carrier frequency(f_c)	2.5 GHz
FFT/IFFT size	2048	Bit rate	10 Gbps
Subcarrier Spacing	15 kHz		
Cyclic prefix length	144		

4.2 Directly received test

Directly received test focus on measuring the quantizing noise of DSM system, i.e., we remove the VPI block in Figure 4-1 and directly receive the output signal of DSM. Thus, the directly received EVM can directly be mapped to the internal noise of DMS systems.

4.2.1 Input and output properties for three DSMs

The baseband signals used in this simulation are 200MHz signals. The system structures are already discussed in chapter 3. Next, about the sampling frequency of ΔΣ modulator, the sampling frequency of DSM type I is set as 10 GHz ($4 \times f_c$) and 5 GHz ($2 \times f_c$) for DSM type II. The purpose of this operation is to get the same OSR for ΔΣ modulators. For EDSM, because of harmonic effect, we set the sampling frequency as 40 GHz ($16 \times f_c$) to achieve high OSR to weaken the harmonic effect.

Figure 4-2 provides details of signal processing corresponding to the positions in Figure 3-14 (before and after the ΔΣ modulators). Figure 4-2 (a) shows the analog RF signal in frequency domain before the ΔΣ modulator (at the position of (a) in Figure 3-14). Figure 4-2 (c) shows the digitized RF signal after the ΔΣ modulator (the DSM output, i.e., at the position of b in Figure 3-14) in the time and frequency domain, respectively. From Figure 4-2 (c), it is seen that most of quantizing noise is shaped out from the signal band by the ΔΣ modulator. Hence the directly demodulated signal has an EVM of -

41.01 dB shown in Figure 4-2 (d). According to the principles of EVM discussed in chapter 2, the directly demodulated SNR is 41.01 dB. For DSM, we only consider that the SNR in signal band, i.e., the SNR of the peak, such as the 200 MHz bandwidth peak in Figure 4-2 (c). So, this SNR in DSM is called peak signal to noise ratio (PSNR), which equals the directly demodulated SNR measured from the constellation diagram. Note that the calculated PSNR is 44.53 dB. The difference between the simulated and calculated PSNR is due to the non-flatness stopband of the Chebyshev-based NTF (see Figure 3-10), which introduces additional quantizing noise. Finally, as shown in Figure 4-2 (b), the output of the DSM, i.e., the digitized RF signal, is an NRZ stream of pulses. However, the spectrum of this signal is quite different from PSD of a random NRZ signal by comparing Figure 4-2 (c) and Figure 2-2 (a). On the contrary, in the frequency domain, the peak of the DSM signal is similar to an analog RF signal. Thus, the digitized RF signal is just an NRZ form signal in the time domain, and in the frequency domain, it is still an analog RF signal.

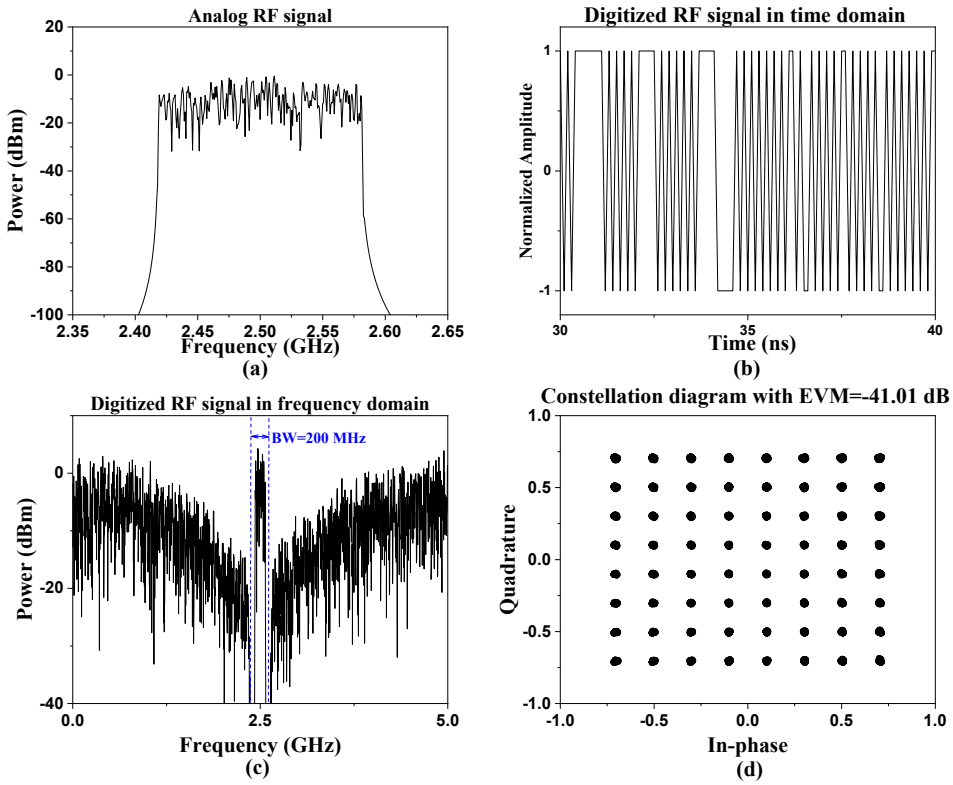

Figure 4-2 (a) Analog RF signal at the position of a, (b) digitized RF signal in time domain at the position of b, (c) spectrum of the signal at the position of b, and (d) signal constellation at the position of b. The positions of a and b are marked in Figure 3-14.

Figure 4-3 illustrates the processing details of the signal at the positions of a, b, and c marked in Figure 3-16. Figure 4-3 (a) shows the baseband signal spectrum at the position of a, i.e., before the lowpass ΔΣ modulator. Figure 4-3 (b) shows the signal spectrum at the position of b, i.e., after the lowpass ΔΣ modulator. Figure 4-3 (c) and (d) show the output spectrum and constellation of the signal at the position of c, i.e., the output of the DSM. The directly demodulated signal has an EVM of -40.85 dB in Figure 4-3 (d), which is approximately equal to the EVM of the DSM Type-I, -41.01 dB in Figure 4-2 (d) because both of them have the same OSR. On the contrary, as discussed in section 3.4.2, since the digital carrier of DSM Type-II is rectangular pulses, the bandwidth of the digital carrier is not negligible, which makes the digitized RF signal have a wider bandwidth than the baseband signal of 200 MHz (Figure 4-3 (c)), i.e., wider than 200 MHz. Moreover, the bandwidth of signal before and after ΔΣ modulator is equal to 200 MHz because it is the digital carrier, rather than the ΔΣ modulator, that expands signal bandwidth.

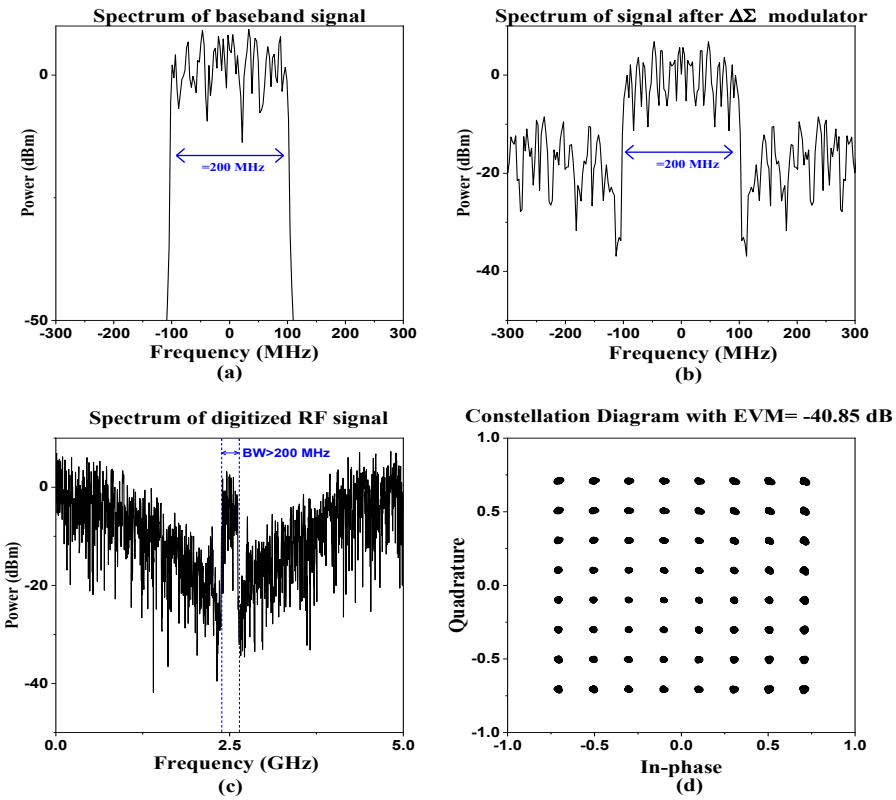

Figure 4-3 (a) Baseband signal spectrum at the position of a, (b) signal spectrum at the position of b, (c) signal spectrum at the position of c, and (d) signal constellation at the position of c. The positions of a, b

and c are marked in Figure 3-16

As shown in Figure 4-4 (a), the quantizing noise in the envelope branch is shaped out from the signal band, and Figure 4-4 (b) shows that the harmonics in the phase branch are generated after the sign quantizer. As discussed in section 3.5.2, because of the harmonic effect, the quantizing noise is still overlapped with the signal band after being multiplexed with the phase branch. Thus, the noise floor of the digitized RF signal created by EDSM, as shown in Figure 4-4 (c), is higher than two bandpass DSMs. Moreover, the quantizing noise introduced by ΔΣ modulator just achieves PSNR 36.24 dB, but the PSNR of final digitized RF signal is 27.82 dB, in which 86.7% of noise comes from harmonic effect.

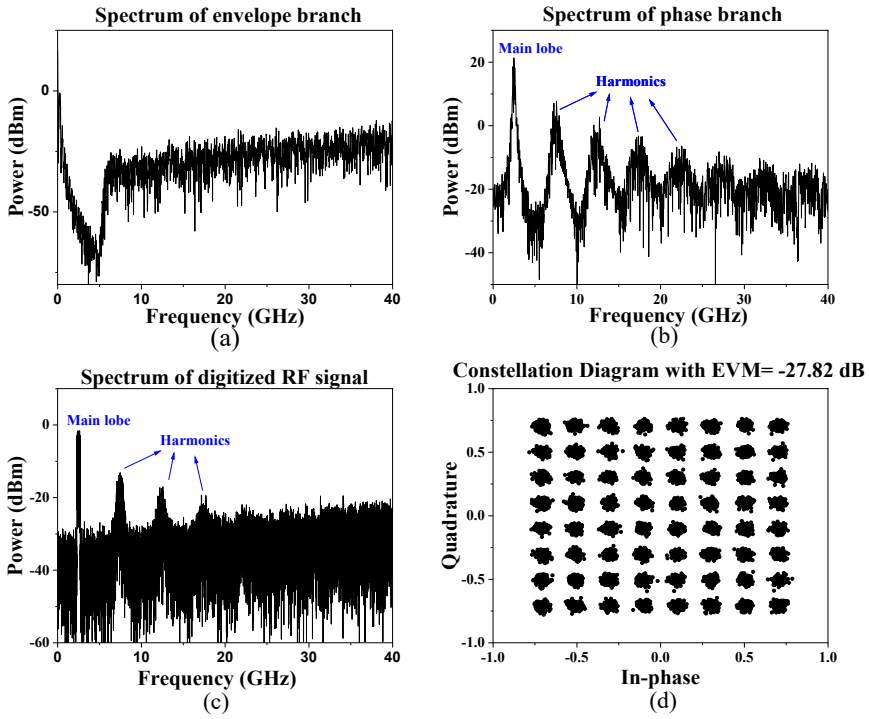

Figure 4-4 (a) Envelope signal spectrum at the position of a, (b) phase signal spectrum at the position of b, (c) output signal spectrum at the output of the DSM, i.e., the position of c, and (d) signal constellation at the output of the DSM, i.e., the position of c. The positions of a, b and c are marked in Figure 3-20

4.2.2 Order of DSM

This section focused on simulation about the order of DSMs, i.e., the order of loop filter in ΔΣ modulator. The results are available in Table 4-2, where the yellow mark is the order selected in future simulations. The sampling frequencies of ΔΣ modulators are the same as section 4.2.1, i.e., 10 GHz for bandpass ΔΣ modulators and 5 GHz for lowpass ΔΣ modulators. There are just even orders (except 1) in

Table 4-2 because odd order is meaningless and unstable for bandpass ΔΣ modulators. Moreover, the EVM for the first order bandpass ΔΣ modulator is not shown because the minimum order of ΔΣ modulator is two to make the zeros and poles are symmetric about the real axis.

First, by comparing the first row, the EVM just improves 1~2 dB after increasing the system order. At the same time, in the second row, the step between each column is about 3~5 dB before 6 order, and it becomes as stable as the first row. The same pattern can be concluded by analyzing the third and last row. Moreover, by comparing each column, for determining bandwidth, i.e., 20 MHz or 200 MHz, the performances of ΔΣ modulator are similar for both lowpass and bandpass ΔΣ modulators. The reason is that the performance of ΔΣ modulator is decided by the mainly OSR, and the OSR of lowpass and bandpass ΔΣ modulators are set as same for a fair comparison. In conclusion, first, the order of ΔΣ modulator should be matched with input signal bandwidth. In detail, the order of the loop filter decides the stopband of NTF, which is also the bandwidth of ΔΣ modulator systems. If the system bandwidth is not wider than the input signal, additional quantizing noise will mix with input signal. Match means the system order is the minimum order that can make the system bandwidth wider than input signal. If the system order is already matched with the input signal, continuing to increase the system order is meaningless because it can only get a little improvement but will affect the stability of the system.

Table 4-2 Directly received EVM with different system order

	Order / BW	1	2	4	6	8
Lowpass ΔΣ modulator	20 MHz	-38.76 dB	-39.97 dB	-41.51 dB	-43.83 dB	-44.20 dB
	200 MHz	-26.77 dB	-31.95 dB	-36.80 dB	-40.85 dB	-41.57 dB
Bandpass ΔΣ modulator	20 MHz	None	-40.10 dB	-40.84 dB	-41.96 dB	-42.59 dB
	200 MHz	None	-21.95 dB	-31.12 dB	-41.01 dB	-41.28 dB

4.3 Simulation of DSM transmission over fiber

This section focuses on the performances of three DSMs transmission over optical fiber. The system layout is already shown in Figure 4-1. The simulation follows Fig. 1. A direct modulation laser at 1550

nm with relative intensity noise (RIN) of -120 dB/Hz and output power of 0 dBm, and a PIN photodiode with 1 A/W responsivity as well as thermal noise (load impedance of 50 Ω, noise figure of 10 dB and bandwidth of 6 GHz) are used [48]. The optical link is a standard single mode fiber with an attenuation of 0.2 dB/km. The fiber has chromatic dispersion of 17 ps/(nm·km) at 1550 nm, dispersion slope of 0.08 ps/(nm^2·km) and, Kerr nonlinearity of $2.6 \times 10^{-20}\ m^2/W$, which is set based on standard signal mode fiber parameters [25]. The signal frequency carrier is set at 2.5 GHz. The baseband signals used in this section are the same as section 4.2.1, and an ideal bandpass filter after the optical receiver has a 300-MHz bandwidth, which is used to convert an NRZ signal to an RF signal. Finally, since the jitter in experiments is not negligible and uncontrollable, a constant time jitter 6 ps, which is measured from experiments, is involved in simulations.

4.3.1 Dispersion and Kerr effect

First, we consider the impact of fiber transmission with four cases of fiber loss only, fiber loss plus group-velocity dispersion (GVD), fiber loss plus Kerr effect, and all included, as shown in Fig. 10. EVM penalty is used to describe the performance, and the EVM in Figure 4-2 is chosen as the reference for Fig. 10, which is the best achieved EVM for the three DSMs.

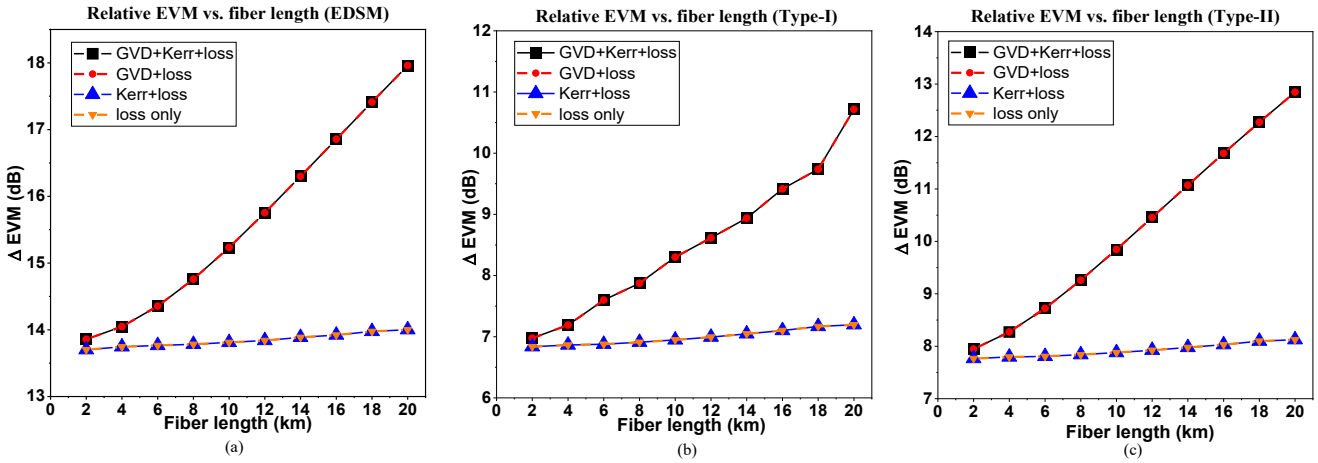

Figure 4-5 EVM penalty vs. fiber length for (a) EDSM, (b) DSM Type I, and (c) DSM Type II. A common reference of EVM=-41.01 dB is used. The oversampling frequency is 10 GHz for two BP-DSMs and 40 GHz for EDSM.

For all the three DSMs, first, even there is only fiber loss, the EVM penalty reaches about 7 dB for

two bandpass DSMs and 14 dB for EDSM. The difference between EDSM and two bandpass DSMs is the harmonic effect in EDSM. Moreover, because the equipment used in lab experiments makes the whole system noise-dominated, the simulation circumstances in this section are also set as noise-dominated to match with lab experiments. That is the reason that the EVM penalty of two bandpass DSMs is around 7~8 dB. What is more, a clear observation is that the GVD has a large impact and induced a large degradation with the increase of fiber length because the NRZ bit rate is 10 Gb/s for the two BP-DSM and 40 Gb/s for the EDSM. Due to the optical power of 0 dBm, the Kerr effect is negligible. Moreover, the DSM Type-II results in a larger EVM penalty than the DSM Type-I with the increase of fiber length. This is because the signal spectrum generated by the DSM Type-II is broader than 200 MHz, which is induced by the digital carrier in Figure 3-16. For example, for a 200 MHz baseband signal, the DSM Type-I in which the carrier is a sinusoid generates a signal of 200 MHz, but the DSM Type-II generates a signal of 250 MHz. Figure 4-5 (a) shows the EDSM leads to the worst performance. This is because of the 3rd harmonic quantizing noise as described in section 3.5.2. This is the reason why the EVM penalty is about 14 dB for without fiber transmission.

Obviously, Fig. 10 shows that a DSM-generated NRZ signal is much more sensitive to fiber GVD than the conventional NRZ signal (for the conventional NRZ, the impact of fiber dispersion on transmission is negligible for fiber of up to 20 km at 10 Gb/s). Figure 4-6 (a) and (b) show two optical spectrums of DSM Type-I generated NRZ and conventional NRZ at 10 Gb/s. It is obvious that the two optical spectrums are quite different, and the optical spectrum of the DSM generated NRZ is distributed roughly over three peaks in addition to two narrow peaks in between the three peaks (the two peaks are located at 2.5 GHz and 2.5 GHz is the RF carrier). It is known that the impact of GVD is very sensitive to optical spectrum distribution, so it is understood that the DSM-generated NRZ signal should be more sensitive to fiber GVD, i.e., quite different from the conventional NRZ signal. This is the reason why the EVM penalty in Figure 4-5 is degraded severely with the increase of fiber distance.

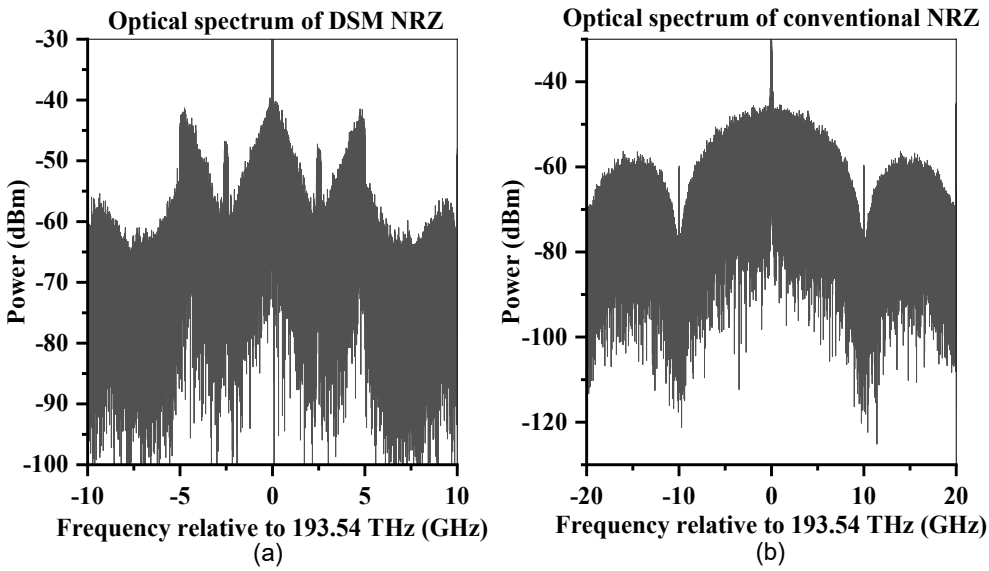

Figure 4-6 Optical spectrum of (a) DSM generated NRZ signal, and (b) conventional NRZ signal, both at bitrate 10 Gb/s. Both signals are modulated by an intensity modulator at 1550 nm (193.54 THz). Optical power is 0 dBm.

4.3.2 Optical power

Under the simulation conditions in section 4.3.1, we continue to consider the effect of optical power and the Kerr nonlinear effect. The optical power that goes into the fiber is controlled by an attenuator. Since all three DSM signals have the same waveform in the time domain, we use DSM type I as examples here. The results are shown in Figure 4-7. The line style means the parameters setup of the fiber, i.e., with and without Kerr effect. And the line color means the optical power. Overall, the dash lines (without Kerr effect) and the solid lines (with Kerr effect) overlap together for any determined optical power from -5 dBm to 5 dBm. It can prove that the DSM signal has resistance to Kerr nonlinearity is because of its NRZ waveform in the time domain. Obviously, if the input signal only has two power levels, there will also be only two power levels in the output signal no matter what nonlinear distortion is introduced by the system. Next, in Figure 4-7(a), the EVM improves about 0.2~0.8 dB when increasing the optical power because higher optical power will get a higher signal-to-noise ratio (SNR) on the receiver side. And fiber loss is the only reason to make the EVM worsen by increasing the fiber length. However, the effect of each parameter is not a simple superposition. As a result, when GVD impact is included in

Figure 4-7(b), the EVM increases about 5.4 dB after 20 km fiber transmission for all optical powers, and the distance between each line does not change when increasing fiber length. In conclusion, the Kerr nonlinear effect does not affect the transmission performance of DSM signal because the NRZ waveform provides DSM resistance to nonlinearity, and this resistance is independent of optical power.

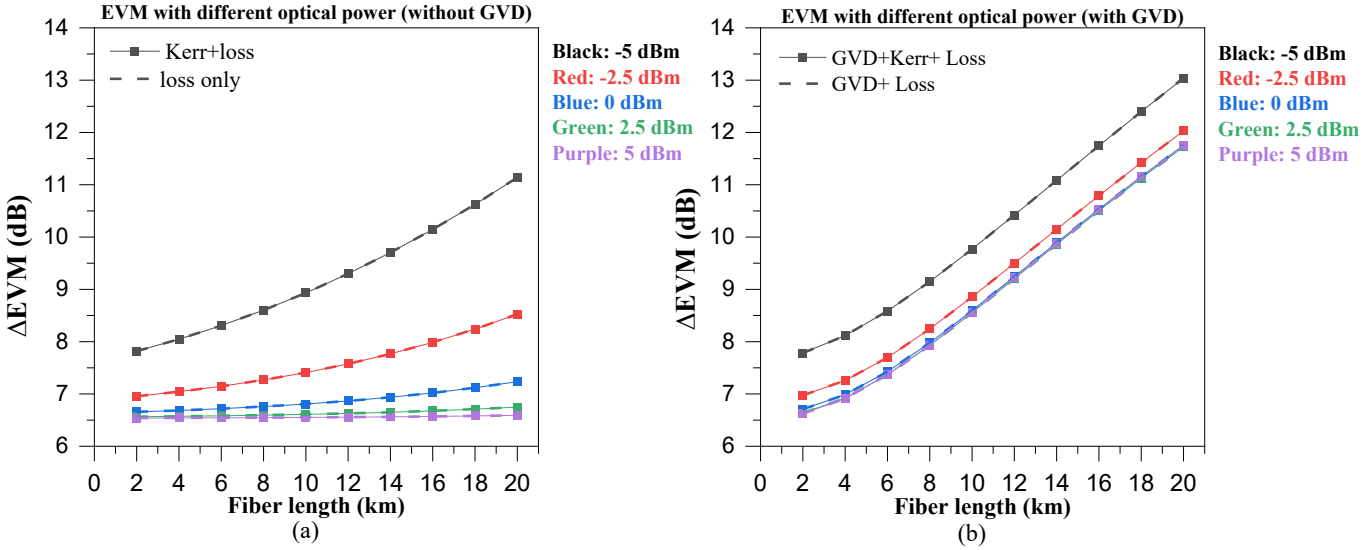

Figure 4-7 EVM penalty vs. fiber length with different optical power for (a) without GVD impact and (b) with GVD impact. DSM type I is used as example and EVM=-41.01 dB is used as reference. Note that the blue, green, and purple lines in (b) are overlapped because their distances are only about 0.1 dB.

4.3.3 Harmonic noise in EDSM

To further show the impact of the harmonic quantizing noise in the EDSM, the EVM penalty at the oversampling frequency of 16fc, 8fc, 4fc, and 2fc is compared in Figure 4-8. The referenced EVM of -27.28 is selected from Figure 4-4 (d) because the EDSM only is considered here. It is observed that the EVM penalty is increased significantly by the decrease of the oversampling frequency, e.g., at fiber length of 0 km, an increase of about 10 dB EVM is obtained between the cases of 16fc and 2fc. This is because the harmonic noise is increased by the decrease of the oversampling frequency, as explained in section 3.5.2. Moreover, the optical bit rate is increased with the increase of the oversampling frequency. Therefore, the dependence of the EVM penalty at a larger oversampling frequency is stronger with the increase of fiber length, as shown in Figure 4-8. On the other hand, if the oversampling frequency is reduced, the quantizing noise left in the signal band increases. Thus, there is a trade-off between increase

of bitrate and decrease of quantizing noise in choosing an oversampling frequency. Note that the percentage of the harmonic noise is always around 82-87% for the above oversampling frequencies, which means harmonic noise is always dominated in Figure 4-8.

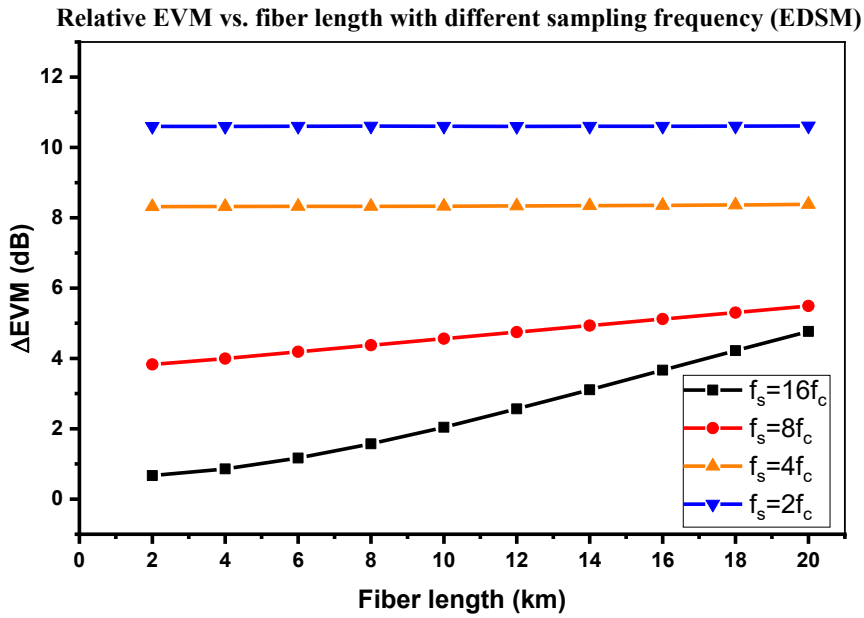

Figure 4-8 EVM penalty vs. fiber length for EDSM with oversampling frequency as indicated in the figure. The referenced EVM=-27.82 dB is used.

To prove that the EVM penalty in Figure 4-8 is caused by harmonic effect instead of fiber transmission, Figure 4-9 (a) and (b) provides the constellation diagram of signal with f_s=16f_c and f_s=4f_c after 20 km fiber transmission, i.e., black line and orange line in Figure 4-8. In Figure 4-9 (a), the EVM of this signal is -25.58 dB, and there is no error symbol in the constellation diagram. However, the signal in Figure 4-9 (b) already suffers distortion, and the EVM is just -19.28 dB. As discussed in previous sections, there is no in-band phase noise in EDSM, the quantizing noise is similar to white noise, and the harmonic effect will introduce addition quantizing noise. Therefore, the overall boundary of Figure 4-9 (b) is still a square to prove that there is only amplitude noise and no phase noise. The reference the constellation diagram in Figure 4-9 (c) is a standard 64 QAM signal polluted by phase noise only. It is clear that the constellation diagram becomes a group of concentric circles because amplitudes of signal do not change. Finally, if the signal suffers both amplitude and phase noise, the symbols in the

constellation diagram will distribute as a circle. Thus, the EVM penalty in Figure 4-8 is caused by the worsening of harmonic effect.

Next, about the slope decreasing while decreasing sampling frequency. It is seen that with the OSR of EDSM decreasing, the increasing trend of EVM penalty becomes slow, and it is going to stop at $f_s \leq 4f_c$. The reason is that the harmonic effect has already become the dominant factor in transmission. In other words, the transmission results are not the summation of each impact, such as GVD and harmonic effect. Instead, it is decided by which one is dominated. For example, for two bandpass DSMs, the GVD impact is dominated in fiber transmission because their internal noise is very small compared with channel noise. On the contrary, if the internal noise is large enough to beat with channel noise, such as EDSM with less OSR, the transmission performance is mainly decided by internal noise.

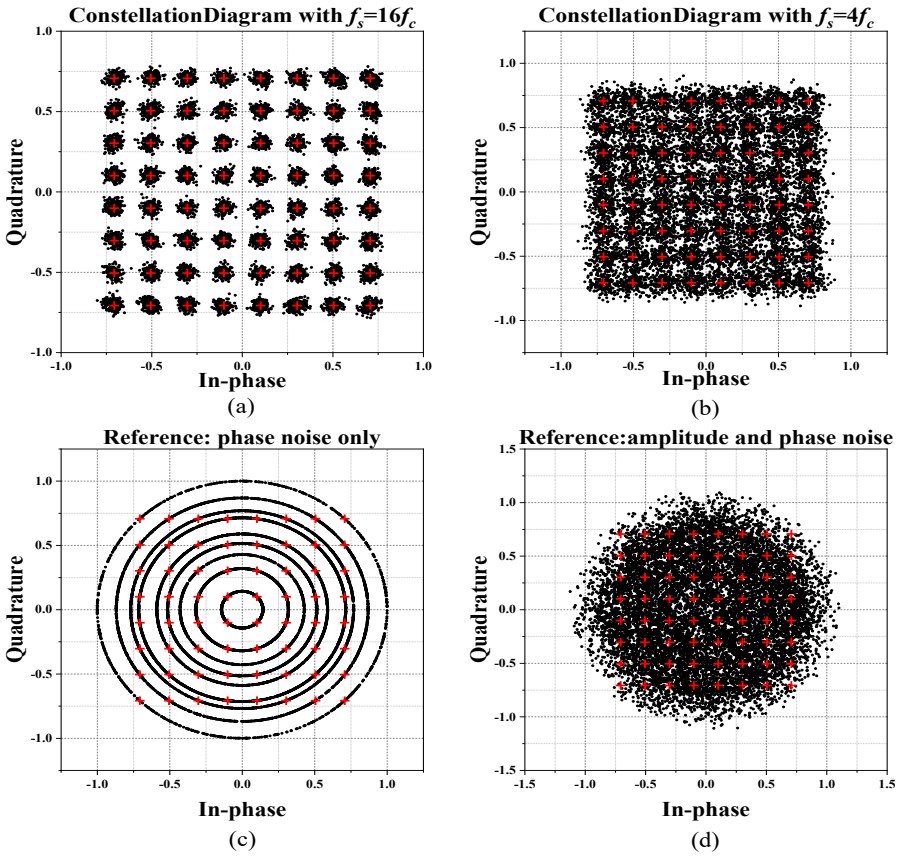

Figure 4-9 Constellation diagram of (a) signal with f_s=16f_c, (b) signal with f_s=4f_c, and (c) and (d) two references.

4.3.4 Up-sampling for bandpass DSM

The last simulation is about up-sampling for bandpass DSM. Note the up-sampling can also be applied to DSM Type-I and EDSM too, but it is not considered in this work. By considering the difficulty of implementation, bandpass DSM Type-II is selected as the object because it is an all-digital system and, up-sampling can be directly implemented by programable IC. The results are shown in Figure 4-10. Because the intensity of GVD impact is relative to the pulse width of NRZ waveform and up-sampling for NRZ signal can decrease the minimum pulse, as shown in Figure 3-19. This operation can be equalized reduce the bit rate, i.e., When no up-sampling is used, the optical bit rate is 10 Gb/s as stated above, and thus bit rates are equalized to 5 Gb/s, 3.3 Gb/s, and 2.5 Gb/s for the up-sampling ratio N of 2, 3, and 4, respectively. Figure 3-19 shows the simulated EVM for the DSM Type-II with the up-sampling ratio of 1~4 for comparison. It is clearly seen that the EVM is much less sensitive to fiber length with the increase of the up-sampling ratio as expected. However, since the real bit rate, i.e., the bit rate setup in simulation software and lab equipment, is still 10 Gbps, and it is the bit frame size that increases by N times. Thus, the cost of this operation is the efficiency.

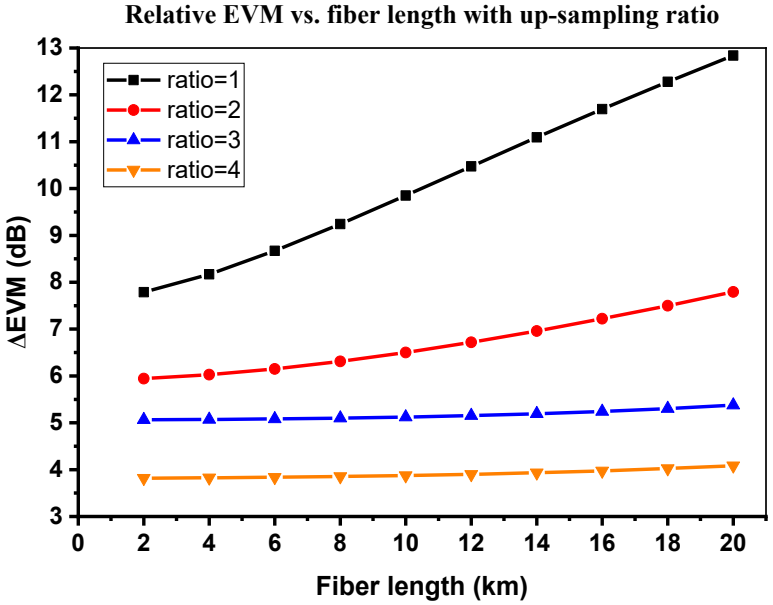

Figure 4-10 Simulated EVM for DSM Type-II plus up-sampling with indicated ratios. The referenced EVM=-41.01 dB is used.

4.4 Simulation Summary

First, by comparing the structures and directly received results of the above three DSMs, the DSM Type I and EDSM are based on a mixed signal system, while the DSM Type II is based on an all-digital system, which can be implemented by programmable devices directly, such as field-programmable gate arrays. Moreover, additional synchronization may be required in the DSM Type-II and EDSM because of possible time delay imbalance between the two branches. By comparison of the DSM Type-I and Type-II, the DSM Type-II needs two lowpass ΔΣ modulator chips, instead of one bandpass ΔΣ modulator in the DSM Type-I, but its loop filter is more difficult to design.

Moreover, compared with the above two bandpass DSMs, the envelope DSM has additional harmonic quantizing noise that may mix with the signal. In order to reduce this harmonic noise, a much higher OSR than the above two bandpass DSMs is required. Generally, it seems that the EDSM does not show advantages for a broadband signal because it has a higher noise floor than the two bandpass DSMs. On the contrary, for a relative narrowband signal, such as 5 MHz [5][22], the EDSM only needs the sampling frequency of $2f_c$, while the two bandpass DSMs still require the sampling frequency of $4f_c$. Thus, the lower sampling in EDSM makes the EDSM output signal less sensitive to fiber dispersion and time jitter for its lower bitrate. Consequently, the EDSM has a high potential to be the best solution for narrowband signals.

Chapter 5 Experiments and discussions

5.1 Experiment setup

The experiment is implemented by following Figure 5-1 and Figure 5-2. The baseband and DSM signal are implemented in MATLAB. Then, the DSM signal is loaded into an arbitrary waveform generator (AWG), which generates an NRZ bit sequence at 10 Gb/s (bit rate = fs=4fc) for all the three DSMs. For the RoF link, the laser and photodiode module of MITEQ SCMT-100M6G-28-20-M14 [48] (6 GHz bandwidth link and direct laser modulation) is used. The others are the same as for the simulation. The black lines in Figure 5-1 mean document transmission, blue lines mean electrical cables, and red lines mean optical fibers.

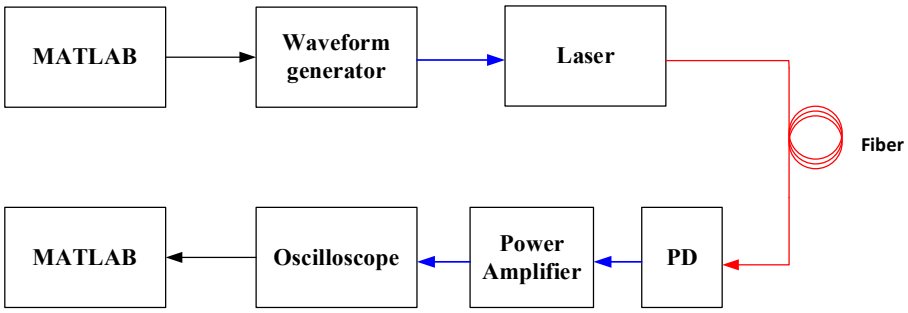

Figure 5-1 Block diagram of lab experiment setup. PD: photodiode

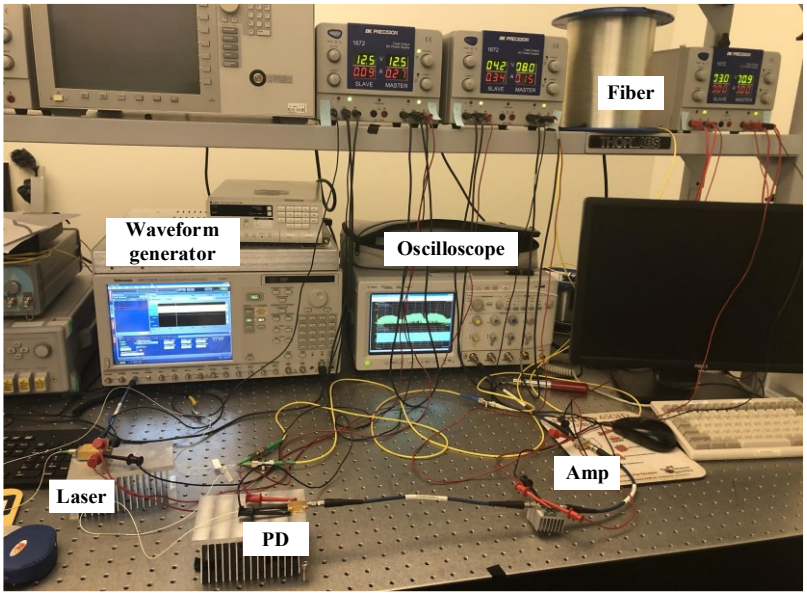

Figure 5-2 Equipment setup in laboratory. Amp: amplifier

5.2 Transmission over fiber

Because of the limitation of equipment, the full digitalized RF signal is too long for the waveform generator and oscilloscope. Thus, the transmission in experiments is frame based because the output of DSM is NRZ form signal which can also be treated as bit 0 and 1. First, we break the output of DSM into bit frame and add a head and trail for each frame. The frame size is decided by the oscilloscope to make sure that the time windows of the oscilloscope can sample a full frame. After all frames are transmitted, the system will regroup them before demodulation.

5.2.1 Directly received performance

The directly received test in the experiment section means connecting the AWG and oscilloscope directly by a short coaxial RF cable, and the results are given in Table 1. It is seen that the DSM Type-I leads to the best performance, and the EDSM leads to the worst performance, as predicted by the simulation.

Table 5-1 Measured EVM without RoF link

Type	EVM (dB)
Bandpass DSM Type I	-34.5
Bandpass DSM Type II	-31.5
Envelope DSM	-25.6

Since Bandpass DSM Type I gets the best performance in experiments, we chose this system for waveform and spectrum plotting, and result is shown in Figure 5-3. It is clear that the quantizing noise is shaped outside the signal band in the frequency domain, and it is an NRZ form signal in the time domain where the eye diagram in Figure 5- 4 can also show its NRZ form in the time domain.

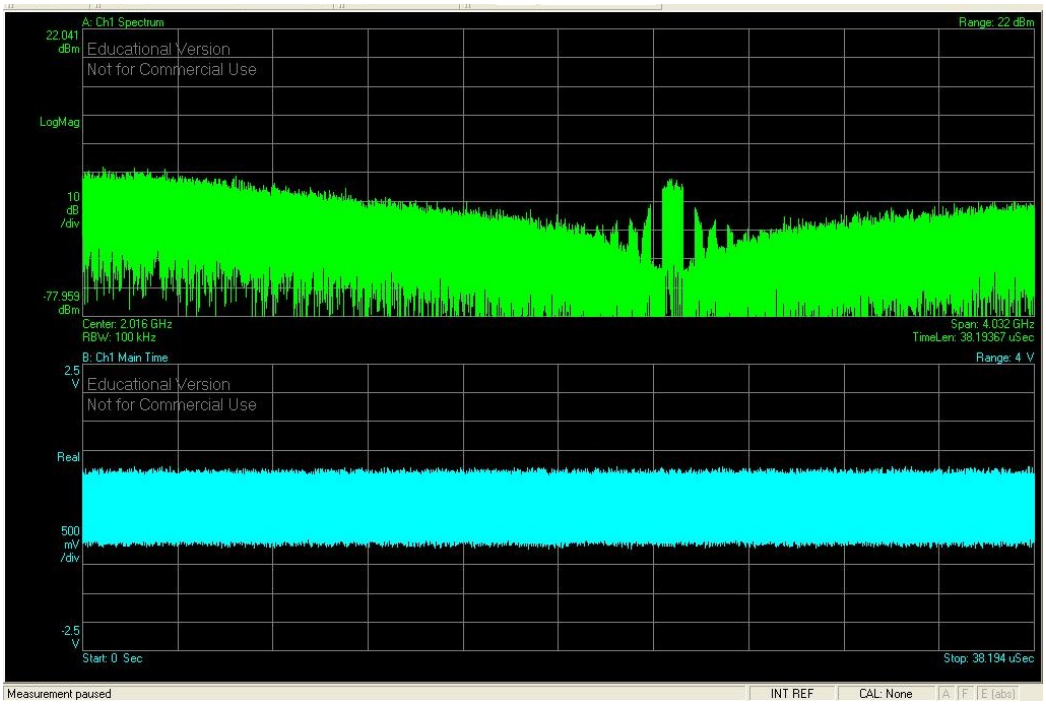

Figure 5-3 Measured spectrum and waveform of bandpass DSM Type I

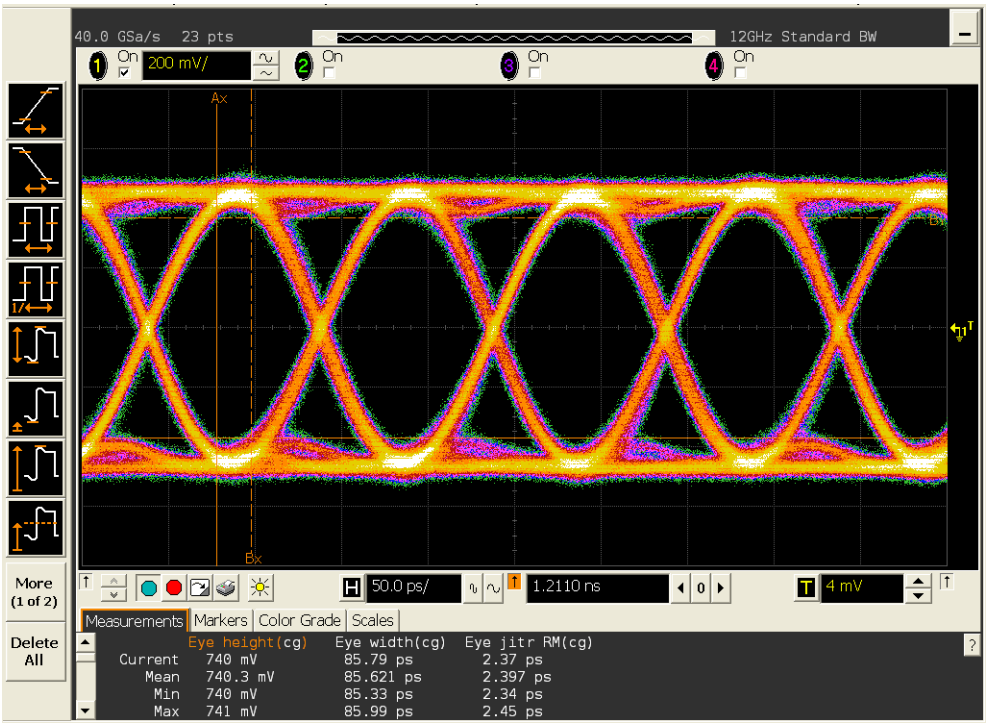

Figure 5- 4 Measured eye diagram of bandpass DSM Type-I

Finally, about the bandwidth expansion effect in bandpass DSM type-II, the output signal spectrums of two bandpass DSMs are shown in Figure 5-5. With a 200 MHz width window (the blue rectangular

Figure 5-5), it is obvious that the bandwidth of signal generated by bandpass DSM type-II is wider than 200 MHz, and the reason has already been explained in section 3.4.2. This experiment result meets the simulation results shown in Figure 4-2 and Figure 4-3.

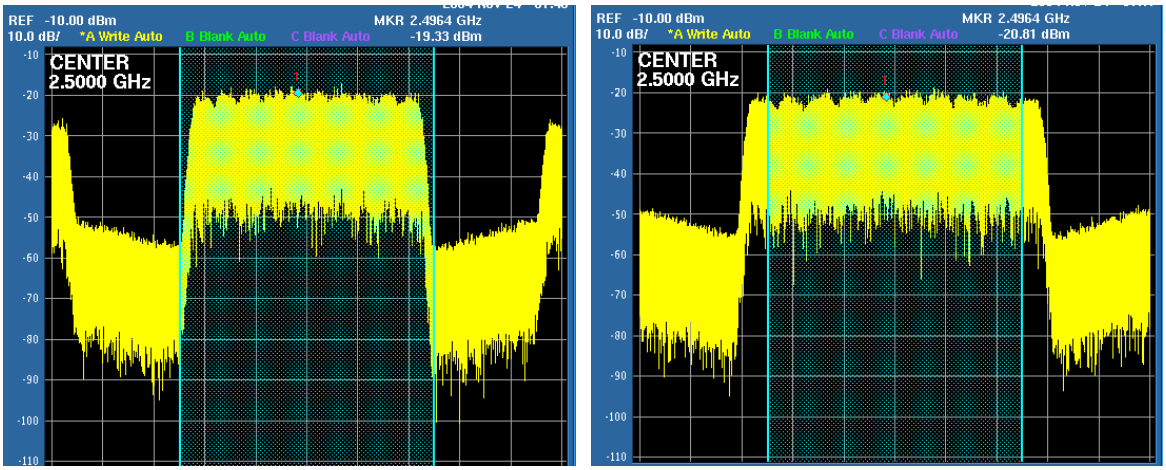

Figure 5-5 Output signal spectrum of (left) bandpass DSM Type-I and (right) and bandpass DSM type-II, where the width of the bule rectangular is 200 MHz.

5.2.2 Transmission over fiber

The experiment in this section discusses the transmission performance in RoF link. Since there are just three rolls of transmission fiber with lengths 2 km, 8 km and 20 km, the transmission distances are set as the combination of them up to 20 km, i.e., 0, 2, 8, 10, and 20 km, where 0 km means connecting the laser and photodiode with a short fiber directly.

Figure 5-6 shows the measured EVM for the RoF link with each of the two BP-DSMs, where the EVM of the DSM Type-I in TABLE 1 is selected as the reference. The measured EVM penalty is very similar to Figure 4-5, and again it is shown that the performance has a strong dependence on fiber length. The performance of the DSM Type II is always 1.5 dB worse than that of the DSM Type I as explained in simulation. Based on the requirement of 64-QAM in IEEE 802.11, a minimum EVM of -21.93 dB is required, which is also shown in Figure 5-6. It is found that the maximum fiber distance of about 10 km can be transmitted, far less than future requirements. The measured EVM for the RoF link with the EDSM is very poor, such as -22.4 dB for the back-to-back RoF, and -19.7 dB for the RoF with 2 km fiber. Thus, this case is not shown in Figure 5-6. The EDSM based RoF link is limited by harmonic noise as well as

the effect of power amplifier, which will be discuss in section 5.2.4.

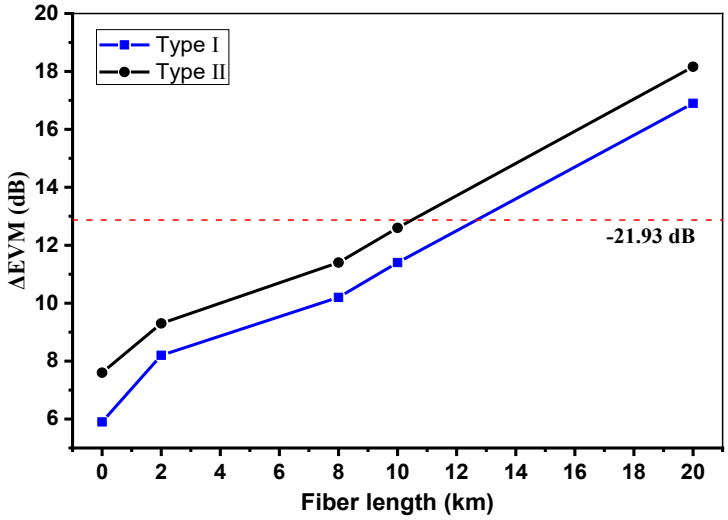

Figure 5-6 Measured EVM for RoF with either of Type I or II bandpass DSM. The referenced EVM=-34.5 dB is used. The red dash line is -21.93 dB, indicating the minimum EVM requirement of 64 QAM in IEEE 802.11 [49].

However, by comparing Figure 4-5 and Figure 5-6, it is found that the increasing slope of EVM in Figure 5-6 is higher than Figure 4-5. The reason is that there is additional phase noise in experiments. Using the results of bandpass DSM Type I as an example here, as shown in Figure 5-7, the signal symbols already deviate from the reference signal (red cross in Figure 5-7). Usually, there are two groups of reference symbols at the left and right sides of the transmitted signal in the constellation diagram, i.e., z=0.707+0j and z= -0.707+0j. Because these two symbols are determined instead of random, they could be use as reference at receiver side. With these reference symbols, the signal processing unit on the receiver side will use them to make the received symbol align with reference signals before EVM measurement. However, the reference symbols after 20 km transmission have already suffered distortion. In that case, the signal processing algorithm cannot perfectly align the received signals with reference signals, which makes the measured EVM in experiments in inaccurate. Obviously, manual correction for the symbol is meaningless. That is the reason that the measured EVMs are higher than simulation results.

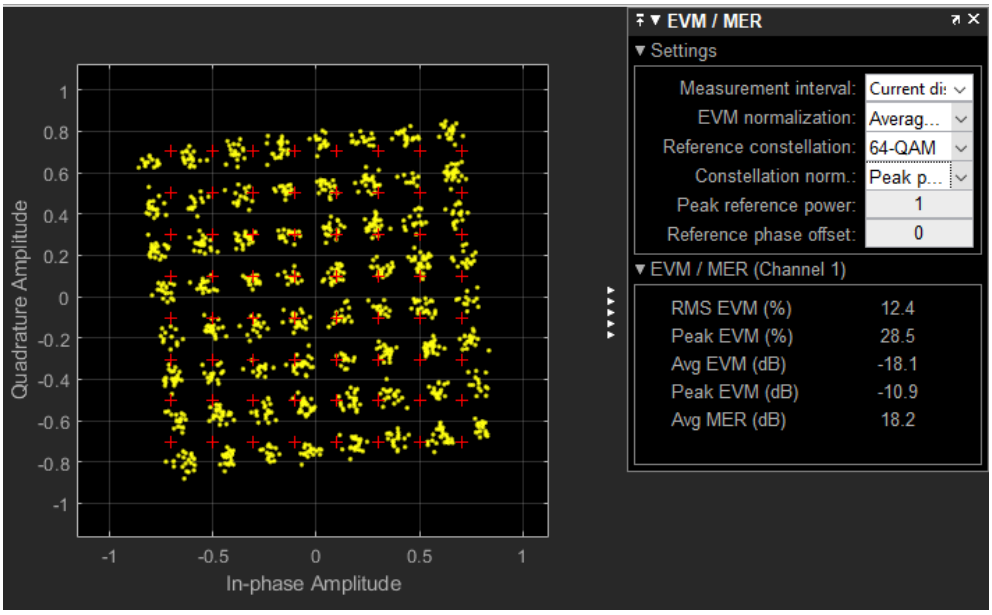

Figure 5-7 Constellation diagram of received signal after 20 km transmission in experiment, where the yellow points are signal symbols and red cross are reference.

5.2.3 Up-sampling for bandpass DSM

In order to improve the fair performance in Figure 5-6, the up-sampling after the DSM Type-II can be used as stated above. Figure 5-8 shows measured EVM for the RoF link using the DSM Type-II plus the up-sampling with ratios of 1~4. With the up-sampling ratio of 4, the measured EVM achieves -36.0 dB without the RoF link, which is the referenced EVM in Figure 5-8. As expected, with the increase of the up-sampling ratio, the measured EVM is much less sensitive to fiber length, and the EVM is also reduced significantly, a very similar behavior as simulated in Figure 4-10. For example, the EVM is improved by 13 dB by using an up-sampling ratio of 4 after 20 km fiber transmission compared to without up-sampling.

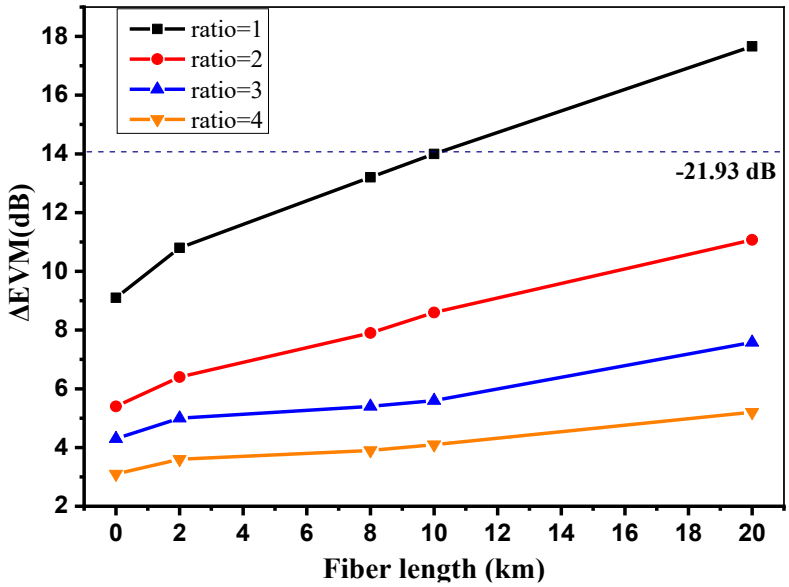

Figure 5-8 Measured EVM for RoF link using DSM Type II plus up-sampling with ratios indicated in the figure. The referenced EVM=-36.0 dB is used.

5.2.4 Effect of RF power amplifiers for EDSM

Figure 5-9 provides the measured step response of power amplifier (PA) used in experiments. The pattern is similar but a little worse than the result in Figure 2-16. As discussed in section 2.1.4, this PA cannot hold a voltage for a long time.

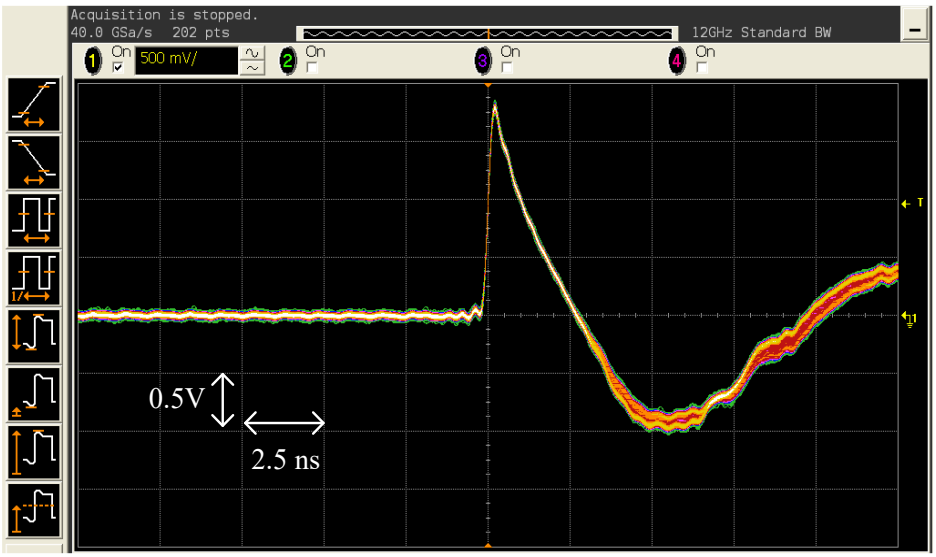

Figure 5-9 Measured step response of power amplifier

As discussed in section 3.5, the EDSM implements the multiplication of envelope and phase branch signal by a logic and gate. And it is known that the 1-bit PM signal, i.e., the signal after *sign(x)* in Figure 3-20, is a periodic rectangular waveform with a 50% duty cycle. As a result, in half of period, the power level of the final digitalized RF signal is constant, and the rest of them is PDM signal, shown in Figure 5-10 (a). At the receiver side, the PDM part does not affect by PA, but the constant power part is distorted because of the PA effect. As shown in Figure 5-10 (b), even there is a decision circuit, it is impossible to find a threshold to recover the original signal. Unfortunately, there is no switching-mode power amplifier in our laboratory for EDSM signal transmission in RoF link, and the power after photodiode is too small to measure without PA. So, the experiment results for EDSM are not shown in Figure 5-6.

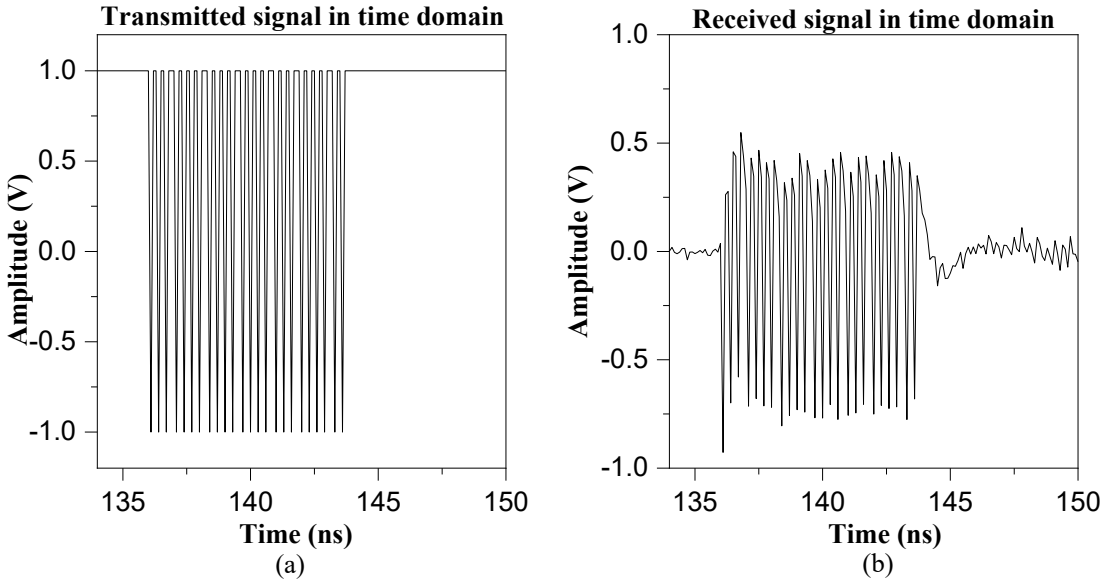

Figure 5-10 A part of (a) transmitted and (b) received EDSM signal in experiments.

5.3 Experiment summary

Overall, the experimental outcomes agree with the simulated counterparts and most of them meet the 64 QAM LTE criteria of below -21.93 dB. The EDSM signal transmitting in RoF link shows the worst performance because of harmonic effect and power amplifier effect. The performances of two bandpass DSMs are similar, and bandpass DSM Type II is about 1.5 dB worse than Type I because signal generated by DSM Type II has wider bandwidth. Finally, the up-sampling operation can improve the transmission performance with the cost of efficiency.

One of problem in experiment is synchronization. As said in the beginning of this chapter, the experimental system is frame-based transmission. Generally, there must be a clock synchronization become the transmitter and receiver, i.e., AWG and oscilloscope. However, the oscilloscope we used do not support external clock from AWG because they come from different manufactures. As a result, the length of sent and received signals may not be the same, which will make the experiment fail.

Chapter 6 Conclusions and future work

6.1 Thesis conclusion

Digitized RoF links using 1-bit DSM has been investigated and compared for three DSMs, i.e., two bandpass DSMs and one envelope DSM, in which an LTE signal of 200 MHz is used. First, from the perspective of system structure, bandpass DSM type I is the simplest structure which is the combination of a standard I/Q upconverter and a bandpass ΔΣ modulator. However, since it is a mixed-signal system, i.e., the signal after upconverter is analog and ΔΣ modulator is a discrete-time system, there is a sampling operation required before ΔΣ modulator. Moreover, because the STF in bandpass DSM type I is a bandpass filter, the design difficulty of bandpass DSM type I is higher than DSM type II and EDSM, whose STFs are lowpass filter. Finally, bandpass DSM type I can be applied to any modulation methods, not just for OFDM. For bandpass DSM type II, it simplifies the design difficulty by applying ΔΣ modulators to baseband signal instead of the RF signal. And the sampling frequency of ΔΣ modulators of Type II also decreases by half compared with DSM type I. Furthermore, since the baseband signal of bandpass DSM type II must be orthogonal modulated signal, such as OFDM, it required two ΔΣ modulators for both in-phase and quadrature branch. Finally, the carrier used for modulation in bandpass DSM type II is also digitalized. As a result, bandpass DSM type II becomes the primary choice of FPGA implementation. The EDSM continues to simplify the number of ΔΣ modulator by dividing the input signal into envelope and phase, instead of in-phase and quadrature. Because there is no in-band noise in phase branch after a 1-bit quantizer, there is just one lowpass ΔΣ modulator required in envelope branch. Nevertheless, the harmonics are also generated after the phase signal is modulated and quantized, which makes EDSM suffer harmonic effect and always gets higher noise floor than two bandpass DSMs. The most efficient method to weaken harmonic effect is increasing OSR, which makes EDSM show less advantages for 200 MHz bandwidth signal. On the contrary, for relative narrow bandwidth signal, the EDSM may require lower sampling frequency than two bandpass DSMs, which makes the signal generated by EDSM show less sensitivity to fiber dispersion and time jitter.

Next, in RoF transmission, among three DSMs, it has been found that additional noise, i.e., 3rd

order harmonic quantizing noise, is added to the signal band in EDSM, which significantly reduces the transmission performance, thus the EDSM based RoF links are first limited by this noise. The DSM Type-I results in the best performance, whose EVM just increases about 4 dB after 20 km fiber transmission. Bandpass DSM type II in simulation and experiment shows the fair performance. Because of the bandwidth expansion effect caused by the non-perfect digital carrier, the signal generated by DSM type II will be more sensitive to fiber dispersion because GVD impact is relative to the signal bandwidth.

Overall, the output signals of three DSMs are NRZ form in time domain. So, the output of DSM could overcome the limitation of analog RF signal, i.e., nonlinear effect. However, it has been found that the optical signal spectrum of DSM-generated NRZ is quite different from the conventional NRZ signal, and it is similar to the spectrum of a double-sideband amplitude modulation signal. Thus, the GVD impact in the frequency domain will directly introduce distortion to components carried with information, which makes the DSM-based optical transmission much more sensitive to fiber dispersion.

Finally, up-sampling after the DSM is proposed for equalized reduction of optical bit rate, and thus less sensitivity to fiber transmission is obtained in addition to low-speed optics. It has been shown that by using up-sampling with a ratio of 4, i.e., bit rate of 10 Gb/s reduced to 2.5 Gb/s, EVM is improved by 13 dB after 20 km fiber transmission. At the same time, the system efficiency is only 25% of the original one because the length of the transmitted bit sequence is also multiplied by four times. Generally, by considering balance between performance and efficiency, up-sampling ratio of 2 may be the best.

6.2 Future work

Due to the limitation of equipment, the experiment results are not as good as simulated. One of the reasons is the amplifier used in experiments is not a switching-mode power amplifier which leads to the distortion of waveforms, especially for EDSM. Another problem is the synchronization between transmitters and receivers. The bit frame used for transmission is directly codding, and there is no reserved bit for synchronization. Designing a bit frame follow some common optical protocol, such as the frame structure in SONET, may improve the results.

Another potential topic for DSM is multiplexing. Because the DSM is not a linear system, i.e., the

summation of two 1-bit DSM signals is not a 1-bit DSM, which means that it is difficult to apply frequency division multiplexing in electrical domain, which becomes the limitation for DSM. One of the possible solutions is applying wavelength division multiplexing (WDM) in the optical domain. Because the span between each band in optical domain is much wider than the DSM signal, there is no Inter-band interference for WDM based transmission. Another solution is the dual-band ΔΣ modulator, i.e., there is more than one passband in STF. Unfortunately, this method is limited by the order of loop filter which makes this system only work for narrow bandwidth signal.

References

[1] J. G. Proakis and M. Salehi., Communication systems engineering, 2nd ed. Upper Saddle River, NJ, USA: Prentice Hall, 2002, ch. 1, pp 1-23.

[2] L. G. Alberto and I. Widjaja, "Channelization in telephone cellular networks," in *communication networks: fundamental concepts and key architectures,* New York, NY, USA: McGraw-Hill, 2001, ch. 6, sec. 6.5.4, pp 382-389.

[3] Z. Eustathia and T. Antonakopoulos. "CSMA/CA performance under high traffic conditions: throughput and delay analysis," *comput. Commun.,* vol 25, no. 3 pp: 313-321, Aug. 2000.

[4] R. Consulta, "4G Mobile Networks – Technology beyond 2.5G and 3G," *Wireless Commun.,* vol 3, pp 230-236, 2011.

[5] H. Kim, "Orthogonal Frequency - Division Multiplexing," in *Wireless Communications Systems Design*, Hoboken, NJ, USA: Wiley, 2015, ch7., pp.209-238.

[6] M. Raja. "Literature survey for transceiver design in MIMO and OFDM systems." *J. of Communications,* vol 13, no. 2, pp 45-59, July 2018.

[7] I. Jawad. "4G Features." *Bechtel Telecommun. Tech. J.,* vol. 1, no. 1, pp 11-14, 2002.

[8] *Digital cellular telecommunications system (Phase 2+) (GSM); Universal Mobile Telecommunications System (UMTS); LTE; 5G; Release description; Release 14*, ETSI TR 121 914 V14.0.0, 2018.

[9] Wikipedia. (2021). *Cellular network* [Online]. Available: https://en.wikipedia.org/wiki/Cellular_network

[10] "Cisco Annual Internet Report (2018–2023) White Paper," Cisco Systems Inc., San Jose, CA, USA, Rep. C11-741490-01, 2020.

[11] F. Connect. (2012, Jun. 14). *The radio over fiber system concept* [Online]. Available:

https://www.fiberoptics4sale.com/blogs/archive-posts/95043078-what-is-radio-over-fiber

[12] X. Liu *et al*., "Efficient Mobile Fronthaul via DSP-Based Channel Aggregation," *J. of Lightwave Technol.*, vol. 34, no. 6, pp. 1556-1564, 2016.

[13] S. Hori *et al*., "A digital radio-over-fiber downlink system based on envelope delta-sigma modulation for multi-band/mode operation," in 2016 IEEE MTT-S International Microwave Symposium (IMS), San Francisco, CA, 2016, pp. 1-4.

[14] S. R. Abdollahi *et al*., "Digital Radio over Fibre for Future Broadband Wireless Access Network Solution," in *2010 6th Int. Conf. on Wireless and Mobile Commun.*, Valencia, 2010, pp. 504-508.

[15] J. Cheng *et al*., "Comparison of Coherent and IMDD Transceivers for Intra Datacenter Optical Interconnects," in *2019 Optical Fiber Commun. Conf. and Exhibition (OFC)*, San Diego, CA, 2019, pp. 1-3.

[16] A. Khilo *et al.*, "Photonic ADC: overcoming the bottleneck of electronic jitter," Opt. Express, vol. 20, no. 4, pp 4454-4469, 2012

[17] S. Pavan *et al.*, Understanding delta-sigma data converters, 2nd ed. Hoboken, NJ, USA: John Wiley & Sons, 2017.

[18] S. Haykin, "Baseband pulse transmission" in *communication systems*, 4th ed. New York City, NY, USA: John Wiley & Sons, 2001, ch. 4, pp. 247-296.

[19] L. G. Alberto, "Random process" and "Analysis and processing of random signal" in *Probability, statistics, and random processes for electrical engineering*, 3rd ed. Upper Saddle River, NJ, USA: Pearson Prentice Hall, 2017, ch. 9-10, pp. 487-633.

[20] J. G. Proakis and M. Salehi, "Deterministic and Random signal analysis" in *Digital communications,* 5th ed. New York City, NY, USA: McGraw-Hill, 2008, ch. 2, pp. 17-82.

[21] *Part 11: Wireless LAN Medium Access Control (MAC) and Physical Layer (PHY) Specifications*, IEEE Std 802.11™-2016, 2016.

[22] R. A. Shafik *et. al*, "On the Extended Relationships Among EVM, BER and SNR as Performance Metrics," in *2006 International Conference on Electrical and Computer Engineering*, Dhaka, Bangladesh, 2006, pp. 408-411

[23] A. F. Molisch, "Orthogonal Frequency Division Multiplexing (OFDM)," in *Wireless Communications*, 2nd ed. Chichester, United Kingdom: John Wiley & Sons Ltd, 2011, ch. 19, pp.417-443.

[24] S. Kumar and M. J. Deen, *Fiber optical communications fundamentals and applications*, 1st ed. Chichester, United Kingdom: John Wiley & Sons Ltd, 2014.

[25] Corning inc., "SMF-28® ultra optical fiber," Corning SMF-28 datasheet, 2014.

[26] F. Edalat, "Effect of Power Amplifier Nonlinearity on System Performance Metric, Bit-Error-Rate (BER)," M.S. thesis, Department Electrical Engineering and Computer Science, Massachusetts Institute of Technology, Cambridge, MA, USA, 2003.

[27] Mini-Circuits company, "Super ultra wideband Amplifier," ZVA-213-S+ datasheet, December, 2008.

[28] A. V. Oppenheim, *Discrete-time signal processing,* 3rd ed. Upper Saddle River, NJ, USA: Pearson Higher Education Inc., 2010.

[29] L. Tan and J. Jiang, "Signal Sampling and Quantization," in *Digital Signal Processing: fundamentals and applications*, San Diego, CA, USA: Elsevier, 2019, ch. 2, pp. 13–58.

[30] H. Inose and Y. Yasuda, "A Telemetering System by Code Modulation - Δ- Σ Modulation," in *IRE Transactions on Space Electronics and Telemetry*, vol. SET-8, no. 3, pp. 204-209, Sept. 1962.

[31] B. Li, " Design of multi-bit sigma delta modulators for digital wireless communications," M.S. thesis, Department of Microelectronics & Information Technology, Royal Institute of Technology, Electrum, Kista, Sweden, 2003.

[32] A. Frappe *et al.*, "An All-Digital RF Signal Generator Using High-Speed Delta Sigma Modulators,"

IEEE Journal of Solid-State Circuits, vol. 44, no. 10, pp. 2722–2732, Oct. 2009.

[33] A. Dupuy and Y. E. Wang, “High efficiency power transmitter based on envelope delta-sigma modulation (EDSM),” in *IEEE 60th Vehicular Technology Conference*, Los Angeles, CA, USA, 2004, pp. 2092-2095.

[34] S. Hori, K. Kunihiro, K. Takahashi, and M. Fukaishi, “A 0.7-3GHz envelope ΔΣ modulator using phase modulated carrier clock for multi-mode/band switching amplifiers,” in *2011 IEEE Radio Frequency Integrated Circuits Symposium*, Baltimore, MD, USA, Jun. 2011, pp. 1–4.

[35] M. Tanio *et al.*, "An FPGA-based all-digital transmitter with 28-GHz time-interleaved delta-sigma modulation," in *2016 IEEE MTT-S International Microwave Symposium (IMS)*, San Francisco, CA, USA, 2016, pp. 1-4.

[36] M. Tanio *et al.*, "An FPGA-based 1-bit Digital Transmitter with 800-MHz Bandwidth for 5G Millimeter-wave Active Antenna Systems," in *2018 IEEE/MTT-S International Microwave Symposium - IMS*, Philadelphia, PA, USA, 2018, pp. 499-502.

[37] A. Lorences-Riesgo *et al.*, "Real-Time FPGA-Based Delta-Sigma-Modulation Transmission for 60 GHz Radio-Over-Fiber Fronthaul," in *2018 European Conference on Optical Communication (ECOC)*, Rome, Italy, 2018, pp. 1-3.

[38] J. Wang *et al.*, "Delta-Sigma Modulation for Next Generation Fronthaul Interface," *Journal of Lightwave Technology*, vol. 37, no. 12, pp. 2838-2850, June, 2019.

[39] S. Hori *et al.*, "A 1-Bit Digital Transmitter System using a 20-Gbps Quadruple-Cascode Class-D Digital Power Amplifier with 45nm SOI CMOS," in *2019 IEEE MTT-S International Microwave Symposium (IMS)*, Boston, MA, USA, 2019, pp. 734-737.

[40] T. Soma *et al.*, "A 200 MHz Bandwidth GaAs Switch-Mode Supply Modulator," in *2018 IEEE BiCMOS and Compound Semiconductor Integrated Circuits and Technology Symposium (BCICTS)*, San Diego, CA, USA, 2018, pp. 148-151.

[41] Y. Seo *et al.*, "3 - Level Envelope Delta - Sigma Modulation RF Signal Generator for High - Efficiency Transmitters," *ETRI Journal*, vol. 36, no. 6, pp. 924-930, December, 2014.

[42] J. Engelen and R. Plassche, *Bandpass sigma delta modulators: stability analysis, performance and design aspects*. Boston, MA, USA: Springer, 1999.

[43] M. Neitola, "Lee's Rule Extended," *IEEE Transactions on Circuits and Systems II: Express Briefs*, vol. 64, no. 4, pp. 382-386, April 2017.

[44] N. Kumar and K. Rawat, "Delta Sigma Modulation Based Digital Transmitter for Single and Dual Band Transmission," in *2018 IEEE MTT-S International Microwave and RF Conference (IMaRC)*, Kolkata, India, 2018, pp. 1-4.

[45] T. Maehata *et al.*, "Concurrent dual-band 1-bit digital transmitter using band-pass delta-sigma modulator," in *2013 European Microwave Integrated Circuit Conference*, Nuremberg, Germany, 2013, pp. 552-555.

[46] *LTE; Evolved Universal Terrestrial Radio Access (E-UTRA); Base Station (BS) radio transmission and reception,* 3GPP TS 36.104 version 8.3.0 Release 8, 2008.

[47] *Digital cellular telecommunications system (Phase 2+) (GSM), Universal Mobile Telecommunications System (UMTS), LTE 5G release description Release 14*, 3GPP TR 21.914 version 14.0.0 Release 14, 2018.

[48] MITEQ, "6 GHz SCM fiber optical link," SCMT-100M 6G-28-20-M14 and SCMR-100M 6G-10-20-10 datasheet, March, 2003.

[49] *IEEE draft standard for information technology - telecommunications and information exchange between systems - local and metropolitan area networks - specific requirements - part 11: wireless LAN medium access control (MAC) and physical layer (PHY) specifications*, IEEE Std 802.11™-2016, 2016.